# Mass Spectrometric Analysis of Tyrosine Metabolic Enzymes

Christopher John Vavricka Jr.

Dissertation submitted to the faculty of the Virginia Polytechnic Institute and State University in partial fulfillment of the requirements for the degree of

Doctor of Philosophy

In

Biochemistry

Jianyong Li, Chairperson

Richard Helm

Glenda Gillaspy

Timothy Larson

July 28th, 2009
Blacksburg, Virginia

Keywords: tyrosine metabolism, mass spectrometry, proteomics, post-translational modification, glycosylation, dopachrome, melanogenesis, methyldopa, dopamine

# Mass Spectrometric Analysis of Tyrosine Metabolic Enzymes

Christopher John Vavricka Jr.

## (ABSTRACT)

The metabolism of tyrosine is essential for many critical biochemical events including catecholamine synthesis, melanogenesis and insect cuticle sclerotization. These pathways are highly regulated in both insects and mammals by many well-characterized enzymes including dopa decarboxylase and tyrosine hydroxylase. On the other hand, there are still many enzymes involved in these processes that we know very little about. Dopachrome tautomerase (DCT), dopachrome conversion enzyme (DCE) and α-methyldopa resistant protein (AMD) fall into the category of the less characterized enzymes.

Dopachrome is a pivotal intermediate in melanogenesis. Mammalian DCT and insect DCE both use dopachrome as substrate. DCE catalyzes a decarboxylative structural rearrangement of dopachrome to 5,6-dihydroxyindole (DHI), whereas DCT mediates the isomerization/tautomerization of dopachrome 5,6-dihydroxyindole-2-carboxylic acid (DHICA). DHI is oxidized easily, leading to the production of melanin, as well as reactive oxygen species (ROS). DHICA is less reactive, relative to DHI, and consequently produces less toxic byproducts during melanogenesis; therefore DCT plays an important role in detoxification of DHI and ROS.

Purification and MS analysis of DCE and DCT determined that *N*-glycosylation is a primary post-translational modification. Q-TOF mass spectrometry was used to determine *N*-glycosylation patterns from *Aedes aegypti* DCE and MALDI-TOF/TOF was used to determine multiple glycosylation sites in DCT. *N*-glycosylation is critical for the folding and trafficking of secreted proteins in the endomembrane system. The analysis of glycosylation sites in DCE and DCT therefore is essential toward achieving a comprehensive understanding of their structure and function.

Like DCT, AMD also plays a protective role. The AMD protein was originally identified in *Drosophila* mutants hypersensitive to α-methyldopa, an inhibitor of dopa decarboxylase (DDC). Production of dopamine by DDC is critical for developing insects because dopamine conjugates are used as crosslinking agents for cuticle sclerotization. Although there has been much discussion into the function of AMD, what exactly this protein does has been unknown. AMD shares 48% sequence identity with DDC, however we have found that AMD is an enzyme, which possesses a different catalytic activity. GC-MS analysis of AMD enzymatic reaction components revealed that AMD catalyzes the oxidative decarboxylation of L-DOPA to DOPAL, and also the oxidative decarboxylation of α-methyldopa to 3,4-dihydroxyphenylacetone.

In summary, multiple *N*-Glycosylation sites were characterized in DCT and DCE. Furthermore, a new protein function has been demonstrated for AMD. These experiments were performed using classical biochemistry techniques in combination with mass spectrometry.

# ACKNOWLEDGMENT

First and foremost, I would like to express my sincere gratitude to Dr. Jianyong Li for his guidance and support throughout my graduate studies. Many thanks to Dr. Tim Larson, Dr. Rich Helm and Dr. Glenda Gillaspy, all for taking me on as a student in their labs and serving on my committee. Thank you Dr. Junsuo Li for mentoring me in the study of glycoproteins. Thanks Haizhen Ding for producing so much valuable raw material for protein purification. I am very grateful of my co-authors Keith Ray and Kim Harich for collecting valuable MS data for this dissertation. Thank you Dr. Qian Han for serving as a mentor for me. I would also like to thank Dr. Eugene Gregory, Dr. Helen Crawford, Dr. Jinsong Zhu, Dr. David Bevan, Dr. Bruce Christensen and Dr. Thomas Sitz for playing an important role throughout my studies. Of course, I cannot avoid giving honorable mention to my friends Brian Hickory, Dr. Joseph Germana, Sam Russell, Dr. Amir Guri and Brian Stanek. Last, but not least, I would like to give a special thanks to my mother, Diane Vavricka, and father, Chris Vavricka, for being there for me always.

# DEDICATION

In memory of Anthony Scarpa, my old friend, opponent in chess and the best electrician in south Jersey.

# TABLE OF CONTENTS

# LIST OF FIGURES

CHAPTER 1



CHAPTER 2

CHAPTER 3

CHAPTER 4

APPENDIX

# LIST OF TABLES

CHAPTER 2



CHAPTER 3

# LIST OF ABBREVIATIONS

| | |
|---|---|
| 5-HTP | 5-hydroxytryptophan |
| 5-HT | 5-hydroxytryptamine, serotonin |
| α-methyldopa | 3-(3,4-Dihydroxyphenyl)-2-methyl-L-alanine |
| AADC | aromatic amino acid decarboxylase |
| AANAT | arylalkylamine N-acetyltransferase |
| ALDH | aldehyde dehydrogenase |
| AMD | α-methyldopa resistant protein |
| asn | asparagine |
| bp | base pairs |
| BSTFA | *N*,*O*-Bis(trimethylsilyl)trifluoroacetamide |
| COMT | catechol-O-methyl transferase |
| CID | collision induced dissociation |
| Da | dalton |
| DA | dopamine, L-3,4-dihydroxyphenethylamine |
| DBH | dopamine-β-hydroxylase |
| DCE | dopachrome conversion enzyme |
| DCT | dopachrome tautomerase |
| DDC | dopa decarboxylase |
| DHI | 5,6-dihydroxyindole |
| DHICA | 5,6-dihydroxyindole-2-carboxylic acid |
| DTT | dithiothreitol |

| | |
|---|---|
| GlcNAc | N-acetyl-glucosamine |
| Hex | Hexose |
| L-DOPA | L-3,4-dihydroxyphenylalanine |
| MALDI | matrix assisted laser desorption ionization |
| Man | Mannose |
| MS | mass spectrometry |
| MS/MS | tandem mass spectrometry |
| NADA | N-acetyldopamine |
| NBAD | N-β-alanyldopamine |
| PCR | polymerase chain reaction |
| PMSF | phenylmethylsulfonyl fluoride |
| PNGase F | peptide N-glycosidase F |
| PNMT | phenyletanolamine N-methyltransferase |
| PTM | post-translational modification |
| Q | quadrupole |
| ROS | reactive oxygen species |
| Sf9 | *Spodoptera frugiperda* 9 cell line |
| TEV | tobacco etch virus |
| TH | tyrosine hydroxylase |
| TIC | total ion count |
| TMCS | trimethylchlorosilane |
| TOF | time of flight |
| TRP1 | tyrosinase-related protein 1 |

# I

# INTRODUCTION

## 1.1 Tyrosine Metabolism

Tyrosine or (S)-2-Amino-3-(4-hydroxyphenyl)-propanoic acid is a semi-essential amino acid synthesized from phenylalanine in most animals. Along with tryptophan, tyrosine contributes to a majority of the UV absorbance of proteins. Aside from its role as a protein residue, tyrosine may undergo many different fates in animals depending on the enzymatic or oxidative forces it encounters (Figure 1.1).

Many evolutionary commonalities and differences exist between the precise functions of tyrosine metabolism in insects and mammals. One common link in all animals is the use of tyrosine for the synthesis of catecholamines, 3,4-dihydroxy derivatives of phenylethylamine [1]. The biosynthesis of catecholamines begins with the enzymatic hydroxylation tyrosine to L-DOPA by tyrosine hydroxylase [1]. Decarboxylation of L-DOPA by dopa decarboxylase (DDC) leads to the formation of dopamine (DA), an abundant signaling molecule located primarily in the striatum of mammals [1]. Dopamine appears to have multiple functions, relating to movement, reward, motivation, cognition and learning [2]. Hydroxylation of dopamine by dopamine-β-hydroxylase (DBH) produces norepinephrine [1]. Phenylethanolamine-N-methyltransferase (PNMT) methylates norepinephrine to epinephrine, which is primarily a hormone in the peripheral nervous system [1]. Both the aromatic phenol ring of tyrosine and the catechol ring absorb light strongly in the UV-region making them easy to detect.

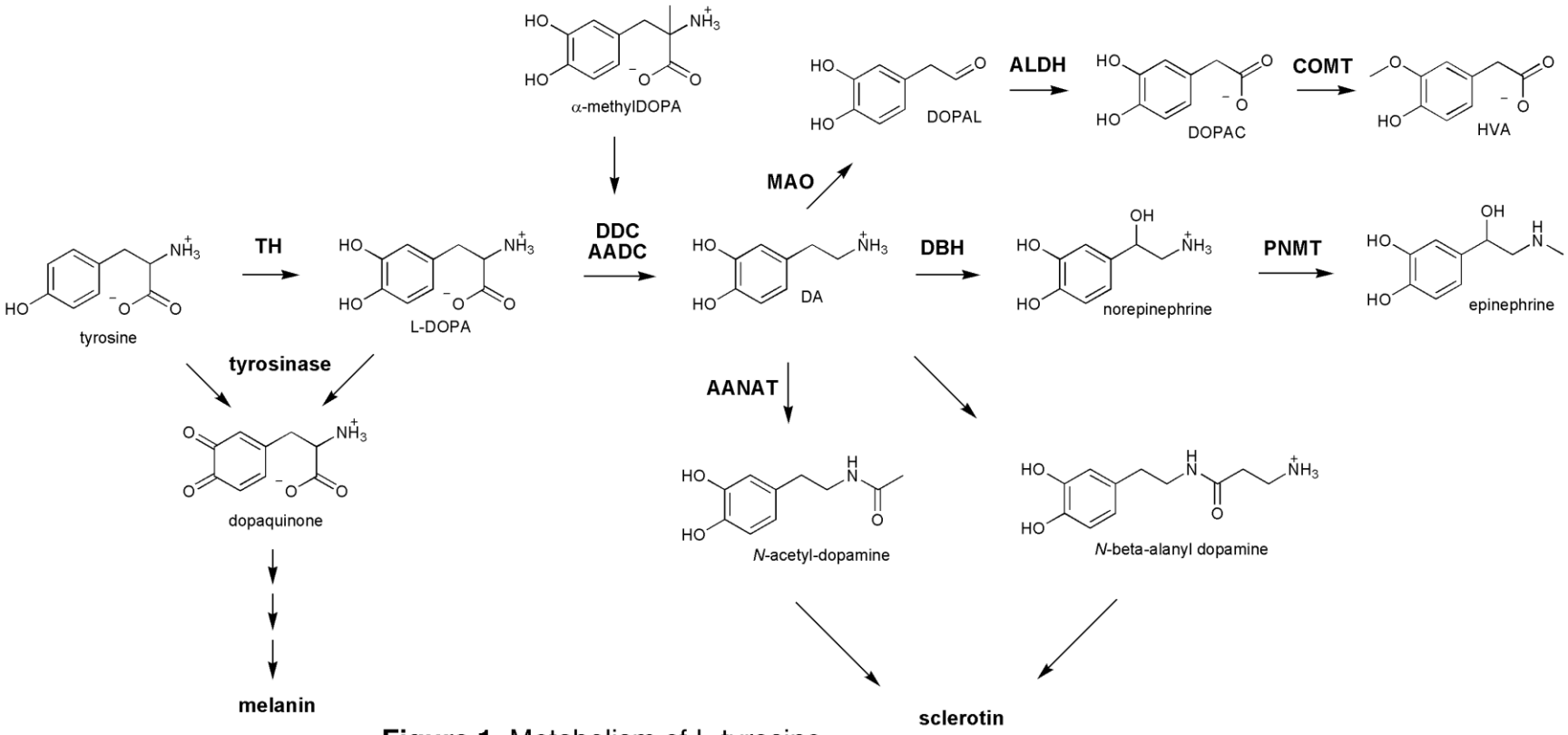


**Figure 1** Metabolism of L-tyrosine

The vicinal diol system of catechol rings is easily oxidized to a quinone [3]. The ability to oxidize catecholamines easily makes them convenient for detection using electrochemical detection. Furthermore, the oxidation of catechol to highly electrophilic quinones is precisely the driving force for melanogenesis and sclerotization [3].

## 1.2 Melanogenesis

Melanin is a large pigment composed primarily of hydroxylated indole residues (Figure 1.2). This complex heteropolymer is present in various bacteria, fungi, plants and animals [4]. It is well established that melanin protects against detrimental UV radiation; however, the presence of melanin in the CNS and inner ear of mammals suggests additional functions [5]. Melanin polymers may participate in either one- or two-electron redox reactions, enabling these polymers to protect against reactive oxygen species [6]. The cuttlefish *Sepia officinalis* secretes a melanin-rich ink as a defense response [7]. Furthermore, melanin has also been demonstrated to be involved in various immune responses [6], chelating of metals [8], mosquito eggshell hardening [9], and possibly signal transduction [5].

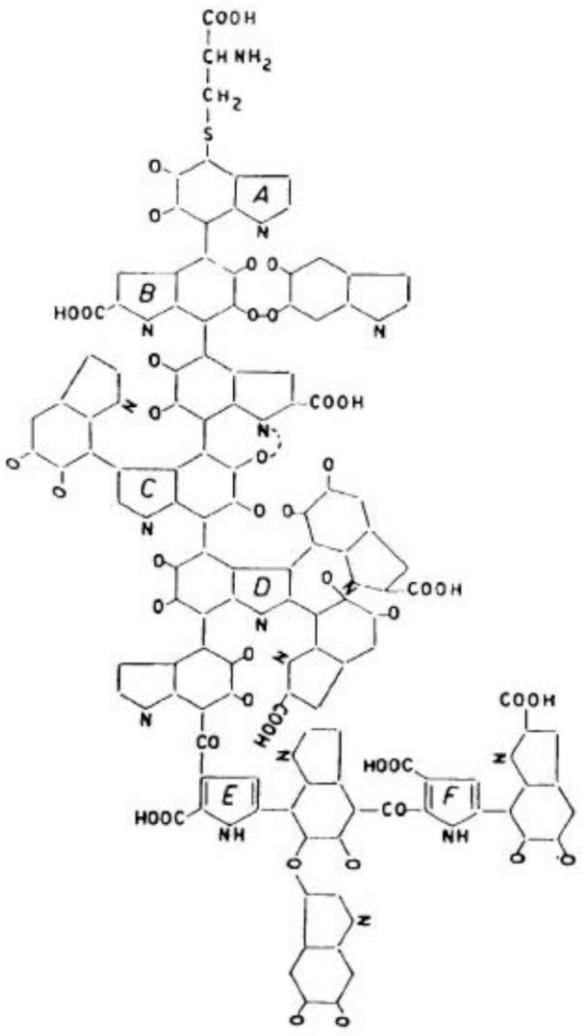


**Figure 1.2** Structure of Sepia melanin proposed by Nicolaus RA [10]. Due to the irregular nature of this polymer, no exact crystal structures currently exist of melanin.

Melanin biosynthesis in mammals is regulated by over 100 different genes [11]; however, the actual reactions are directly catalyzed by very few enzymes [4]. In mammals three proteins, named tyrosinase, tyrosinase-related protein 1 (TRP1) and trysoinase related protein 2 (TRP2), are directly involved in melanogenesis (Figure 1.3) [4]. TRP2 catalyzes the isomerization and tautomerization of dopachrome to DHICA; therefore, it was also named dopachrome tautomerase (DCT) in some literature (Figure 1.3). In insects, the tyrosinase equivalent is named phenoloxidase (PO) and their DCT counterpart is named dopachrome conversion enzyme (DCE). Although PO and tyrosinase use the same substrates and catalyze the same reactions in the melanization pathway, their primary sequences share no apparent similarity. For example, mouse tyrosinase and *Drosophila* diphenol oxidase A2 share only 8% sequence identity. Insect DCE and mammalian DCT, similar to insect PO and mammalian tyrosinase, use the same dopachrome substrate, but their enzymatic product is different. As a result, the properties of biological melanin produced in the presence or absence of DCT or DCE vary considerably. For example, in the presence of DCT, much more carboxylated 5,6-dihydroxyindole-2-carboxylic acid (DHICA) melanin is produced, and in the presence of DCE, a higher proportion of decarboxylated 5,6-dihydroxyindole (DHI) melanin is produced (Figure 1.3). DHI melanin is reported to be darker and less soluble as compared to DHICA melanin, which is more brownish with higher solubility [12].

The process of melanogenesis beings with the oxidation of tyrosine or L-DOPA to dopaquinone by the enzyme tyrosinase in bacteria, fungi and mammals; or by the enzyme PO in insects (Figure 1.3) [6]. At this point in the pathway, everything else may proceed spontaneously under oxidizing conditions and therefore many bacteria do not posses

other enzymes to manipulate this process aside from tyrosinase. Dopaquinone is highly unstable and will cyclize to form dopachrome via a leucodopachrome (cyclodopa) intermediate (Figure 1.3) [3]. Dopachrome may spontaneously undergo decarboxylative structural rearrangement to form DHI, however the non-enzymatic conversion of dopachrome to DHI proceeds very slowly (Figure 1.3) [3].

Virtually all melanin arising from tyrosine in non-mammalian species goes through the decarboxylative pathway leading to formation of the black, insoluble DHI melanin [4]. DHI is easily oxidized to its *o*-quinone that polymerizes to form melanin. Unlike bacteria, mammals and insects have evolved a set of enzymes to control this process to meet their specific demands.

Although the decarboxylative rearrangement of dopachrome to DHI occurs spontaneously under neutral conditions, this process is not adequate for insects whose melanization pathway is a major biochemical event in cuticle hardening. The cuticle (also named exoskeleton) provides insects with protection against physical injury and water loss, rigidity for muscle attachment and mechanical support, and flexibility for joints. The highly protective cuticle is one of the reasons why insects are the most successful animals on earth. During larval development, continued growth requires that insects periodically shed their old cuticle and produce a new one. The newly formed cuticle is soft and elastic, which allows it to stretch and expand to accommodate the increased body size, but at this time the insect cuticle also is vulnerable to adverse environmental conditions and must be hardened or solidified shortly after insects shed their old cuticle. Consequently, the melanization of insect cuticle must be completed in a short period. DCE that facilitates the dopachrome to DHI pathway accelerates tremendously the insect

melanization process, which likely explains why DCE is evolved only in insects [13] [14]. To illustrate this, mosquito eggs can darken from white to black within a 2 hour-period [9].

On the other hand, mammals have much more time to invest into the process of melanogenesis. DHI is highly reactive and toxic to various cell lines [13]. DCT catalyzes the specific non-decarboxylative tautomerization of dopachrome to DHICA, which can polymerize in a similar manner to DHI. Therefore, DCT protects the cell against the formation of DHI, a toxic intermediate [13]. Although DCT shares approximately 40% sequence identity with tyrosinase and contains the same highly conserved metal binding histidine residues, the active site of DCT has a very different function and has nothing to do with the binding of molecular oxygen (see appendix).

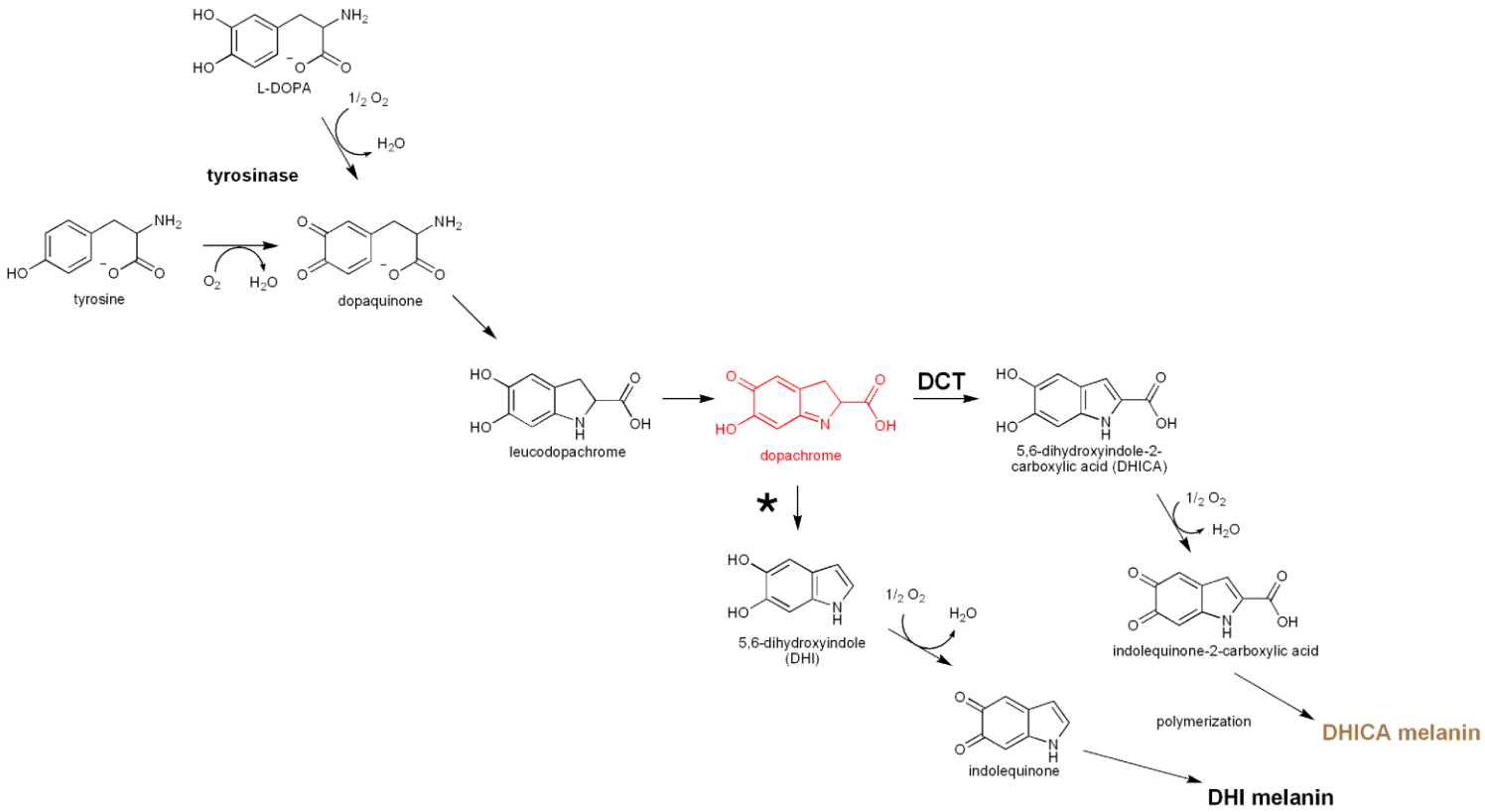


**Figure 1.3** Melanogenesis. The decarboxylative rearrangement of dopachrome to DHI (indicated by the asterisk), proceeds spontaneously under physiological conditions, or may be accelerated by the insect protein DCE. Non-enzymatic oxidation of catechols or hydroxylated indoles by molecular oxygen produces semiquonone radical. Polymerization of DHI and DHICA often results in C-C bonding at the 4'-7 positions of the indole ring.

By preserving the side-chain carboxyl group of the indole ring, DCT not only protects against formation of a toxic molecule, but also produces a unique melanin found only in higher eukaryotes. In this respect, DCT is the most influential enzyme currently known in terms of affecting the quality and properties of melanin. The DHICA melanin, resulting from the action of DCT, has different properties than ubiquitous DHI melanin: higher solubility and lighter color [4]. Molecular weight, size and redox properties of DHICA melanin may also be altered, which is postulated to play a direct role in the etiology of melanoma [14]. Furthermore, high DCT expression levels have been found to correlate with radiation and chemotherapy resistant melanoma lines [15-17]. Although melanogenesis should be able to proceed spontaneously after the point of tyrosine oxidation, mutations in *DCT* result in a grey coat color in mice, hence the gene for DCT has been termed *slaty* [18]. In addition to its importance in relation to melanogenesis and melanoma, DCT is also a critical factor for the differentiation of neurons [19].

A third mammalian enzyme, TRP1, shares high sequence identity to tyrosinase and DCT and is encoded by the mouse *brown* locus [20]. Mice with mutations in TRP1 display a brown coat phenotype in contrast to the black coat of the agouti mouse [20]. Mutations in human TRP1 are responsible for oculocutaneous albinism type 3, resulting in mild hypo-pigmentation [21]. Due to high sequence similarity, the TRP1 gene was mistaken as tyrosinase and was consequently the first of the three tyrosinase-related protein genes to be cloned [22]. Specific immunoaffinity purification of TRP1 yielded an enzyme with similar activity as tyrosinase [23]. Further investigation indicated that TRP1 likely functions as a better DHICA oxidase than tyrosinase [24]; however confusion has arisen due to discrepancies between the activity of human and mouse TRP1 [25].

Furthermore, TRP1 has been found to form a heterodimeric complex with tyrosinase [26]. Therefore the precise function of TRP1 is not entirely clear.

Among the three proteins directly involved in mammalian melanogenesis, tyrosinase has been the most well-characterized biochemically. A 3-D structure for a *Streptomyces* tyrosinase has been solved [27]. Although its primary sequence shares relatively limited sequence identity (29%) with mammalian tyrosinase and is only about half the size of the mammalian enzyme, the structural basis of substrate binding and catalysis of the mammalian tyrosinase likely is similar to that of the bacterial enzyme. DCT is very interesting in terms of its substrate specificity and catalysis, since it contains a "tyrosinase" domain yet catalyzes a completely different type of reaction. This, in addition to the ease in detecting dopachrome activity, has made DCT an ideal starting point for the structure and function analysis of the tyrosinase-related protein family. As for TRP1, there is much to learn about its physiological function.

### 1.3 Processing of Secreted Proteins

Many of the proteins involved in melanogenesis contain a signal peptide and undergo extensive processing and trafficking before reaching their functional state and destination. This has been a major area of research for the tyrosinase related protein family [28]. DCE also contains a signal sequence and is processed and glycosylated in the ER (Chapter 3).

Proteins secreted into the ER undergo various co- and post-translational modifications including *N*-glycosylation and disulfide bond formation [29]. N-glycosylation normally

occurs at Asn residues with the Asn-X-Ser/Thr motif, where X can be any amino acid except proline [29]. A core $Glc_3Man_9GlcNAc_2$ oligosaccharide unit is transferred to the *N*-glycosylation site of glycoproteins in the ER, and processing begins with the removal of the 3 terminal glucose residues by α-glucosidase I and II [30]. Before the third glucose is removed by α-glucosidase II, the monoglucosylated oligosaccharide moiety is able to bind with the ER lectin chaperones calnexin and calreticulin [31]. Once the protein is folded and the third glucose is removed, the protein may then enter the Golgi complex, where it undergoes further glycan processing [29].

Incorporation of an *N*-glycosylation site has been demonstrated to increase secretion of heterologous proteins in yeast [32]. Due to the heavy involvement of the *N*-glycosylation into the proper folding and processing of secreted proteins, proteins in this class are very unlikely to express as soluble recombinant protein in a bacterial expression system. Therefore, if there is difficulty in obtaining protein from native sources, as it is the case with the tyrosinase-related proteins, a eukaryotic expression system like yeast, insect cells or mammalian Chinese hamster ovary (CHO) cells must be utilized.

*O*-glycosylation of serine or threonine protein residues may occur at a later point (after *N*-glycosylation) in the processing of secreted proteins in the *Golgi*. Due to the importance of *N*-glycosylation for interactions with the chaperones calnexin and calreticulin in the ER, there is an emphasis on *N*-glycosylation in the study of the tyrosinase-related proteins. However, *O*-glycosylation has also been demonstrated to play an important role in the processing of secreted proteins, like synaptotagmin [33], and there is evidence that tyrosinase may contain *O*-glycosylation sites [34].

## 1.4 Insect Catecholamine Metabolism

A major difference between insects and mammals in regards to tyrosine metabolism is the use of dopamine in the process of cuticle sclerotization. This process is highly related to melanogenesis and occurs simultaneously. Insects produce *N*-acetyl-dopamine and N-beta-alanyldopamine as crosslinking precursors to promote the hardening of the cuticle (Figure 1.1) [35]. It is understood that highly reactive quinones, similar to those arising from melanogenesis, also function to crosslink components in the cuticle [35]. One major difference between the known intermediates in melanogenesis and sclerotization is the presence of a free amino group able to promote intramolecular cyclization.

α-Methyldopa is a competitive inhibitor of DDC and therefore prevents the formation of dopamine from L-DOPA [36]. In a similar manner, α-methyltyrosine is also a competitive inhibitor of TH and is slowly metabolized to α-methyldopa [1]. Catecholamines stimulate the sympathetic nervous system, which is activated during a response to stress (fight-or-flight response). Therefore, catecholamines often result in increased blood pressure and α-methyldopa has been marketed as the drug aldomet to treat hypertension [1]. Insects, which require dopamine to form sclerotin, especially during cuticle development, are especially susceptible to inhibition of DDC [37]. While studying the effect of α-methyldopa on DDC mutants, strains of *Drosophila* that are hypersensitive to this inhibitor were identified [37]. A new gene adjacent to DDC was identified and the product was termed α-methyldopa resistant protein (AMD) [37]. This protein shares approximately 40% sequence identity with DDC and is expressed as two

isoforms with variation in their N-terminal sequence, however the function of the two AMD isoforms has yet to be reported.

# LITERATURE CITED


1. Molinoff, P.B. and J. Axelrod, *Biochemistry of catecholamines.* Annu Rev Biochem, 1971. **40**: p. 465-500.

2. Schultz, W., *Multiple dopamine functions at different time courses.* Annu Rev Neurosci, 2007. **30**: p. 259-88.

3. Ito, S. and K. Wakamatsu, *Chemistry of mixed melanogenesis--pivotal roles of dopaquinone.* Photochem Photobiol, 2008. **84**(3): p. 582-92.

4. Prota, G., *Melanins and melanogenesis*. 1992, San Diego: Academic Press. xiii, 290 p.

5. Nicolaus, B.J.R., *A critical review of the function of neuromelanin and an attempt to provide a unified theory.* Medical Hypotheses, 2005. **65**(4): p. 791-796.

6. Riley, P.A., *Melanin.* International Journal of Biochemistry & Cell Biology, 1997. **29**(11): p. 1235-1239.

7. Russo, G.L., et al., *Toxicity of melanin-free ink of Sepia officinalis to transformed cell lines: identification of the active factor as tyrosinase.* Biochemical and Biophysical Research Communications, 2003. **308**(2): p. 293-299.

8. Sarna, T., J.S. Hyde, and H.M. Swartz, *Ion-Exchange in Melanin - Electron-Spin Resonance Study with Lanthanide Probes.* Science, 1976. **192**(4244): p. 1132-1134.

9. Li, J.S.S. and J.Y. Li, *Major chorion proteins and their crosslinking during chorion hardening in Aedes aegypti mosquitoes.* Insect Biochemistry and Molecular Biology, 2006. **36**(12): p. 954-964.

10. Nicolaus, R.A., M. Piattelli, and E. Fattorusso, *The structure of melanins and melanogenesis. IV. On some natural melanins.* Tetrahedron, 1964. **20**(5): p. 1163-72.

11. Bennett, D.C. and M.L. Lamoreux, *The color loci of mice - A genetic century.* Pigment Cell Research, 2003. **16**(4): p. 333-344.

12. Orlow, S.J., M.P. Osber, and J.M. Pawelek, *Synthesis and characterization of melanins from dihydroxyindole-2-carboxylic acid and dihydroxyindole.* Pigment Cell Res, 1992. **5**(3): p. 113-21.

13. Pawelek, J.M. and A.B. Lerner, *5,6-Dihydroxyindole is a melanin precursor showing potent cytotoxicity.* Nature, 1978. **276**(5688): p. 626-8.

14. Sarangarajan, R. and S.P. Apte, *The polymerization of melanin: a poorly understood phenomenon with egregious biological implications.* Melanoma Research, 2006. **16**(1): p. 3-10.

15. Pak, B.J., et al., *Lineage-specific mechanism of drug and radiation resistance in melanoma mediated by tyrosinase-related protein 2.* Cancer Metastasis Rev, 2001. **20**(1-2): p. 27-32.

16. Pak, B.J., et al., *Radiation resistance of human melanoma analysed by retroviral insertional mutagenesis reveals a possible role for dopachrome tautomerase.* Oncogene, 2004. **23**(1): p. 30-8.

17. Pak, B.J., et al., *TYRP2-mediated resistance to cis-diamminedichloroplatinum (II) in human melanoma cells is independent of tyrosinase and TYRP1 expression and melanin content.* Melanoma Res, 2000. **10**(5): p. 499-505.

18. Costin, G.E., et al., *Mutations in dopachrome tautomerase (Dct) affect eumelanin/pheomelanin synthesis, but do not affect intracellular trafficking of the mutant protein.* Biochem J, 2005. **391**(Pt 2): p. 249-59.

19. Jiao, Z., et al., *Dopachrome tautomerase (Dct) regulates neural progenitor cell proliferation.* Dev Biol, 2006. **296**(2): p. 396-408.

20. Jackson, I.J., *A cDNA encoding tyrosinase-related protein maps to the brown locus in mouse.* Proc Natl Acad Sci U S A, 1988. **85**(12): p. 4392-6.

21. Boissy, R.E., et al., *Mutation in and lack of expression of tyrosinase-related protein-1 (TRP-1) in melanocytes from an individual with brown oculocutaneous albinism: a new subtype of albinism classified as "OCA3".* Am J Hum Genet, 1996. **58**(6): p. 1145-56.

22. Shibahara, S., et al., *Cloning and expression of cDNA encoding mouse tyrosinase.* Nucleic Acids Res, 1986. **14**(6): p. 2413-27.

23. Jimenez, M., K. Tsukamoto, and V.J. Hearing, *Tyrosinases from two different loci are expressed by normal and by transformed melanocytes.* J Biol Chem, 1991. **266**(2): p. 1147-56.

24. Jimenez-Cervantes, C., et al., *A new enzymatic function in the melanogenic pathway. The 5,6-dihydroxyindole-2-carboxylic acid oxidase activity of tyrosinase-related protein-1 (TRP1).* J Biol Chem, 1994. **269**(27): p. 17993-8000.

25. Boissy, R.E., et al., *Human tyrosinase related protein-1 (TRP-1) does not function as a DHICA oxidase activity in contrast to murine TRP-1.* Exp Dermatol, 1998. **7**(4): p. 198-204.

26. Jimenez-Cervantes, C., et al., *Molecular interactions within the melanogenic complex: Formation of heterodimers of tyrosinase and TRP1 from B16 mouse melanoma.* Biochemical and Biophysical Research Communications, 1998. **253**(3): p. 761-767.

27. Matoba, Y., et al., *Crystallographic evidence that the dinuclear copper center of tyrosinase is flexible during catalysis.* J Biol Chem, 2006. **281**(13): p. 8981-90.

28. Branza-Nichita, N., et al., *N-glycosylation processing and glycoprotein folding - Lessons from the tyrosinase-related proteins.* Chemical Reviews, 2000. **100**(12): p. 4697-+.

29. Varki, A., *Essentials of glycobiology*. 2nd ed. 2009, Cold Spring Harbor, N.Y.: Cold Spring Harbor Laboratory Press. xxix, 784 p.

30. Roth, J., M. Ziak, and C. Zuber, *The role of glucosidase II and endomannosidase in glucose trimming of asparagine-linked oligosaccharides.* Biochimie, 2003. **85**(3-4): p. 287-94.

31. Caramelo, J.J. and A.J. Parodi, *Getting in and out from calnexin/calreticulin cycles.* Journal of Biological Chemistry, 2008. **283**(16): p. 10221-10225.

32. Sagt, C.M.J., et al., *Introduction of an N-glycosylation site increases secretion of heterologous proteins in yeasts.* Applied and Environmental Microbiology, 2000. **66**(11): p. 4940-+.

33. Atiya-Nasagi, Y., et al., *O-glycosylation is essential for intracellular targeting of synaptotagmins I and II in non-neuronal specialized secretory cells.* J Cell Sci, 2005. **118**(Pt 7): p. 1363-72.

34. Halaban, R., et al., *Regulation of Tyrosinase in Human Melanocytes Grown in Culture.* Journal of Cell Biology, 1983. **97**(2): p. 480-488.

35. Andersen, S.O., M.G. Peter, and P. Roepstorff, *Cuticular sclerotization in insects.* Comparative Biochemistry and Physiology B-Biochemistry & Molecular Biology, 1996. **113**(4): p. 689-705.

36. Lovenberg, W., et al., *Characteristics of the Inhibition of Aromatic L-Amino Acid Decarboxylase by Alpha-Methylamino Acids.* Arch Biochem Biophys, 1963. **103**: p. 9-14.

37. Marsh, J.L. and T.R.F. Wright, *Evidence for Regulatory Variants of the Dopa Decarboxylase and Alpha-Methyldopa Hypersensitive Loci in Drosophila.* Genetics, 1986. **112**(2): p. 249-265.

# II

# DOPACHROME TAUTOMERASE

## 2.1 Abstract

Dopachrome tautomerase (DCT) catalyzes the non-decarboxylative tautomerization of dopachrome to 5,6-dihydroxyindole-2-carboxylic acid (DHICA) in the melanogenesis pathway. In the absence of DCT, dopachrome spontaneously undergoes decarboxylative structural rearrangement to form 5,6-dihydroxyindole (DHI), which is more easily oxidized that DHICA, leading to higher levels of reactive oxygen species. DCT plays a critical role in lowering oxidative stress resulting from melanogenesis. Levels of DCT are elevated in melanoma cell lines that are especially resistant to chemotherapy and radiation. DCT is also processed as a melanoma antigen and is being explored as a potential target for immunotherapy. In order to establish a more complete understanding of the contributions that DCT may offer in the treatment of melanoma skin cancer, isolation of highly pure and properly processed protein is necessary. Purification of native DCT has been problematic due to a hydrophobic transmembrane anchor and interactions with melanin. In this study, DCT was expressed, without its carboxy-terminal transmembrane region, using a Sf9 insect cell protein expression system and its recombinant protein was purified by various chromatographic techniques. Analysis of its tryptic peptides by MALDI-TOF/TOF determined *N*-glycosylation as a primary DCT post-translational modification. Our success in the expression of soluble mammalian DCT and the characterization of *N*-glycosylation should serve as a useful reference toward a comprehensive understanding of the structure / function relationship of mammalian DCT.

## 2.2 Introduction

Dopachrome tautomerase (DCT, TRP-2) catalyzes a tautomerization of L-dopachrome to 5,6-dihydroxyindole-2-carboxylic acid in the mammalian melanogenesis pathway (Figure 2.1) [1]. In the absence of DCT, dopachrome undergoes a decarboxylative structural rearrangement to form 5,6-dihydroindole that is easily oxidized by molecular oxygen, leading to the production of reactive oxygen species. By preserving the carboxylic acid group of its substrate, DCT protects the cell against the formation of 5,6-dihydroxyindole, a highly toxic intermediate [2].

Unfortunately, DCT not only protects healthy melanocytes, but also contributes significantly to the resistance of melanoma to many various forms of treatment. Transfection of WM35 human melanoma cells with *DCT* has been reported to confer resistance to the chemotherapeutic drug, CDDP [3, 4]. Later, it was demonstrated that DCT is significantly elevated at the mRNA and protein level in WM35 cell lines that display increased resistance to X-ray radiation, UV radiation and chemotherapy [5]. Furthermore, DCT is presented as a melanoma surface antigen that is recognized by cytotoxic T-cells and is therefore a potential target for immunotherapy [6-8].

The ability to obtain purified DCT is essential to our understanding of its function in resistant melanoma lines. Although there is high DCT activity in melanocytes and melanoma cells, a carboxy-terminal transmembrane domain has made it difficult to purify native DCT. Furthermore, melanosomal proteins are often covalently linked to melanin, making them even less soluble [9]. Immune-affinity purification of native DCT has been reported; however, this was done using antibodies specific for a portion of the carboxy-terminal membrane region [10]

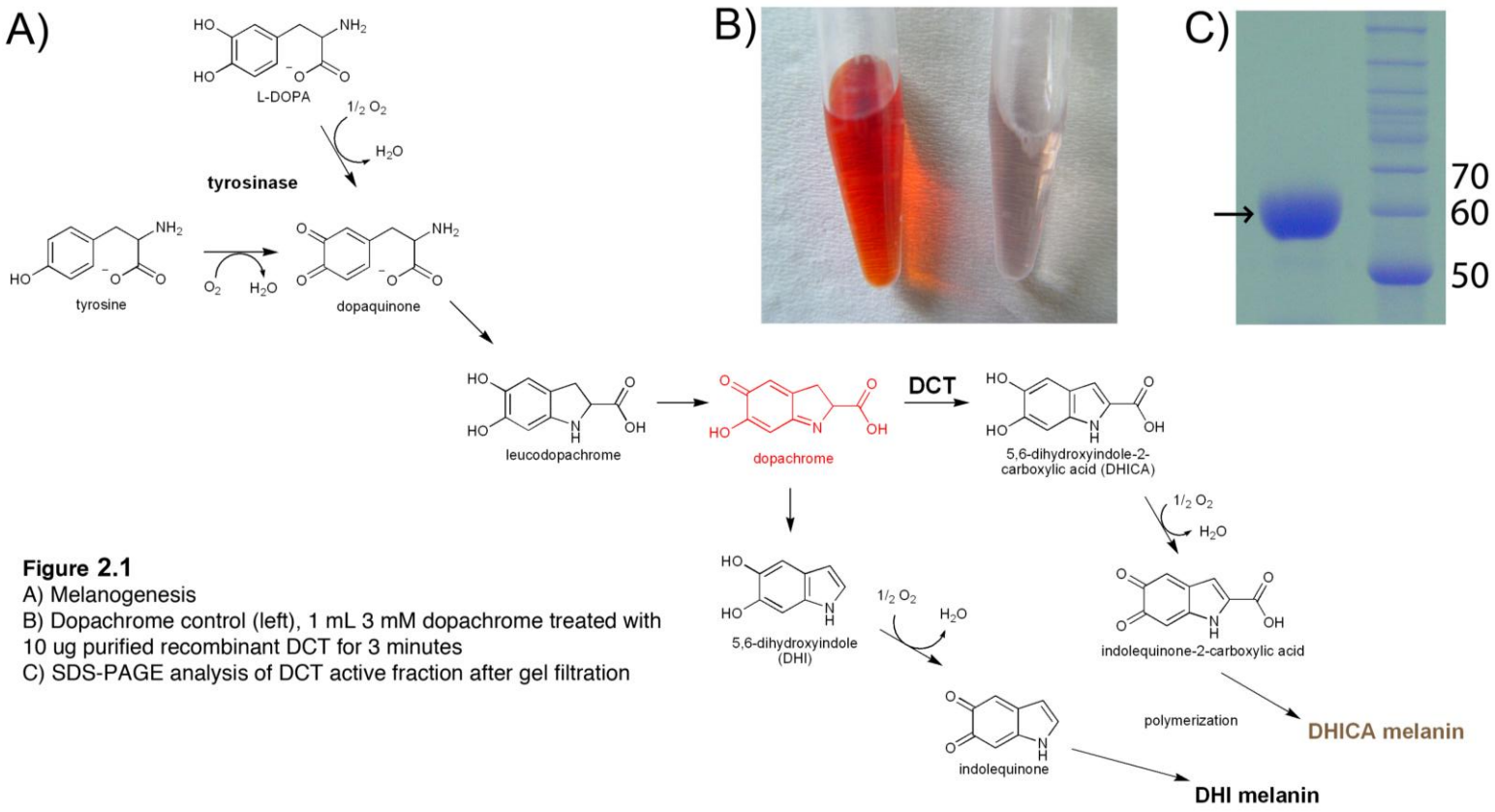


**Figure 2.1**
A) Melanogenesis
B) Dopachrome control (left), 1 mL 3 mM dopachrome treated with 10 ug purified recombinant DCT for 3 minutes
C) SDS-PAGE analysis of DCT active fraction after gel filtration

In the study described herein, functionally active recombinant DCT was expressed, without this problematic hydrophobic region, using a Sf9 insect cell expression system. This recombinant DCT was purified without the use of detergents that often interfere with separation and cannot simply be removed with dialysis. Expression of DCT in a eukaryotic system has proved necessary largely due to extensive *N*-glycosylation of DCT, which is critical for correct processing and trafficking in the ER and Golgi [11]. Transient interactions between protein *N*-glycan structures and ER lectin-like resident chaperones are extremely important for folding of glycoproteins [12, 13]. This maturation process in the endomembrane system has been extensively studied using tyrosinase and tyrosinase-related protein 1, the proteins most closely related to DCT [12, 13]. However, no direct investigation into the glycosylation sites of DCT has previously been reported [14]. In the analysis of recombinant DCT using MALDI-TOF/TOF, two out of the seven potential *N*-glycosylated sites were found to be occupied.

## 2.3 Materials and Methods

*Materials*

*Spodoptera frugiperda* (Sf9) insect cells, pBlueBac4.5, linearized *Autographa californica* multicapsid nucleopolyhedrovirus (AcMNPV) viral DNA, and Cellfectin$^{R}$ Transfection Reagent were from Invitrogen (Carlsbad, CA, USA). Grace's Insect Medium was from Gibco (Carlsbad, CA, USA) and fetal bovine serum was from Innovative Research (Novi, MI, USA). B16 murine melanoma cells and Dulbecco's Modified Eagle's Medium were obtained from ATCC (Manassas, VA, USA). 3,4-

dihydroxyphenylalanine (L-DOPA), sodium periodate, phenylmethylsulfonyl fluoride (PMSF) and Octyl-Sepharose were from Sigma (St. Louis, MO, USA). Mono-Q and Superose were from Amersham Biosciences (Piscataway, NJ, USA). CHT™ Ceramic Hydroxyapatite was obtained from Bio-Rad (Hercules, CA, USA). PNGase F expression vector, pOPH6, was a gift from Dr. Shaun Lott (University of Auckland, New Zealand).

*Expression of Recombinant DCT*

Total mRNA was isolated from B16 mouse melanoma cells and reverse transcribed to cDNA. A forward primer (ACTAGTATGCTAGCATGGGCCTTGTGGGAT) containing an NheI restriction site and a reverse primer (ACTAGGATCCCTATGAGAGAGTTGTGGACC) containing an EcoRI restriction site were used for PCR amplification of the DCT coding sequence from the B16 cDNA library. PCR parameters: 64$^{o}$C annealing temperature, (45 s); 72$^{o}$C extension (2 min, 20 s); 36 cycles. This led to the amplification of a 1416 bp truncated DCT coding sequence (without the carboxyl-terminal membrane domain of 135 bp). The gene fragment amplified using the above primers encode a truncated DCT protein with the C-terminal sequence SEEEAPVWSTTLS

The PCR product was ligated into the baculovirus transfer vector pBlueBac4.5 between the NheI and EcoRI restriction sites. The resulting recombinant baculovirus transfer vector was amplified in *E. coli*. DNA from purified recombinant baculovirus was PCR amplified using the forward primer TTTACTGTTTTCGTAACAGTTTTG and reverse primer CAACAACGCACAGAATCTAGC. PCR parameters: 60$^{o}$C annealing temperature, (45 s); 72$^{o}$C extension (2 min, 30 s); 36 cycles. A 1.85 kb fragment was

observed, matching the calculated size of the DCT coding sequence (1.41 kb) and b aculovirus sequence (435 bp). No wild-type virus amplified DNA fragment was present when analyzing the PCR products with agarose gel electrophoresis.

The DCT recombinant pBlueBac4.5 transfer vector and linearized Bac-N-Blue™ viral DNA were co-transfected into log phase Sf9 cells using Cellfectin$^{R}$ Reagent. Pure recombinant baculovirus was purified by a plaque assay. Viral DNA was isolated for PCR analysis to determine the purity of the recombinant virus. A high-titer viral stock of a pure recombinant virus was generated through amplification in suspension cultured Sf9 cells.

DCT activity was detected in transfected Sf9 cells one day after inoculation of DCT recombinant baculovirus and reached its peak activity four days after viral infection. Sf9 cells were cultured in TNM-FH medium containing 10% fetal bovine serum and harvested 4 days after inoculation of DCT recombinant virus by centrifugation (800 *g* for 15 min at 4°C). Cell pellets were stored at -80°C until use.

*Dopachrome Tautomerase Activity Assay*

The preparation of fresh L-dopachrome and assay of DCT activity were according to the methods of Aroca et al. [15]. Briefly, an equal volume of 4 mM L-DOPA was mixed with 8 mM sodium periodate. Dopachrome activity was assessed visually by the disappearance of dopachrome, which is bright red, or by the decrease in absorbance at 475 nm. Dopachrome has a molar extinction coefficient of 3,700 $M^{-1}$ $cm^{-1}$. Sf9 insect cells transfected with baculovirus encoding an unrelated protein was used as a control to

determine that there was no background DCT activity in the expression system (data not shown).

*DCT Purification*

Harvested Sf9 cells (12g wet weight) were solubilized in 20 mM sodium phosphate (pH 6.8) with 1 mM PMSF. After sonication and incubation on ice for one hour, cell lysates were centrifuged for 45 min at 35,000 *g* at 4°C. The pellet was re-extracted in the same manner and the supernatants were combined to a total volume of 250 mL. Ammonium sulfate (49.5 g) was added to the crude cell extract to make the final concentration 1.5 M and the sample was loaded onto 20 mL Octyl Sepharose column (15 x 170 mm) at a flow rate of 1.5 ml $min^{-1}$ in a 4$^{o}$C cold room. After washing with 3 column volumes of 1.5 M ammonium sulfate, protein was eluted with a linear gradient of ammonium sulfate (1.5 - 0 M) prepared in 50 mM sodium phosphate, pH 6.8. DCT active fractions were combined and immediately dialyzed against 20 mM sodium phosphate (pH 7.5) with 5% glycerol at 4$^{o}$C.

A hydroxyapatite column was packed using 20-µm particle CHT ceramic hydroxyapatite (Bio-Rad) with a bed volume of 5 mL (1.0 x 6.4 ml). The column was washed with 50 ml of 400 mM sodium phosphate (pH 7.5) and then equilibrated with 20 mM sodium phosphate (pH 7.5) with 5% glycerol. The dialyzed DCT active fractions from Octyl Sepharose chromatography were applied to the hydroxyapatite column at a flow rate of 0.8 ml $min^{-1}$. The recombinant DCT did not bind to hydroxyapatite under the applied conditions; the flow through was collected and then immediately applied to Mono Q.

A Mono Q column (8 mL, 10 x 100 mm) was equilibrated with 20 mM sodium phosphate (pH 7.5) and the hydroxyapatite flow through was applied to the column. Proteins were eluted by a linear NaCl gradient (0 - 400 mM) made up in 20 mM sodium phosphate (pH 7.5) with 5% glycerol.

DCT active fractions were combined and concentrated using a membrane concentrator with a molecular weight cutoff of 30,000. During concentration, the buffer was exchanged with sodium phosphate (pH 6.8) with 150 mM NaCl and 5% glycerol and the DCT active sample was loaded onto a Superose 6 gel filtration column (24 mL, 10 x 300 mm) at a flow rate of 0.2 mL $min^{-1}$. DCT active fractions were collected and concentrated again using the membrane concentrator. DCT was stored at -20$^{o}$C in 20 mM sodium phosphate (pH 6.8) with 5% glycerol.

*SDS-PAGE*

12% polyacrylamide gels were used for SDS-PAGE separations. Protein samples were heated to 95$^{o}$C in loading buffer containing DTT. Samples were loaded and run at a current of 15 mA. Gels were stained with Coomassie Blue and destained using 40% methanol containing 7% acetic acid.

*In-Gel Digestion of DCT*

DCT, separated by SDS-PAGE, was cut into 1 mm cubes and transferred to a low retention microcentrifuge tube. The gel cubes were extensively washed and destained using a washing buffer containing 25 mM $NH_4HCO_3$ and 50% acetonitrile (pH 8.0). Next, the gel pieces were dehydrated using 100% acetonitrile, followed by DTT (35 mM)

reduction and iodoacetamide alkylation (80 mM). Before digestion with trypsin, the gel cubes were washed using the same washing buffer and dried under vacuum in a Speed Vac. DCT was digested with 1 µg / mL trypsin for 16 hours at 37°C. Peptides were extracted from the gel pieces with 0.1% TFA and desalted using ZipTip $C_{18}$.

*PNGase F Deglycosylation*

Glycoamidase PNGase F was produced according to the methods of Loo et al. (see section A.1 of the appendix) [16]. Recombinant His-tagged PNGaseF from *Flavobacterium meningosepticum* was overexpressed in BL21(DE3) *E. coli* and purified with a Ni-NTA column. Purified DCT (0.25 mg) was digested with 0.1 mg PNGase F (0.1 mg) for 48 hours at 37°C in a reaction volume of 0.5 mL. After deglycosylation, the sample was separated by SDS-PAGE and processed for in-gel digestion in the same manner as the glycosylated DCT.

*MALDI-TOF/TOF Analysis*

The MALDI-TOF/TOF analysis of DCT tryptic peptides was carried out by the Virginia Tech Mass Spectrometry Incubator (http://www.mass.biochem.vt.edu/). Approximately 1 µL of each desalted sample was deposited onto a dried matrix spot on a MALDI target plate. The matrix spot was 1 µL of a 4 mg/mL α-cyano-hydroxycinnamic acid solution in 40% acetonitrile, 60% water supplemented with 0.5% formic acid and 20 mM ammonium dihydrogen citrate. MS data were acquired using an Applied Biosystems 4800 MALDI TOF/TOF operated in positive ion reflectron mode for m/z range 800 to 4000. MS/MS data were then collected utilizing the positive ion MS/MS 1kV mode

(without the use of a CID gas) for the predominant peaks observed in the MS spectrum. Typically, data for 500 to 1000 laser shots (or more if needed for adequate signal to noise) were collected and averaged for each spectrum. DCT peptides were identified by manual *de novo* sequencing of peptides tandem TOF/TOF spectra.

## 2.4 Results

*DCT Purification*

Although the soluble protein sample from transfected insect cells displayed DCT activity, no apparent protein band corresponding to DCT was observed when the crude supernatant was analyzed by SDS-PAGE. A three-step procedure ending with gel filtration chromatography gave DCT as the major protein band in the collected fraction and displayed activity toward dopachrome (Figure 2.1).

DCT eluted from Octyl-Sepharose at approximately 750 mM ammonium sulfate Although DCT did not bind to the hydroxyapatite column under the applied conditions (20 mM phosphate buffer, pH 6.8, containing 5% glycerol), approximately 50% of the excess proteins were retained and thereby eliminated by the hydroxyapatite column. This allowed for the separation of many problematic proteins that co-elute with DCT from anion exchange and hydrophic interaction chromatography. The hydroxyapatite flow through was then passed through a Mono-Q column (GE Health) and DCT activity eluted at 100-150 mM NaCl. When applied to a Superose 6 gel filtration column, DCT behaved as a protein with a relative molecular weight of 56,000 Da, suggesting that the protein was present as a monomer in the applied buffer conditions during chromatography.

Glycerol was immediately included after separation by Octyl-Sepharose to increase the stability of the enzyme. The purified recombinant DCT retained its activity after 6 months of storage in 25% glycerol at -20$^{o}$C.

*MALDI-TOF/TOF Analysis*

DCT in-gel digestion and subsequent analysis of its tryptic peptides by tandem mass spectrometry resulted in the identification of a number of interesting peptide ions (Table 2.1, Figure 2.2). Due to the presence of many complex and modified peptides, only ions with clear MS/MS spectra were reported. DCT contains many cysteine residues, which were all found to contain carboxyamidomethyl (CAM) modification after iodoacetamide treatment. A CAM alkylated histidine residue was also found upon MS/MS analysis of peptide ion *m/z* 1925.91 (AIDFSHQGPAFVTWHR). Trypsin digestion also generated an unexpected peptide ion, *m/z* 2721.34, which was verified as SAANDPVFVVLHSFTDAIFDEWLK.

**Table 2.1** Identification and PTMs of DCT peptides. All peptides were confirmed by manual analysis of tandem MS spectra.
* Peptide ion m/z 1249.86 was not seen in the MALDI-TOF/TOF analysis, but was seen using Q-TOF. This method is described by Li et al. [17].

| Observed mass (m/z) | Deduced mass (m/z) | Start | End | Sequence |
|---|---|---|---|---|
| 1249.86* | 1249.63 | 28 | 38 | VCMTLDGVLNK ($C^{29}$-CAM) |
| 2277.00 | 2276.99 | 39 | 58 | ECCPPLGPEATNICGFLEGR ($C^{40}$, $C^{41}$ and $C^{52}$- CAM) |
| 1343.59 | 1343.58 | 79 | 88 | NQDDREQWPR |
| 1209.49 | 1209.48 | 111 | 120 | FGWTGPDCNR |
| 1168.62 | 1168.58 | 129 | 138 | NIHSLTAQER |
| 1216.68 | 1216.67 | 195 | 205 | DTLLGPGRPYK |
| 1868.91 | 1868.90 | 206 | 221 | AIDFSHQGPAFVTWHR |
| 1925.91 | 1925.90 | 206 | 221 | AIDFSHQGPAFVTWHR ($H^{211}$-CAM) |
| 1925.83 | | | | |
| 1186.57 | 1186.57 | 221 | 229 | RYHLLWLER $R^{229}$ -99.08 |
| 1129.60 | 1129.59 | 222 | 229 | YHLLWLER |
| 1722.68 | 1722.74 | 252 | 266 | NECDVCTDELLGAAR ($C^{254}$ and $C^{257}$-CAM) |
| 1868.84 | 1868.79 | 252 | 266 | NECDVCTDELLGAAR ($N^{252}$-Fuc, $C^{254}$ and $C^{257}$-CAM |
| 2019.76 | 2019.76 | 279 | 294 | FSTWEIVCDSLDDYNR ($C^{286}$-CAM) |
| 1496.65 | 1496.64 | 296 | 308 | VTLCDGTYEGLLR ($C^{299}$-CAM) |
| 1824.82 | 1824.82 | 334 | 348 | FDSPPFFQDSTFSFR $N^{300}$ deamidated after PNGase F treatment |
| 2026.90 | 2026.91 | 334 | 348 | FDSPPFFQNSTFSFR ($N^{342}$-HexNAc) $N^{342}$ deamidated after PNGase F treatment |
| 2700.06 | 2700.16 | 334 | 348 | FDSPPFFQNSTFSFR ($N^{342}$-$Hex_2$-$HexNAc_2$-Fuc) |
| 2721.34 | 2721.33 | 385 | 408 | SAANDPVFVVLHSFTDAIFDEWLK |
| 2116.89 | 2116.88 | 410 | 428 | NNPSTDAWPQELAPIGHNR |

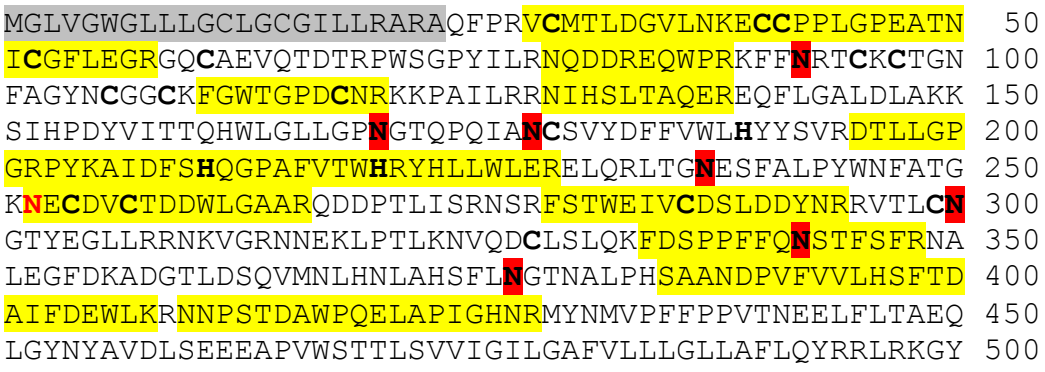


**Figure 2.2** Annotated sequence of the truncated DCT recombinant protein expressed in this study. Identified peptides are highlighted in yellow, potential *N*-glycosylation sites are highlighted in red, the putative signal peptide is highlighted in grey, cysteine residues and conserved metal binding histidine residues are in bold.

Peptide ions *m/z* 2700.06, 2862.10 and 3008.15 were separated by an interval of 162 (hexose) and 146 (fucose) (Figure 2.3), which indicated multiple glycoforms of a glycosylated peptide. Examination of the MS/MS spectra of all 3 ions confirmed their identity as *N*-glycosylated $^{334}$FDSPPFFQ**N**STFSFR$^{348}$ (Figure 2.4 and 2.5, spectra of *m/z* 2862.10 is provided in the appendix). This monoisotopic mass of the non-glycosylated $(M+H^+)^+$ peptide ion is 1823.8; therefore, peptide ion *m/z* 2700.06 contains an additional 876 Da, peptide ion *m/z* 2862.10 contains an additional 1038 Da, and peptide ion *m/z* 3008.15 contains an additional 1184 Da. This 876 Da corresponds to the oligosaccharide structure "$Man_2$-GlcNAc(Fuc)GlcNAc-," 1038 Da corresponds to "$Man_3$-GlcNAc(Fuc)GlcNAc-," and 1184 corresponds to "$Man_3$-GlcNAc($Fuc_2$)GlcNAc-." The addition of 876, 1038 and 1184 mass units were also discovered in our detailed analysis of *N*-glycosylation in mosquito dopachrome conversion enzyme [17]. Later, another peptide ion (*m/z* 2026.90) was confirmed as the same peptide ($^{334}$FDSPPFFQ**N**STFSFR$^{348}$) with the addition of a single *N*-acetylated hexose. Furthermore, all of the glycosylated $^{334}$FDSPPFFQ**N**STFSFR$^{348}$ peptides were no longer seen in the PNGase F digested sample; however, the deamidated version ($^{334}$FDSPPFFQ**D**STFSFR$^{348)}$ was observed (*m/z* 1824.72), which confirms the identity of this *N*-glycosylation site. This particular *N*-glycosylation sequon is conserved in tyrosinase-related protein 1, but not in tyrosinase [18].

Another potentially *N*-glycosylated peptide ion, *m/z* 1868.84, was identified as $^{252}$NECDVCTDELLGAAR with the addition of 146 Da (Figure 2.6). In this case, the additional 146 Da was attached to a nonstandard NXC *N*-glycosylation sequon. The

observation of 146 Da to $N^{252}$ is suggestive of *N*-fucosylation. The same peptide without any modification was also identified as peptide ion *m/z* 1722.68 (Figure 2.6).

The deamidated potential glycopeptide *m/z* 1496.65 VTLCDGTYEGLLR was identified in the PNGase F digested sample (Figure 2.7), however its glycosylated counterpart was not identified in the native sample. The presence of peptide ion *m/z* 1496.65 only in the deglycosylated sample is a strong indication that this particular peptide is *N*-glycosylated as well. This method to identify glycosylation sites by searching for deamidated peptides after PNGase F treatment has been documented with the human protein nephrin [19].

The peptide ion *m/z* 2116.89 NNPSTDAWPQELAPIGHNR from the PNGase F treated sample was almost considered a deamidated NDPSTDAWPQELAPIGHNR because these two sequences would yield the same $y_1 - y_{17}$ ions. However, the NPS sequon is rarely glycosylated because proline disrupts the peptide backbone, and the same ion *m/z* 2117 was also found in the untreated sample. Our results confirm that the $N^{411}$ is not glycosylated (Figure 2.8).

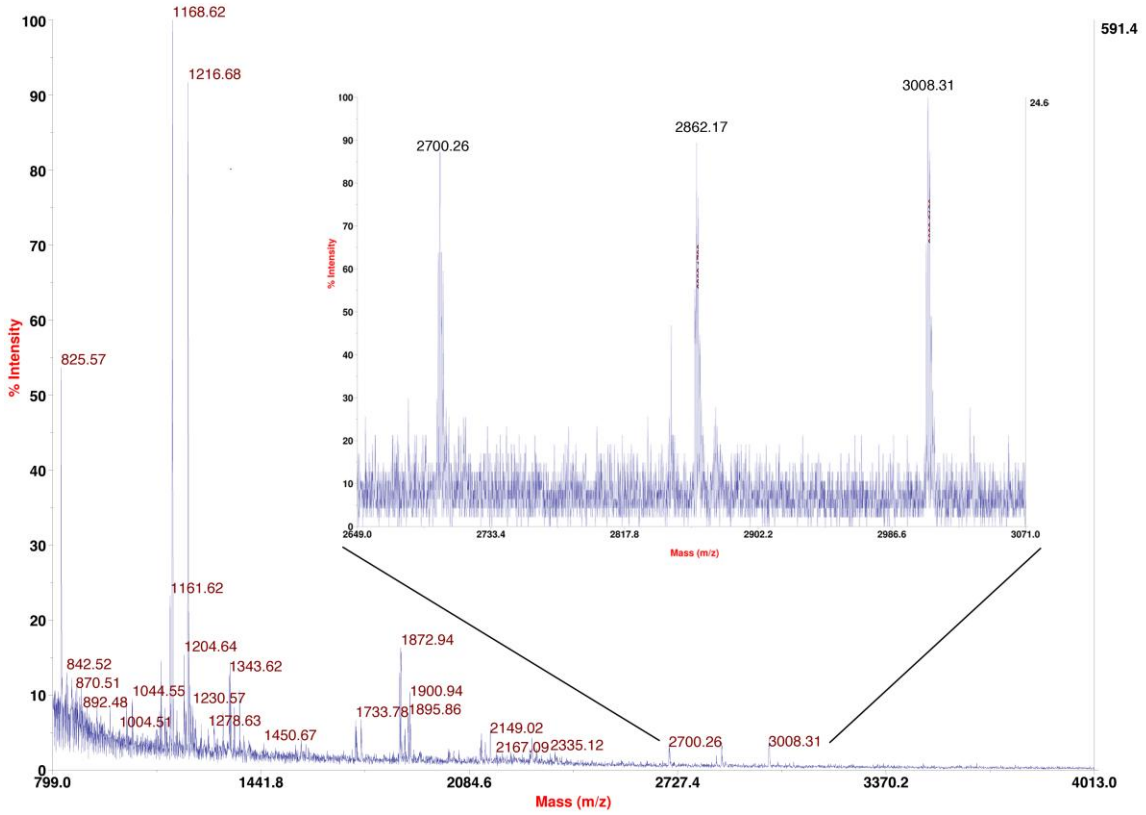


**Figure 2.3** MALDI-TOF peptide map of a DCT tryptic digest. The inset shows a close-up of the glycosylated peptide ions *m/z* 2700.26, 2862.17 and 3008.31.

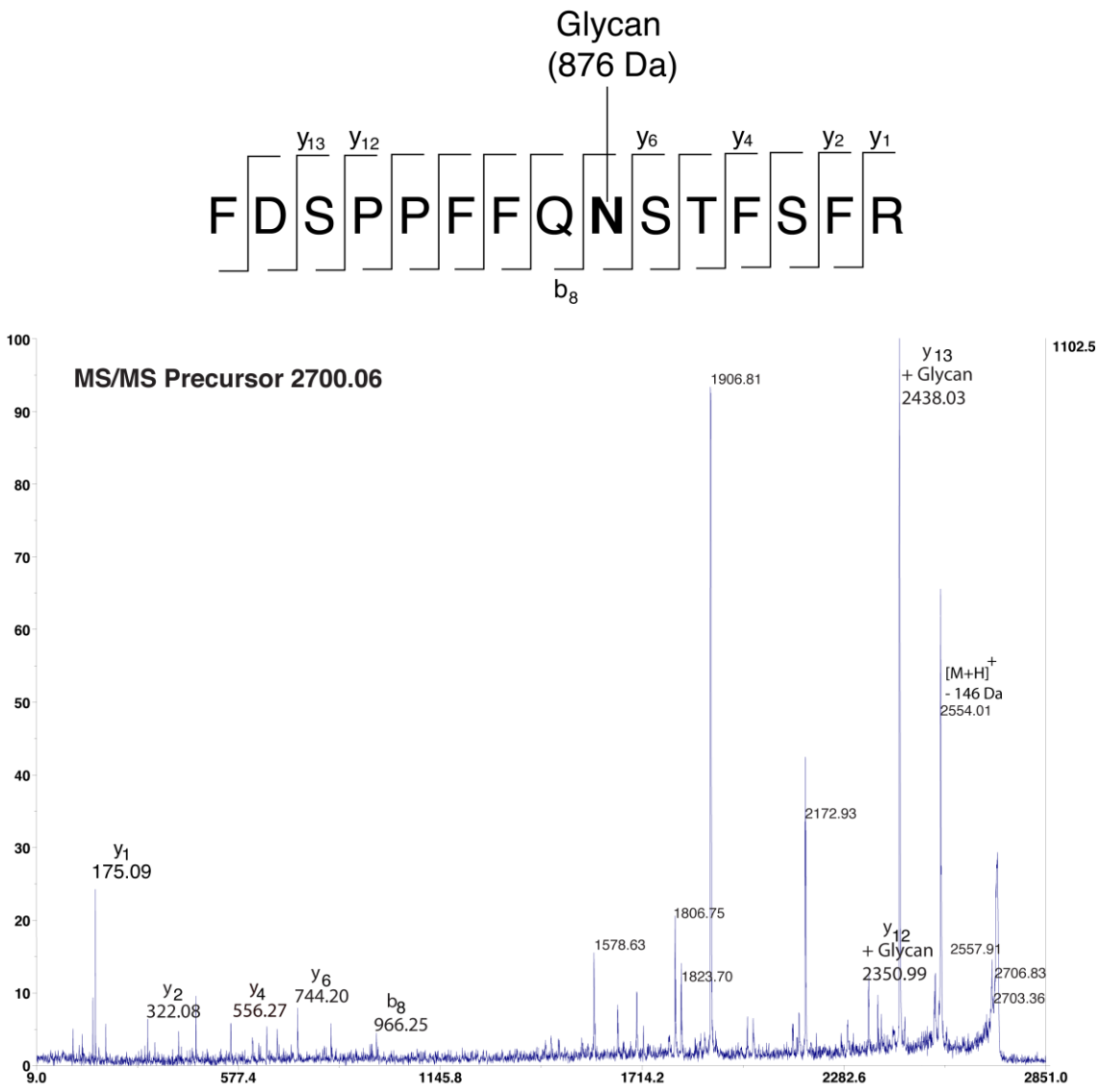


**Figure 2.4** MALDI-TOF/TOF spectra of *N*-glycosylated DCT peptide *m/z* 2700.06 (FDSPPFFQ**N**STFSFR).

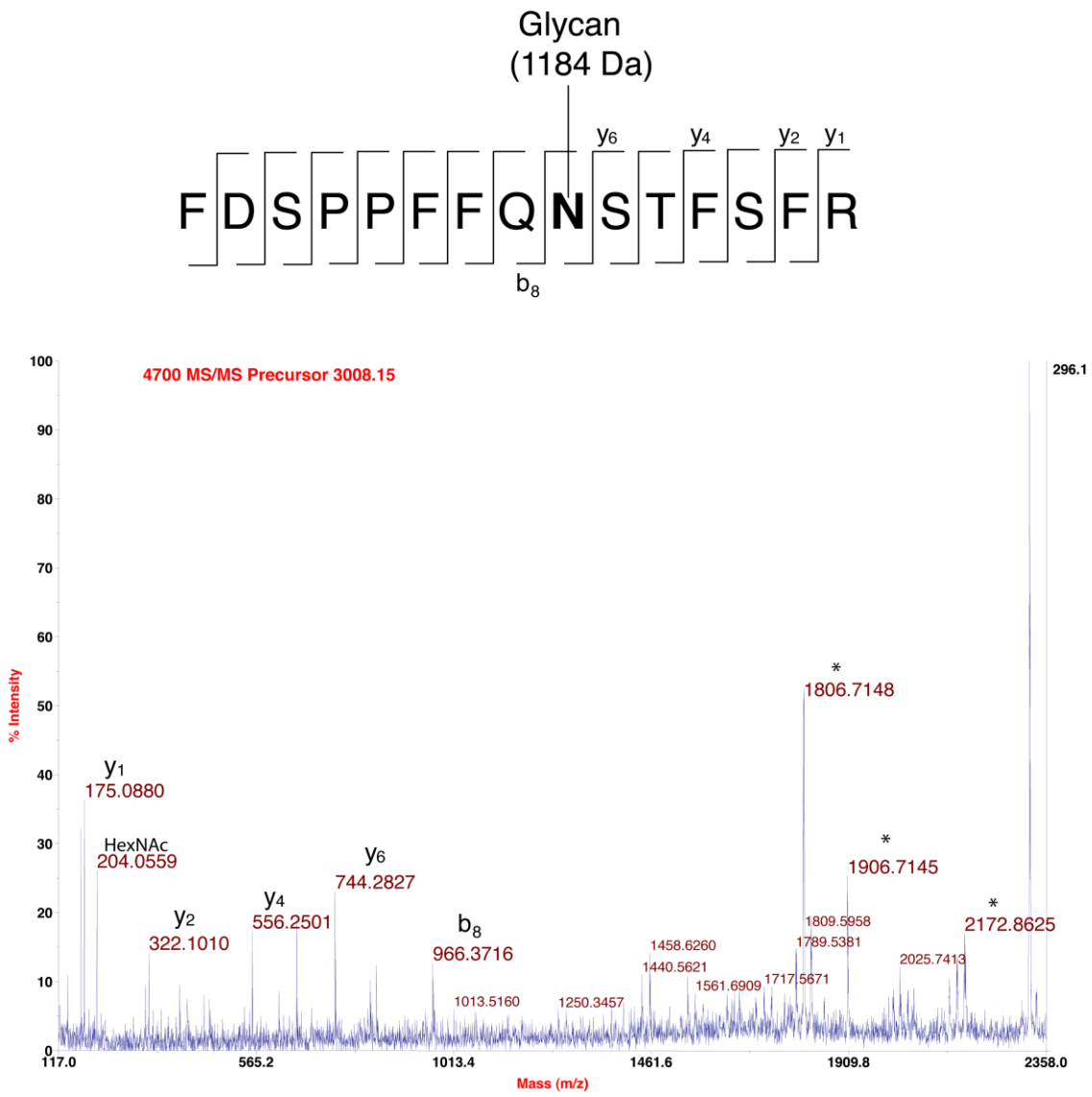


**Figure 2.5** MALDI-TOF/TOF spectra of *N*-glycosylated DCT peptide *m/z* 3008.15 (FDSPPFFQ**N**STFSFR). Ions indicated with * also appear as dominant ions in Figure 2.3, however due to complex fragmentation of glycopeptides with MALDI-TOF/TOF remain elusive.

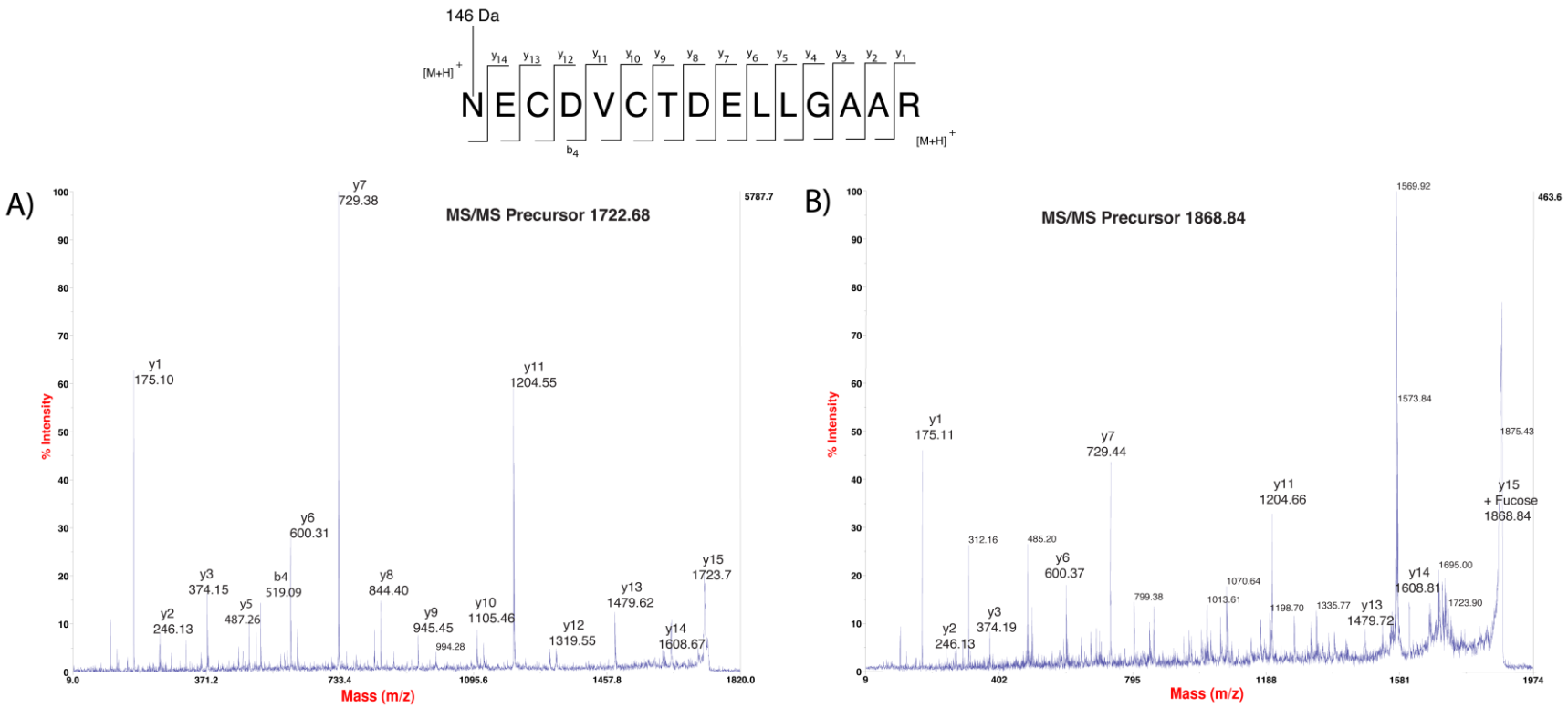


**Figure 2.6** MALDI-TOF/TOF spectra of the DCT peptide NECDVCTDELLGAAR, A) with addition of 146 Da, and B) with no modification

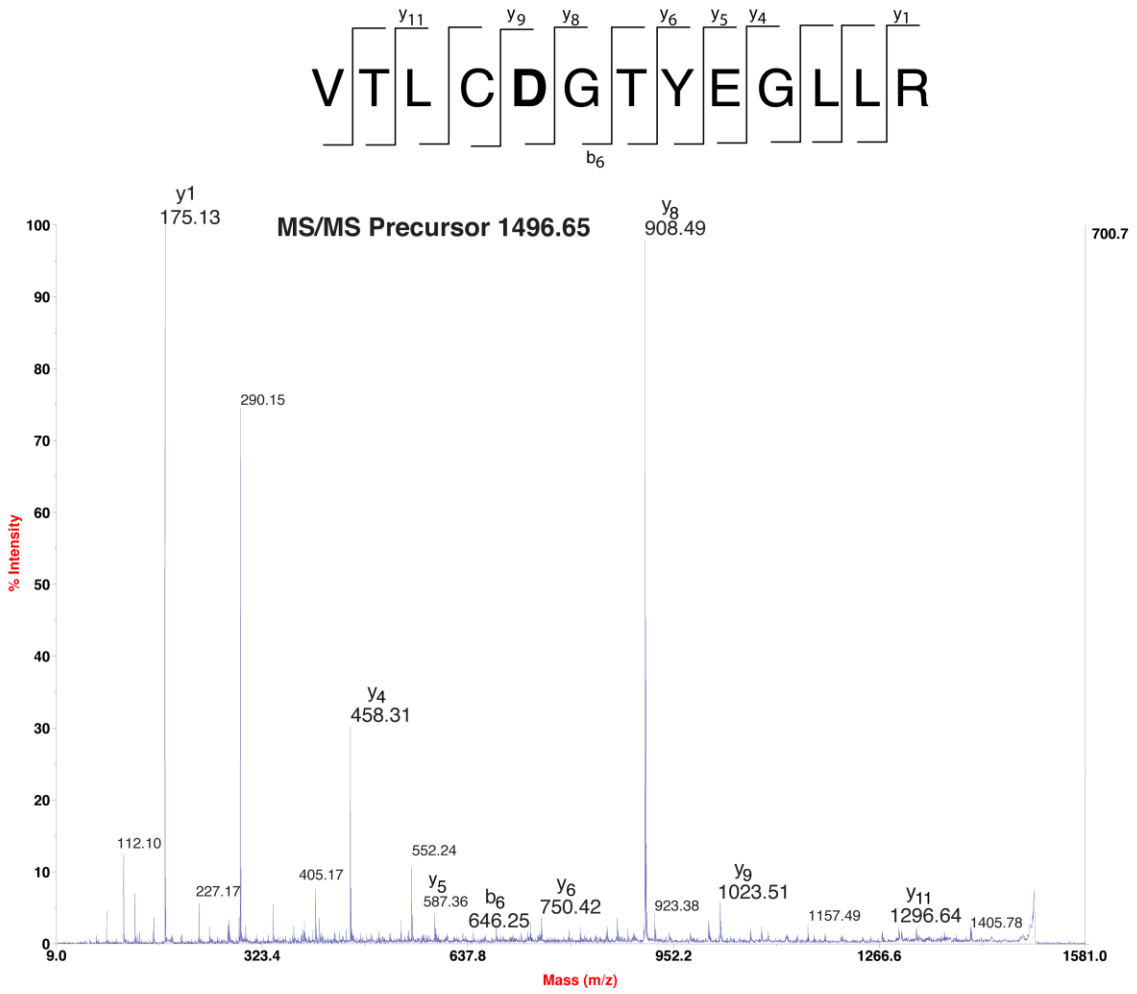


**Figure 2.7** MALDI-TOF/TOF spectra of the PNGase F deglycosylated DCT peptide $^{296}$VTLC**D**GTYEGLLR$^{308}$. Note: cysteine is modified with carboxyamidomethyl (CAM).

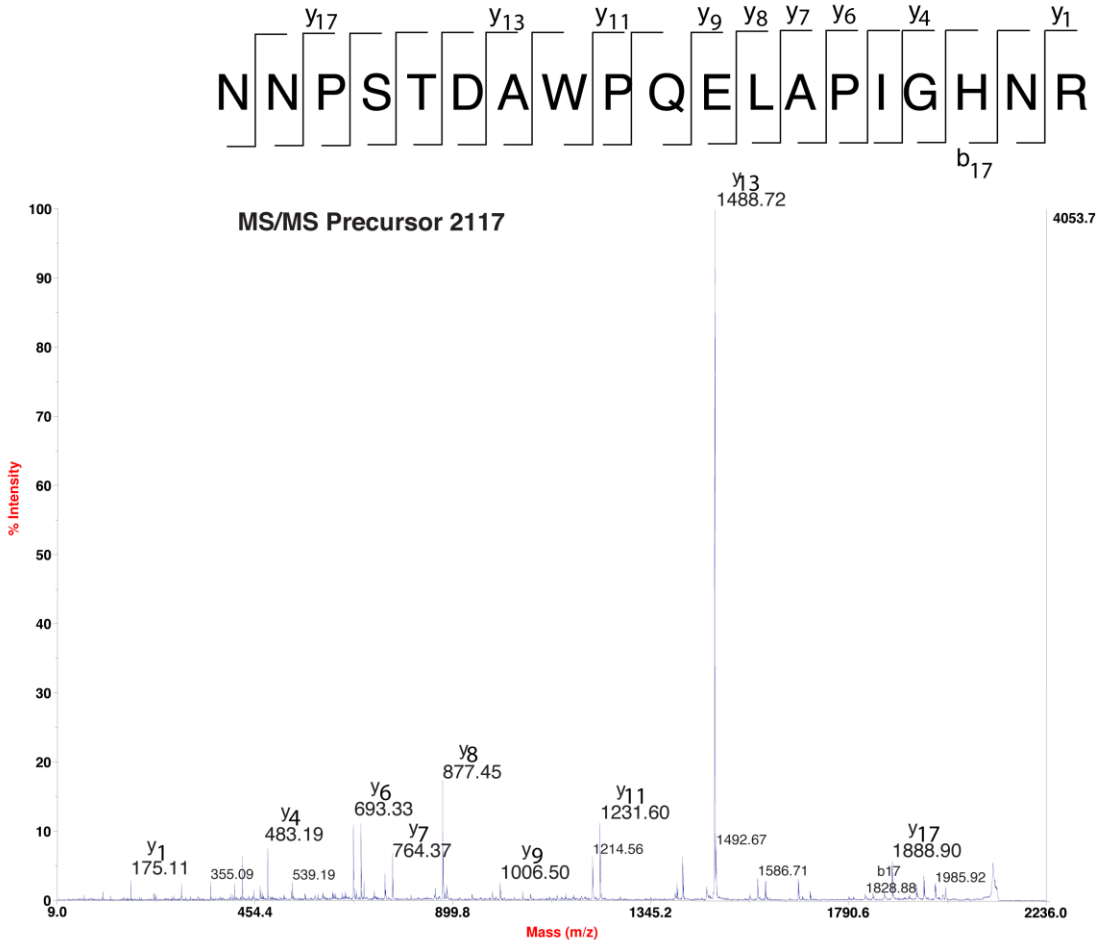


**Figure 2.8** MALDI-TOF/TOF spectra of the non-glycosylated DCT peptide NNPSTDAWPQELAPIGHNR.

## 2.5 Discussion

There has been considerable interest in the structure and function of DCT due to its involvement in the resistance of melanoma cell lines to radiation and chemotherapy. Furthermore, DCT is processed through the trans-Golgi network, where it may end up in the melanosome or as melanoma surface antigen [11]. Although it is well known that the trafficking of DCT is heavily reliant upon *N*-glycosylation, no direct investigations into the exact sites of glycosylation have been previously carried out [14].

The major obstacle in the structural characterization of DCT has proven to be the ability to attain purified, functional protein. Purification of native DCT from melanoma is very problematic due to the hydrophobic transmembrane domain and interactions with melanin. The use of a eukaryotic expression system to express recombinant DCT without the membrane domain has solved this problem and allowed for the production of soluble, active and glycosylated DCT.

Although the complexity of *N*-glycosylation structures varies between mammalian and insect systems, in most cases the same sites of a particular protein are glycosylated in both insect and mammalian cells [20-23]. Glycoproteins produced in insect cell expression systems contain lower complexity glycan structures than mammalian or yeast systems, which results in a more homogeneous protein [21]. Less complex and more homogeneous glycan structures, in addition to the increased solubility of recombinant DCT, will increase the future potential for obtaining quality protein crystals.

DCT is one of only three mammalian proteins that are currently known to directly participate in melanin biosynthesis. These three proteins, DCT, tyrosinase and tyrosinase-

related protein 1 all share approximately 40% sequence identity. Like DCT, tyrosinase and tyrosinase-related protein 1 are both glycoproteins that are processed as melanoma antigens. *N*-glycosylation has recently been reported to enhance the presentation of a tyrosinase MHC Class I-restricted epitope [24]. Because of the high level of similarity between these three proteins, the work described in this manuscript should also offer insight into the purification and *N*-glycosylation of tyrosinase and tyrosinase-related protein 1.

**Acknowledgements**

The MALDI-TOF/TOF analysis of DCT was carried out by Dr. Keith Ray at the Virginia Tech Mass Spectrometry Incubator (VT-MSI). This work is supported by College of Agricultural Life Sciences, Virginia Tech and NIH grant AI 19769.

# LITERATURE CITED


1. Bernard, K., et al., *Functional proteomic analysis of melanoma progression.* Cancer Res, 2003. **63**(20): p. 6716-25.

2. Pawelek, J.M. and A.B. Lerner, *5,6-Dihydroxyindole is a melanin precursor showing potent cytotoxicity.* Nature, 1978. **276**(5688): p. 626-8.

3. Chu, W., et al., *Tyrosinase-related protein 2 as a mediator of melanoma specific resistance to cis-diamminedichloroplatinum(II): therapeutic implications.* Oncogene, 2000. **19**(3): p. 395-402.

4. Pak, B.J., et al., *TYRP2-mediated resistance to cis-diamminedichloroplatinum (II) in human melanoma cells is independent of tyrosinase and TYRP1 expression and melanin content.* Melanoma Res, 2000. **10**(5): p. 499-505.

5. Pak, B.J., et al., *Radiation resistance of human melanoma analysed by retroviral insertional mutagenesis reveals a possible role for dopachrome tautomerase.* Oncogene, 2004. **23**(1): p. 30-8.

6. Wang, R.F., et al., *Identification of TRP-2 as a human tumor antigen recognized by cytotoxic T lymphocytes.* J Exp Med, 1996. **184**(6): p. 2207-16.

7. Umansky, V., et al., *Melanoma-specific memory T cells are functionally active in Ret transgenic mice without macroscopic tumors.* Cancer Res, 2008. **68**(22): p. 9451-8.

8. Lu, X., et al., *Adoptive transfer of pTRP2-specific CTLs expanding by bead-based artificial antigen-presenting cells mediates anti-melanoma response.* Cancer Lett, 2008. **271**(1): p. 129-39.

9. Chi, A., et al., *Proteomic and bioinformatic characterization of the biogenesis and function of melanosomes.* J Proteome Res, 2006. **5**(11): p. 3135-44.

10. Tsukamoto, K., et al., *A second tyrosinase-related protein, TRP-2, is a melanogenic enzyme termed DOPAchrome tautomerase.* Embo J, 1992. **11**(2): p. 519-26.

11. Negroiu, G., R.A. Dwek, and S.M. Petrescu, *The inhibition of early N-glycan processing targets TRP-2 to degradation in B16 melanoma cells.* J Biol Chem, 2003. **278**(29): p. 27035-42.

12. Toyofuku, K., et al., *Oculocutaneous albinism types 1 and 3 are ER retention diseases: mutation of tyrosinase or Tyrp1 can affect the processing of both mutant and wild-type proteins.* Faseb J, 2001. **15**(12): p. 2149-61.

13. Wang, N., R. Daniels, and D.N. Hebert, *The cotranslational maturation of the type I membrane glycoprotein tyrosinase: the heat shock protein 70 system hands off to the lectin-based chaperone system.* Mol Biol Cell, 2005. **16**(8): p. 3740-52.

14. Gupta, G., et al., *Probing into the role of conserved N-glycosylation sites in the Tyrosinase glycoprotein family.* Glycoconj J, 2008.

15. Aroca, P., et al., *A new spectrophotometric assay for dopachrome tautomerase.* J Biochem Biophys Methods, 1990. **21**(1): p. 35-46.

16. Loo, T., et al., *Using secretion to solve a solubility problem: high-yield expression in Escherichia coli and purification of the bacterial glycoamidase PNGase F.* Protein Expr Purif, 2002. **24**(1): p. 90-8.

17. Li, J.S., et al., *Proteomic analysis of N-glycosylation in mosquito dopachrome conversion enzyme.* Proteomics, 2007. **7**(15): p. 2557-2569.

18. Branza-Nichita, N., et al., *N-glycosylation processing and glycoprotein folding-lessons from the tyrosinase-related proteins.* Chem Rev, 2000. **100**(12): p. 4697-712.

19. Khoshnoodi, J., et al., *Identification of N-linked glycosylation sites in human nephrin using mass spectrometry.* J Mass Spectrom, 2007. **42**(3): p. 370-9.

20. James, D.C., et al., *N-glycosylation of recombinant human interferon-gamma produced in different animal expression systems.* Biotechnology (N Y), 1995. **13**(6): p. 592-6.

21. Altmann, F., et al., *Insect cells as hosts for the expression of recombinant glycoproteins.* Glycoconj J, 1999. **16**(2): p. 109-23.

22. Yeh, J.C., et al., *Site-specific N-glycosylation and oligosaccharide structures of recombinant HIV-1 gp120 derived from a baculovirus expression system.* Biochemistry, 1993. **32**(41): p. 11087-99.

23. Lopez, M., et al., *Microheterogeneity of the oligosaccharides carried by the recombinant bovine lactoferrin expressed in Mamestra brassicae cells.* Glycobiology, 1997. **7**(5): p. 635-51.

24. Ostankovitch, M., et al., *N-glycosylation enhances presentation of a MHC class I-restricted epitope from tyrosinase.* J Immunol, 2009. **182**(8): p. 4830-5.

# III

# DOPACHROME CONVERSION ENZYME

## 3.1 Abstract

A novel dopachrome conversion enzyme (DCE) is present in insects and involved in their melanization pathway. DCE shares no sequence homology with any noninsect species from bacteria to humans. Several DCE sequences have been available, but enzyme structure and catalytic mechanism are unclear. This study concerns DCE PTMs, especially glycosylation. A mosquito DCE was purified and its monosaccharide composition, *N*-glycosylation site, and oligosaccharide structures were determined. Results showed that *N*-acetyl D-glucosamine and D-mannose are the major monosaccharides and L-fucose, D-xylose, and D-arabinose are the minor ones in mosquito DCE. Glycosylation site and oligosaccharide structures were elucidated from MS and MS/MS spectra of trypsin-digested DCE glycopeptides. A single *N*-glycosylation site ($Asn^{285}$-Glu-Thr) was identified in DCE and was proven to be fully glycosylated. $Man_3GlcNAc_2$, $Man_3(Fuc)_{1-2}GlcNAc_2$, and their truncated structures were the dominant oligosaccharides. In addition, high hexose (likely mannose) type structures ($Hex_{4-7}(Fuc)GlcNAc_2$) were also identified. Removal of DCE N-oligosaccharides with PNGase F decreased its activity and thermal stability. However, partial DCE deglycosylation with α-mannosidase or α-fucosidase somewhat stimulated its activity and improved its thermal stability. During mass spectrometric analysis of DCE glycopeptides, their CID patterns were highly intriguing, in that some glycopeptides underwent both C-terminal rearrangement and formation of dimeric structures during CID. Results of this study provide an interesting example in terms of potential complexity of the glycopeptide CID fragmentation pattern.

## 3.2 Introduction

An enzyme from *Aedes aegypti* was recently determined to catalyze a decarboxylative structural rearrangement of dopachrome to 5,6-dihydroxyindole in the melanization pathway [1]. Based on its function, this protein was termed dopachrome conversion enzyme (DCE). Sequence comparison determined that mosquito DCE belongs to a mosquito yellow gene family. The yellow gene family is insect-specific; members of the yellow gene family in different insect species have sequence homology, but they share no similarity with proteins from any non-insect species. Among the yellow genes, Drosophila yellow-y gene has attracted considerable attention, because loss of the yellow-y function due to mutation prevents normal pigmentation in Drosophila cuticle [2]. Recently, there were also extensive studies concerning the molecular regulation of the yellow gene [3–5]. Although a number of potential functions have been suggested for the Drosophila yellow-y gene in flybase (http://flybase.org/reports/FBgn0004034.html), the exact chemical mechanism by which the yellow-y protein promotes normal Drosophila pigmentation is unclear. To achieve a comprehensive understanding of the structure/function relationship of DCE and yellow-y as well as other members of the insect yellow gene family, it is necessary to study them at the protein level.

Our current study demonstrates that DCE is a glycoprotein. In this study, we purified DCE from two mosquito species and determined their *N*-glycosylation site and oligosaccharide structures by direct analysis of glycopeptides using LC-ESI MS/MS. Comparison of DCE sequences with the deduced sequences of other yellow genes from several insect species indicated that a similar *N*-glycosylation site is present in a number of yellow family proteins, suggesting that there might be similar glycosylation pathway

for most of the yellow family proteins in insects. Results of this study provide a basis for understanding the structure/function relationship of the insect yellow family proteins.

### 3.2 Materials and methods

*Materials*

Monosaccharide standards, TFA (protein sequencing grade), 2-aminobenzoic acid, sodium cyanoborohydride, *o*-phenylenediamine, peptide *N*-glycosidase (PNGase F), Jack Bean α-mannosidase, and bovine kidney α-fucosidase were purchased from Sigma (St. Louis, MO, USA). Modified trypsin was from Promega (Madison, WI, USA). PVDF membrane was from Amersham Biosciences (Piscataway, NJ, USA). Centrifugal filters (30,000 MWcut-off) and ZipTip C18 were from Millipore (Bedford, MA, USA). Dialysis membrane tubing (12,000 MW cut-off) was from Spectrum Laboratory (Ft. Lauderdale, FL, USA). Fresh Mini-Q water was used to prepare all buffers. Other laboratory chemicals were purchased from Sigma or Fisher (Fairlawn, NJ, USA).

*DCE Purification*

All operations were performed at 0–4$^{o}$C. Fifty grams (wet weight) of 6-day-old *A. aegypti* larvae were homogenized in 100 mM sodium phosphate buffer (pH 6.5) containing 1 mM PMSF, 1 mM phenylthiocarbamide, 1 mM DTT, and 2 mM EDTA. Homogenates were centrifuged at 25,000 x *g* for 20 min. Supernatant was collected and brought up to 60% ammonium sulfate saturation. The precipitates were then separated from supernatant by centrifugation (10,000 x *g*, 20 min) and resuspended into a minimal

volume of 0.5 M ammonium sulfate in 50 mM phosphate buffer (pH 6.5). After centrifugation at 10,000 x *g* for 20 min, the solution was applied to a phenyl Sepharose column (50 mL, Amersham Biosciences), and eluted using a linear gradient of ammonium sulfate (1.0–0 M) in 10 mM phosphate buffer (pH 6.5). The fractions with DCE activity were collected into dialysis tubes and dialyzed against 10 mM phosphate buffer (pH 6.5). The dialyzed active fraction was applied to a DEAE Sepharose column (20 mL, Amersham Biosciences), and proteins were eluted using a linear NaCl gradient (0–500 mM) prepared in 10 mM phosphate buffer (pH 6.5). DCE fractions were concentrated using membrane filters and further purified sequentially using the following columns, including phenyl-Superose (5 mL), Mono-Q (5 mL, Amersham Biosciences), CHT5-I (hydroxyapatite) (5 mL, BioRad, Hercules, CA, USA), and Superose (30 mL, Amersham Biosciences). Finally, the purity of the DCE fraction was examined by 12% SDS-PAGE. Protein concentration was determined at 280 nm using a U2800A spectrophotometer (Hitachi, Tokyo, Japan). To compare DCE N-glycosylation from different mosquito species, a DCE from *Armigeres subalbatus* larvae was also purified as those described for the purification of the *A. aegypti* DCE.

*DCE Activity Assay*

DCE activity was measured by determining the decrease in dopachrome absorbance at 475 nm ($\varepsilon$ = 3245 $M^{-1}$/cm) using a U2800A spectrophotometer (Hitachi). Dopachrome was generated by mixing 0.5 mM L-DOPA in water with an equal volume of 1.0 mM sodium periodate ($NaIO_4$) in 20 mM phosphate buffer (pH 7.0) (the initial absorbance is 0.98–1.00 at room temperature.)

*Con A Affinity Chromatography*

An aliquot of purified DCE was loaded onto a Con A-Sepharose 4B column (0.5 mL) equilibrated with binding buffer containing 20 mM Tris and 0.5 M NaCl (pH 7.4). After washing with binding buffer, DCE was eluted by a linear α-D-methylmannoside gradient (0.05–0.5 M) prepared in the same buffer solution.

*Monosaccharide Analysis*

Monosaccharide determination was based on methods described by Weitzhandler *et al.* [6] and Anumula [7–9]. SDS-PAGE was performed with 12% polyacrylamide gel and 0.1% SDS [10]. After electrophoresis, protein bands were transferred directly to PVDF membranes using a Hoefer TE22 Mini Transfer Unit (Amersham Biosciences) at 400 mA for 6 h. The protein bands were cut, and put into 1.6 mL polypropylene vials with O-ring seal screw caps (Fisher).

For neutral and amino monosaccharide analysis, DCE on a PVDF membrane was hydrolyzed in 20% TFA at 100$^{o}$C for 6 h. The released monosaccharides were derivatized with 2-aminobenzoic acid and sodium cyanoborohydride [6, 7]. Determination of the derivatized monosaccharides was achieved through the use of a LaChrom D7000 HPLC system with fluorescence detection (Hitachi). HPLC conditions were as follows: $C_{18}$ column, 5 μm particle, 4.6 x 150 mm$^2$; fluorescence detection at Ex360 nm and Em425 nm; mobile phase A, 0.2% v/v 1-butylamine, 0.5% v/v phosphoric acid, and 1.0% v/v THF in water; mobile phase B, 50% ACN in mobile phase A; gradient profile, 5% B from 0 to 10 min, 5–12% B from 11 to 35 min, and 12–100% B from 36 to 40 min, 1

mL/min of flow rate; loading volume, 50 uL.

For sialic acid analysis, the DCE on PVDF was first hydrolyzed with 0.25 M sodium bisulfate at 80$^{o}$C for 20 min, and then derivatized with *o*-phenylenediamine at 80$^{o}$C for 40 min [8]. HPLC conditions were as follows: $C_{18}$ column, 5 mm particle, 4.6 x 150 mm; fluorescence detection at Ex 230 nm/Em 425 nm; gradient profile, 10% B from 0 to 20 min and 10–100% B from 21 to 25 min, 1 mL/min of flow rate; loading volume, 50 uL. The monosaccharide standards and blank were subjected to the same hydrolysis and derivatization processes, and analyzed by HPLC under identical conditions.

*In-gel Digestion*

DCE was electrophorezed by SDS-PAGE, stained with CBB and destained with 40% methanol containing 7% acetic acid. The DCE band was cut from the gel and transferred to a 0.6 mL siliconized microcentrifuge tube (Fisher). After DTT reduction and iodoacetamide alkylation, DCE was digested with 0.01 mg/mL trypsin in 50 mM Tris-HCl (pH 8.0) at 37$^{o}$C for 16–18 h. The peptide products were extracted from the gel using 50% ACN in 0.5% TFA combined with sonication. After evaporation in a Speed Vac, peptides were redissolved in 0.1% formic acid and cleaned-up with ZipTip C18 for subsequent LC-ESI MS/MS analysis.

*Capillary LC-ESI MS/MS*

The capillary LC-ESI MS/MS system consisted of a CapLC XE fitted with a NanoEase 75 mm $C_{18}$ column, an OPTI-PAK $C_{18}$ Trap column, and a Q-TOF micro™ mass spectrometer with a nanospray source (Waters Micromass, Manchester, UK).

Peptide separation was achieved by gradient elution with mobile phase A (5% ACN in 0.1% formic acid) and mobile phase B (90% ACN in 0.1% formic acid). The following gradient profile was applied: 5% B from 0 to 5 min, 5–40% B from 6 to 40 min, and 40–90% B from 40 to 65 min. The ESI/Q-TOF was operated in positive ion mode with a capillary voltage of 3719 V. For MS analysis, precursor ions were scanned from 400 to 1900 Da with a collision voltage of 10 V. The potential glycopeptides were screened by a precursor ion scan using *m*/*z* 163 and 204 as marker ions. During MS/MS analysis, fragmentation was performed with a collision voltage of 35 V and a scan of 50–1900 Da. Only precursor ions having a charge state of +2, +3, or +4 were extracted into the collision cell for dissociation.

*Protein Sequencing, Identification and Glycosylation Analysis*

The raw MS and MS/MS data were analyzed by Masslynx 4.0 (Waters Micromass). Protein was identified by Proteinlynx 2.1 (Waters Micromass), with peptide tolerance set at 0.5 Da and fragment tolerance at 0.2 Da. The glycosylation site and structures were elucidated through MS/MS fragmentation. The *Aedes aegypti* NCBI database was used to search for identified peptides.

*DCE Deglycosylation and Effect on DCE Activity and Stability*

*A. aegypti* DCE (10 mg) was incubated with individual glycosidases at 37$^{o}$C for 12 h: 100 U/mL PNGase F in 50 mM sodium phosphate buffer (pH 7.5) containing 0.5% Triton X-100; 50 U/mL α-mannosidase in 50 mM sodium acetate buffer (pH 5.5) containing 0.5% Triton X-100; 1 U/mL α-fucosidase in 50 mM sodium acetate buffer

(pH 5.5) containing 0.5% Triton X-100. Controls were incubated at identical conditions as the corresponding deglycosylation reactions in the absence of glycosidase. Kinetic parameters and thermal stability (at 45$^{o}$C) of the control and deglycosylated DCE samples were analyzed. $K_m$ and $V_{max}$ were determined by the Lineweaver–Burke plot (Sigma Plot). Aliquots of individual samples were also subjected to SDS-PAGE, in-gel digested with trypsin at 37$^{o}$C overnight, and then analyzed by LC-ESI MS/MS.

## 3.3 Results and Discussion

*DCE Purification*

After separation of DCE from extracted mosquito larval proteins by various chromatographic procedures, a DCE active fraction displayed as a single peak during gel filtration chromatography (Figure 3.1) and a single band during SDS-PAGE analysis (Figure 3.1, inset). The purified DCE showed extremely high activity to dopachrome and was highly stable in neutral buffer. During gel filtration chromatography, DCE behaved like a protein with a relative molecular weight of 55,600, suggesting that it is present as a monomer at the applied chromatographic conditions.

Purified DCE was retained by Con A column, and can be eluted with high concentrations of α-D-methylmannoside (Figure 3.2). This result suggest that DCE is a glycoprotein and its associated oligosaccharides contain high-mannose or paucimannose structures.

*Identification and Modifications of DCE*

The results of *de novo* sequencing of MS/MS data from the *A. aegypti* DCE active fraction matched *A. aegypti* DCE (accession no. AAG01014) in the NCBI nonredundant database, with 20 matched peptides (Table 3.1). Similarly, the spectral data of the purified *A. subalbatus* protein matched *A. subalbatus* DCE (accession no. AY960762) with 21 matched peptides. The sequences of matching peptides and possible post-translation modifications are listed in Table 3.1. In addition to glycosylation, there were several amino acid substitutions within C-terminal of DCE. Furthermore, propionamide modification of cysteine was observed from several peptide ions; this can be explained by exposure of the protein to acrylamide during SDS-PAGE, prior to in-gel digestion.

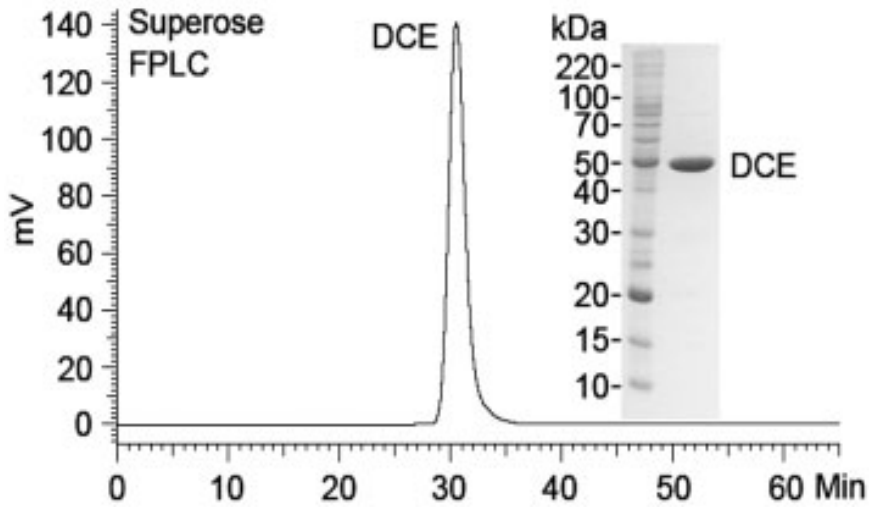


**Figure 3.1** Chromatogram and SDS-PAGE of purified DCE from *A. Aegypti* larvae homogenate.

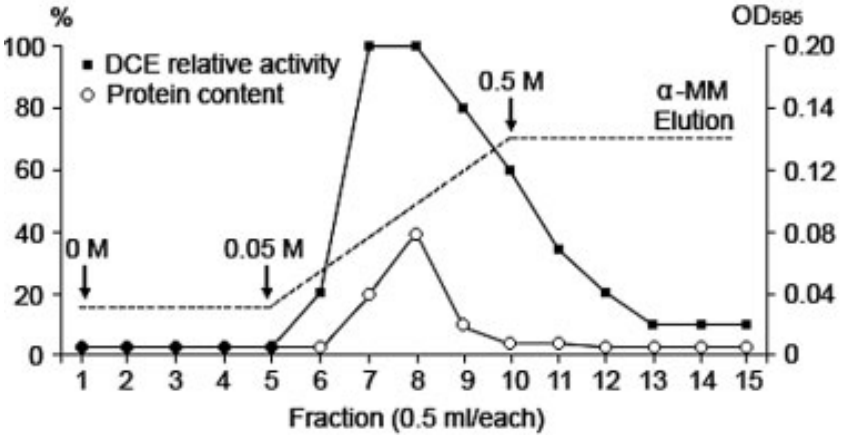


**Figure 3.2** Elution profile (activity and protein) of purified *A. aegypti* DCE from a Con A affinity column (0.5 mL). The elution buffer was 20 mM Tris-HCl (pH 7.4) containing 0.5 M NaCl and 0–0.5 M α-D-methylmannoside (α-MM).

**Table 3.1** Identification and PTMs of *A. aegypti* dopachrome conversion enzyme

| Observed mass (*m/z*)[a] | Deduced mass (*m/z*) | Start | End | Sequences and potential PTMs [b] |
|---|---|---|---|---|
| 2508.07 | 2508.38 | 1 | 22 | MLRLVFLCVVAFAALTVVSGQR |
| 2522.70 | 2522.40 | | | ($M^1$ = O, Acetyl $M^1$, $C^8$-CAM or $C^8$-PAM)[d] |
| 844.41 | 844.48 | 23 | 29 | QVEEVLK[c] |
| 3671.53 | 3671.82 | 30 | 62 | WQQVEFDVPASVLSAPDGYIPINNIPMSGVHYK ($M^{56}$ or $M^{56}$ = O)[d] |
| 3687.61 | 3687.82 | | | |
| 817.43 | 817.49 | 65 | 71 | VFVTVPR[c] |
| 4007.77 | 4008.12 | 74 | 108 | WGIPSTLNVVELEPPYP VTNPVLKPYP SFELNELR[c] |
| 999.39 | 999.48 | 109 | 117 | ADLQPDANR[c] |
| 1003.50 | 1003.60 | 118 | 125 | LVTVYRPR[c] |
| 3378.32 | 3379.72 | 132 | 160 | LWFVDTGMMEIPGNFTVVQ RPSIWSIDLK |
| 3394.34 | 3395.71 | | | (M, $M^{139}$ = O and/or $M^{140}$ = O)[c] |
| 3410.32 | 3411.71 | | | |
| 801.29 | 801.42 | 161 | 167 | SNQPLSR (S for $T^{161}$)[d] |
| 777.36 | 777.41 | 168 | 173 | YEIPQK[d] |
| 3158.23 | 3158.47 | 168 | 195 | YEIPQKDVETGYGLTSITLDVDP DDCSK |
| 3172.26 | 3172.49 | | | ($C^{193}$-CAM, or $C^{193}$-PAM)[c] |
| 2399.94 | 2400.08 | 174 | 195 | DVETGYGLTSITLDVDP DDCSK |
| 2313.96 | 2314.09 | | | ($C^{193}$-CAM, or $C^{193}$-PAM)[c] |
| 1503.65 | 1503.78 | 196 | 207 | VFVYISDLQTYR[c] |
| 1690.68 | 1690.81 | 208 | 220 | MVVYDHQNQKSWR (Q for $E^{214}$)[d] |
| 1262.47 | 1262.58 | 208 | 217 | MVVYDHENQK ($M^{208}$ or $M^{208}$ = O)[c] |
| 1278.49 | 1278.58 | | | |
| 2300.99 | 2301.15 | 264 | 284 | TAYFHALSSNSEFTVST AVLR[c] |
| 3807.50 | 3807.77 | 264 | 290 | TAYFHALSSNSEFTVSTAVLRNETASK |
| | | | | $N^{285}$-Hex2-$HexNAc_2$-Fuc[c] |
| 3963.57 | 3963.87 | 264 | 291 | TAYFHALSSNSEFTVSTAVLRNETASKR |
| | | | | $N^{285}$-Hex2-$HexNAc_2$-Fuc[c] |
| 1094.43 | 1094.50 | 291 | 299 | RGYHGDDFK[c] |
| 938.33 | 938.40 | 292 | 299 | GYHGDDFK[c] |
| 621.31 | 621.37 | 300 | 304 | LLGYR (K for $R^{304}$)[d] |
| 593.33 | 593.36 | | | |
| 3773.29 | 3773.80 | 305 | 338 | GAQSQS SIHGFHPETG VIFFALIQLN AVSCWDTR (C-$CAM^{334}$)[d] |
| 1506.69 | 1506.81 | 339 | 351 | KPFAPQNMAIVYK ($M^{346}$, or $M^{346}$ = O)[c] |
| 1522.69 | 1522.81 | | | |
| 1907.82 | 1907.98 | 339 | 354 | KPFAPQNMAIVYKNDR ($M^{346}$ = O)[d] |
| 3296.35 | 3296.59 | 352 | 379 | NDRDIIYPNDLSIDQEGNVWFMSNSIIK |
| 3312.33 | 3312.58 | | | ($M^{373}$, or $M^{373}$ = O)[d] |
| 2911.23 | 2911.42 | 355 | 379 | DIIYPNDLSIDQEGNVWFMSNSIIK |
| 2927.23 | 2927.41 | | | ($M^{373}$, or $M^{373}$ = O)[c] |
| 2209.00 | 2209.14 | 380 | 396 | LLYTQLSLEEFNFHIWR[c] |
| 928.51 | 928.58 | 397 | 404 | ANIKEIIK[c] |
| 502.34 | 502.32 | 401 | 404 | ELLK[d] |
| 1848.71 | 1848.86 | 405 | 421 | GTVCDPTVPPNVDHGQR |
| 1862.72 | 1862.88 | | | ($C^{408}$-CAM, or $C^{408}$-PAM)[c] |
| 3688.95 | 3689.74 | 405 | 437 | GTVCDP TVPPNVDHGQRFGGEQNADRVTFVEYK |
| | | | | (C-$CAM^{408}$) [d] |
| 1032.39 | 1032.45 | 422 | 430 | WGGEQNADR (W for $F^{422}$)[d] |
| 1887.80 | 1887.90 | 422 | 437 | FGGEQNADRVTFVEYR (R for $K^{437}$)[d] |

a) Monoisotopic masses.
b) PTMs, PTMs. Carboxyamidomethyl cysteine (C-CAM) and propionamide cysteine (C-PAM) was artificial modification during sample preparation.
c) Sequences and modifications were confirmed by ESI-MS/MS.
d) sequences and modifications were based on ESI/MS.

*Monosaccharide Composition*

Significant amounts of *N*-acetyl-D-glucosamine, D-mannose, and L-fucose were detected in *A. aegypti* DCE (Figure 3.3). This result was further confirmed by analysis of peptide-associated oligosaccharide structures. In addition, trace amounts of *N*-acetyl-D-galactosamine, D-arabinose, and D-xylose are likely present in DCE according to this analysis (Figure 3.3), but this was not further confirmed. D-galactose, *N*-glycolyl neuraminic acid, and *N*-acetyl neuraminic acid were not detected (data not shown).

The above determination of monosaccharide composition provided necessary information to describe final oligosaccharide types, amounts, and structures. For example, the residues of hexoses (mannose, glucose, and galactose) or *N*-acetylhexoseamines (*N*-acetylglucosamine and *N*-acetylgalactosamine) have identical mass units of 162 or 203 Da, which makes it impossible to assign the ions by MS data alone. However, the absence of galactose, and *N*-acetylgalactosamine and the presence of *N*-acetylglucosamine in the DCE monosaccharide composition provided a basis to assign *m*/*z* 204 ions to *N*-acetylglucosamine during elucidation of MS/MS data of glycopeptides.

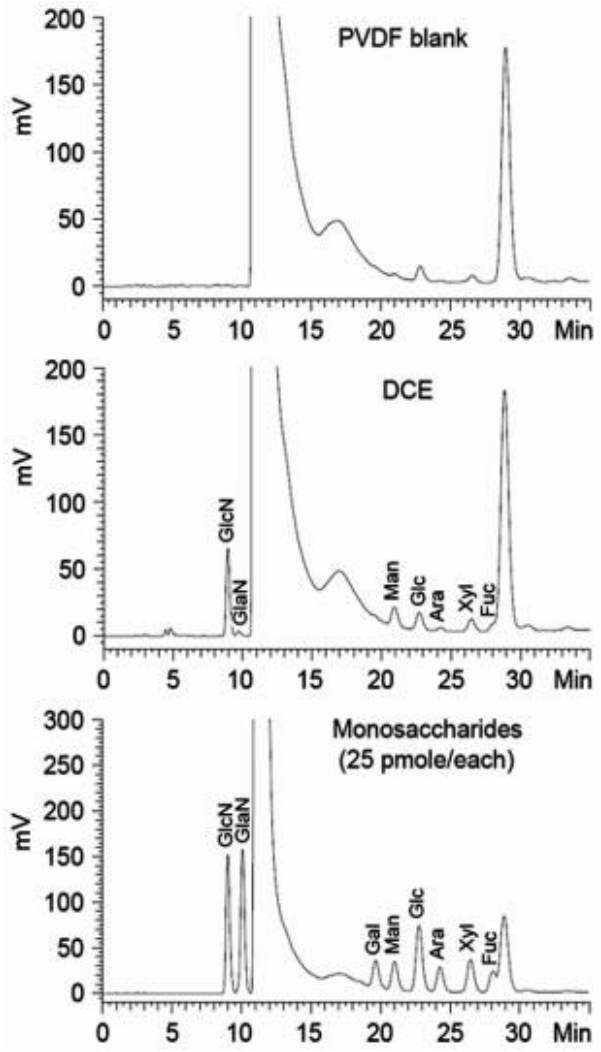


**Figure 3.3** Chromatograms of 2-anthranilic acid-labeled monosaccharides in the TFA-hydrolysate of *A. aegypti* DCE. Top, blank PVDF membrane; middle, DCE monosaccharide profile; bottom, monosaccharide standards (25 pmol each). GlcNAc, *N*-acetyl Dglucosamine; GalNAc, *N*-acetyl D-galactosamine; Gal, galactose; Man, D-mannose; Glc, Glucose; Ara, D-arabinose; Xyl, xylose; Fuc, L-Fucose.

*Glycosylation Site*

Analysis of the deduced *A. aegypti* DCE sequence by an *N*-glycosylation prediction program (http://www.cbs.dtu.dk/services/NetNGlyc) indicated that the enzyme has two potential glycosylation sites ($Asn^{145}$-Phe-Thr and $Asn^{285}$-Glu-Thr) with possible tryptic peptides of $^{132}$LWFVDTGMMEIPG**N**FTVVQRPSIWSIDLK$^{160}$, $^{285}$**N**ETASKR$^{291}$, or $^{285}$**N**ETASK$^{290}$.

Based on the presence of *m*/*z* 163 and 204 in the tandem mass spectra of individual precursor ions, a number of potential glycopeptides were detected (see Figure 3.8). Among these tryptic glycopeptides (3000–4500 Da), *m*/*z* 3963 displayed an MS/MS spectrum with good quality and rich fragmentation data. Therefore, a detailed structural elucidation of *m*/*z* 3963 is illustrated (Figures 3.4 and 3.5). The MS/MS fragmentation pattern of *m*/*z* 3963 was particularly intriguing (Figure 3.4). The presence of strong diagnostic marker ions in the spectrum, such as *m*/*z* 163 [Hex], 204 [GlcNAc], and 366 [HexHexNAc], confirmed the peptide from the precursor ion scan as a glycopeptide (Figure 3.4B). Further *de novo* sequencing suggested that it was the tryptic peptide, $^{264}$TAYFHALSSNSEFTVSTAVLR**N**ETASKR$^{291}$, with two missed trypsin cleavage sites ($Arg^{284}$-$Asn^{285}$ and $Lys^{290}$-$Arg^{291}$), and a sugar moiety (876 Da) attached to its $Asn^{285}$-Glu-Thr motif (Figure 3.4A). Evidently, the conjugated oligosaccharide on $Asn^{285}$ hindered the hydrolysis of the C-terminal side of $Arg^{284}$-$Asn^{285}$.

It was interesting that the glycosylated peptide ion, *m*/*z* 3963 $[M + H]^+$ underwent apparent C-terminal rearrangement during CID, resulting in the loss of the C-terminal arginine residue (156 Da) and formation of a rearrangement ion of *m*/*z* 3807 [$b_{27} + H_2O$] (Figure 3.4E). Peptide ion *m*/*z* 3963 has a lysine residue (a basic residue) at the *n* - 1

position of C-terminal ($Lys^{290}$-$Arg^{291}$), which enhances this intramolecular rearrangement [11, 12]. Hence, the CID spectrum of *m*/*z* 3963 contained fragments from both *m*/*z* 3963 and 3807, which helped explain the complexity of its MS/MS spectrum, *e.g.* the abundant fragment of *m*/*z* 3807 and added sugar signals (also see Figure 3.5).

The unmodified peptide ions, *m*/*z* 3087 ($^{264}$TAYFHALSSNSEFTVSTAVLRNETASKR$^{291}$), *m*/*z* 2931 ($^{264}$TAYFHALSSNSEFTVSTAVLRNETASK$^{290}$), *m*/*z* 649 ($^{285}$NETASK$^{290}$), and *m*/*z* 805 ($^{285}$NETASKR$^{291}$), were not observed in the ESI/MS spectrum. Therefore, the $Asn^{285}$-Glu-Thr site in most of the DCE molecules is occupied. The binding of purified DCE to the Con A column (data not shown) and the monosaccharide composition (Table 3.2) also support this conclusion.

There is another potential *N*-glycosylation motif ($Asn^{145}$-Phe-Thr) in DCE. Several methods were used to determine the possible glycosylation at $Asn^{145}$, including direct detection of glycopeptides, comparison of peptide maps of control and deglycosylated DCE, and enrichment of glycopeptides followed by LC-MS/MS (data not shown). Unglycosylated ($Asn^{145}$-Phe-Thr) tryptic peptides, *m*/*z* 3378 ($^{132}$LWFVDTGMMEIPGNFTVVQRPSIWSIDLK$^{160}$), *m*/*z* 3394 (oxidized $Met^{139}$ or $Met^{1140}$), and *m*/*z* 3410 (oxidized $Met^{139}$ and oxidized $Met^{140}$), were clearly observed (Table 3.1). However, no trace evidence for possible *N*-glycosylation at $Asn^{145}$ was obtained. Based on these data, it seems clear that $Asn^{145}$ is not *N*-glycosylated in DCE.

**Table 3.2** Monosaccharide composition of DCE from *A. aegypti*

| **Monosaccharide** | **Content (ng/13.8 ug DCE)[a)]** | **Percentage in total carbohydrates (%w/w)[b)]** | **Residues per molecule of DCE[c)]** |
|---|---|---|---|
| *N*-acetyl D-glucosamine | 119.8 +/- 5.35 | 39.5 | 1.92 |
| D-Mannose | 98.0 +/- 9.03 | 32.3 | 1.93 |
| L-Fucose | 40.5 +/- 9.35 | 13.4 | 0.88 |

a) Mean +/- SD, *n* = 3.
b) The samples contain small amounts of others sugars that are not further confirmed (see Figure 3.3)
c) Calculation based on 49,000 Da of the molecular weight by SDS-PAGE.

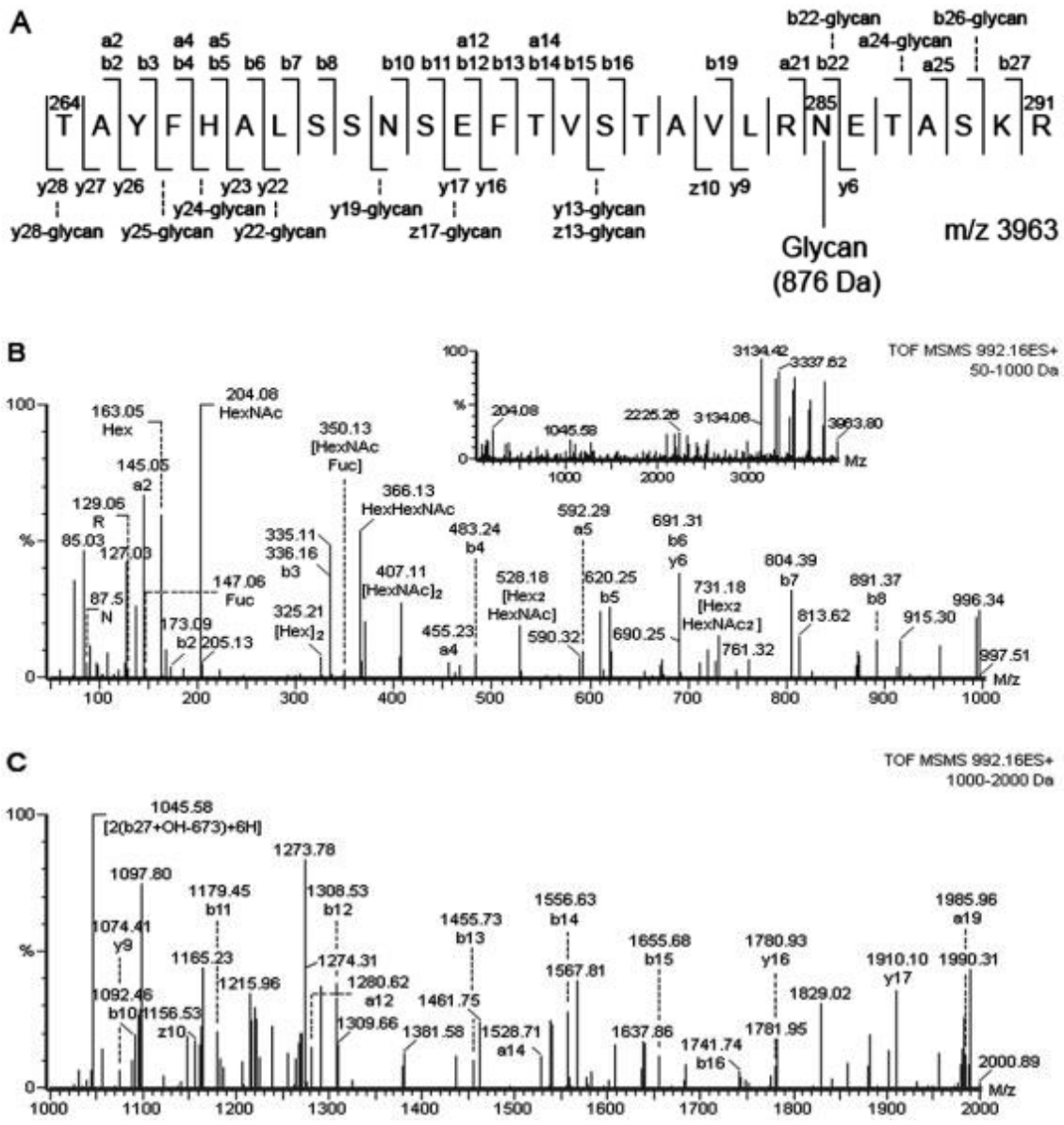


**Figure 3.4** ESI-MS/MS spectrum and structure of the +4 glycopeptide ion *m/z* 992.16 (monoisotopic *m/z* 3963) from *A. aegypti* DCE. (A) *De novo* sequencing; (B)–(E) ESI-MS/MS spectrum and elucidation. m/z 3807 is a proposed fragment derivatized from *m/z* 3963 through C-terminal rearrangement (E). The inset in Fig. 3B shows the entire spectrum of m/z 3963.

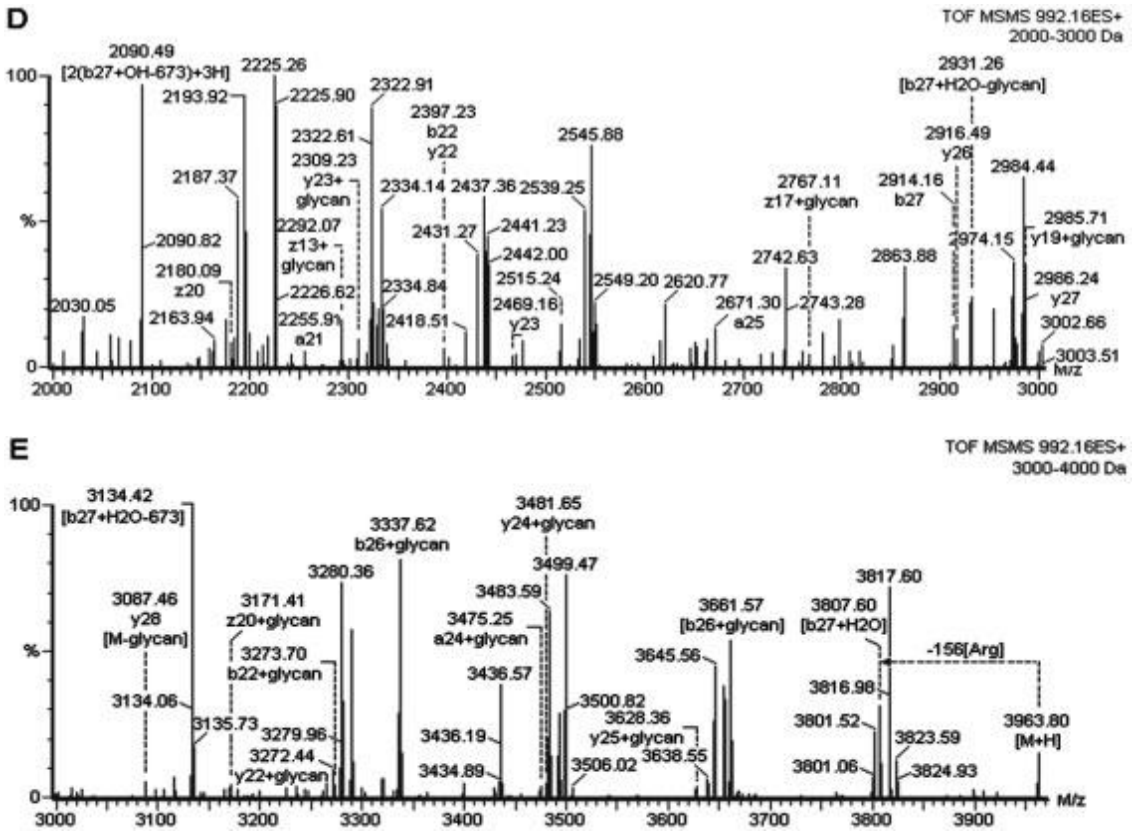


**Figure 3.4 (continued)** ESI-MS/MS spectrum the +4 glycopeptide ion *m/z* 992.16 (monoisotopic *m/z* 3963) from *A. aegypti* DCE. (B)–(E) ESI-MS/MS spectrum and elucidation. m/z 3807 is a proposed fragment derivatized from *m/z* 3963 through C-terminal rearrangement (E). The inset in Fig. 3B shows the entire spectrum of m/z 3963.

*Oligosaccharide Structures*

The sugar moiety structure of *m/z* 3963 is illustrated in Figure 3.5. The presence of *m/z* 163, 204, and 147, in conjunction with results of monosaccharide analysis (Figure 3.3), suggests that this oligosaccharide contains hexose (likely mannose), *N*-acetylglucosamine, and fucose. Examination of the MS/MS spectra of *m/z* 3963 (Figure 3.5) indicates no addition of 146 Da on the $y_1$ ion, which could result from lysine. The strong fragments of *m/z* 3134, 3280, 3290, and 3817, along with *m/z* 350 [FucGlcNAc] and *m/z* 366 [HexGlcNAc], indicate that the $Asn^{285}$-linked GlcNAc residue bears a branched fucose residue. Therefore the presence of *m/z* 147 is extremely suggestive of fucosylation. Because the *N*-oligosaccharide was cleaved by PNGase F, the fucose residue likely joined to the GlcNAc residue through α-1,6-linkage [13]. Figure 3.4 illustrates the assigned structures of these fragments. The y- and b-ion series were dominant fragments in this CID spectrum and signals seemed to be derived from both precursor *m/z* 3963 $[M + H]^+$ and its proposed C-rearrangement ion *m/z* 3807 [$b_{27}$ + H2O] (Figure 3.4B and Figure 3.5C). Based on the above spectral analysis, the associated oligosaccharide was identified as "$Hex_2$-GlcNAc(Fuc)GlcNAc-" (Figures 3.5A and B).

In addition, there were also abundant ion peaks that seemed to be derived from dimers $[2M + 3H]^{3+}$ or $[2M + 6H]^{6+}$ (Figures 3.5D and E). These multiple charged complexes had similar fragmentation pattern as their monomers. For example, in Figure 3.5C, *m/z* 3645 [(F-162) + $H^+$] (F refers fragment) was derived from *m/z* 3807 [F + $H^+$] by the loss of a hexose unit (162 Da). Similarly, in Figure 3.5D, *m/z* 2431 [2(F-162) + $3H^+$] was derived from *m/z* 2539 [2F + 3H] by the loss of two hexose units. In Figure 3.5E, *m/z* 1215 [2(F-162) + 6H] was derived from *m/z* 1269 [2F + 6H] by the loss of two

hexose units. The presence of $[2M + 3H]^{3+}$ or $[2M + 6H]^{6+}$ complexes further complicated this particular MS/MS spectrum. We do not have a specific mechanism to explain why this peptide formed dimeric complexes, but their presence could be clearly derived from the precursor ions. The glycopeptide has large size (3963 Da) and a number of charged residues ($Glu^{275}$, $Arg^{284}$, $Glu^{286}$, $Lys^{290}$, $Arg^{291}$). It is possible that the peptide molecules maintain strong noncovalent interactions in vacuum or gas phase, such as hydrogen bonds and ionic bonds [14].

Another precursor of *m*/*z* 3807 $[M + H]^+$ was produced by trypsin digestion. Analysis of its CID spectrum revealed the sequence $^{264}$TAYFHALSSNSEFTVSTAVLRNETASK$^{290}$, with an oligosaccharide of $Hex_2(Fuc)HexNAc_2$ (876 Da) (data not shown). *m*/*z* 3807 has the same sequence as *m*/*z* 3963 except that it has one missing cleavage site (-$Ser^{289}$-$Lys^{290}$ at C-terminal region). Its fragmentation pathway and complexes were similar to *m*/*z* 3963, but there was no C-terminal rearrangement.

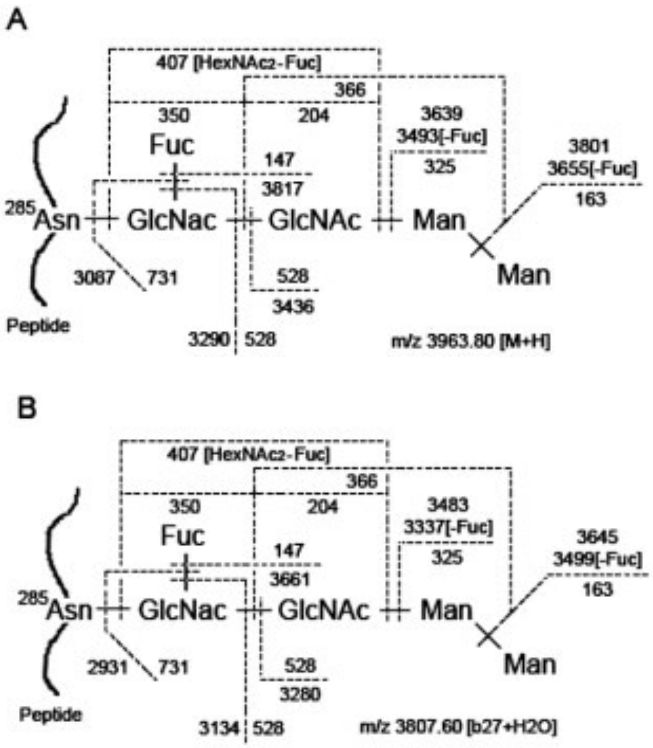


**Figure 3.5** ESI-MS/MS spectrum and structure of the sugar moiety of the +4 glycopeptide ion *m/z* 992.16 (monoisotopic *m/z* 3963) from *A. aegypti* DCE. (A) Fragmentation pathway of *m/z* 3963 [M + H] associated oligosaccharide; (B) fragmentation pathway of *m/z* 3807 [b27 + $H_2O$] associated oligosaccharide (C-terminal rearrangement ion).

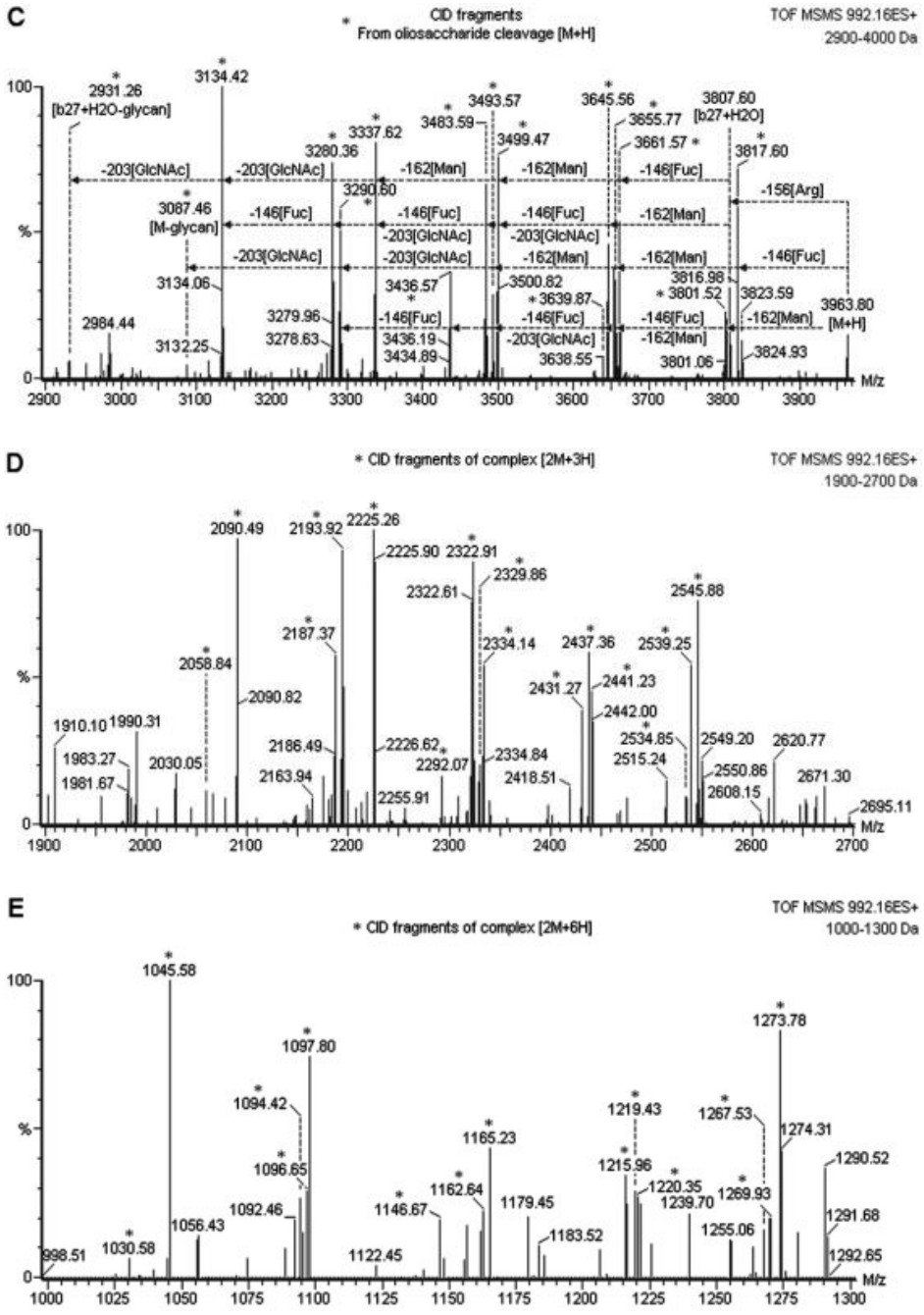


**Figure 3.5 (continued)** ESI-MS/MS spectrum of the +4 glycopeptide ion *m/z* 992.16 (monoisotopic *m/z* 3963) from *A. aegypti* DCE. (C) Elucidation of fragments from the sugar moiety of *m/z* 3963. (D) and (E) are complexes and the fragmentation pattern of their sugar moiety.

*Deglycosylation and its Effect on DCE Function*

Three glycosidases were selected to deglycosylate DCE based on the results of monosaccharide analysis and ESI-MS/MS (Figures 3.6 A–B). Removal of all oligosaccharides by PNGase F decreased DCE activity and stability. In contrast, partial deglycosylation with α-mannosidase or α -fucosidase somewhat improved the enzyme activity or stability. Similar results were also observed in a mammal enzyme, dopachrome tautomerase [15]. The recommended pH of deglycosylation is 5.5 for fucosidase or mannosidase and 7.5 for PNGase F. DCE activity was not affected during a 12 h incubation at pH 7.5 (the $K_m$ and $V_{max}$ of unincubated DCE were 0.36 +/- 0.05 mM and 442.5 +/- 24.0 mmol/min/mg, respectively). However, incubation of DCE at pH 5.5 decreased substantially its activity. Consequently, the much higher activity of the partially deglycosylated DCE by fucosidase or mannosidase, as compared to control sample, might be due to improved stability of the partially deglycosylated DCE rather than increase in DCE specific activity due to partial deglycosylation.

To confirm DCE deglycosylation, the peptide maps of the control and deglycosylated enzyme were determined by LC-ESI MS/MS after SDS-PAGE and trypsin digestion. There was noticeable decrease in DCE molecular weight after PNGase deglycosylation (Figure 3.7A, SDS-PAGE gel) and changes in TIC chromatograms between the control and deglycosylated DCE peptide samples (Figure 3.7A). By screening the peptide of interests in total ion chromatogram, the relevant peptides (glycopeptides or deglycosylated peptides) within the elution window were calculated to obtain an easily recognized-spectrum (Figure 3.7B). Most of the glycopeptides, seen in the ESI/MS spectrum of the control (Figure 3.7B, single asterisk labeled peaks),

A

| Glycosidases | $K_m$, mM | | $V_{max}$, μmol/min/mg | |
|---|---|---|---|---|
| | Control | Deglycosylated | Control | Deglycosylated |
| PNGase F 100 U/mL | 0.38±0.08 | 0.11±0.04 | 436±40.6 | 106±11.3 |
| α-Fucosidase 1 U/mL | 0.11±0.03 | 0.16±0.09 | 14.1±1.28 | 272±48.7 |
| α-Mannosidase 50 U/mL | 0.09±0.04 | 0.26±0.02 | 14.1±1.52 | 272±19.6 |

B

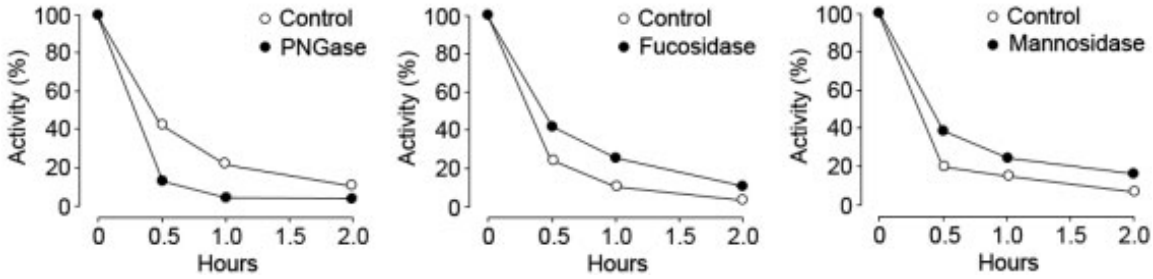


**Figure 3.6** Effect of glycosylation on DCE activity and thermal stability. (A) Kinetic parameters of the control and deglycosylated DCE from *A. aegypti*. The incubation condition was described above. Mean +/- SD, $n$ = 3. (unincubated DCE: $K_m$ 0.36 +/- 0.05 mM and $V_{max}$ 442.5 +/- 24.0 umol/min/mg). (B) Thermal stability of the control and deglycosylated DCE at 45$^{o}$C. All data were means of two repeats.

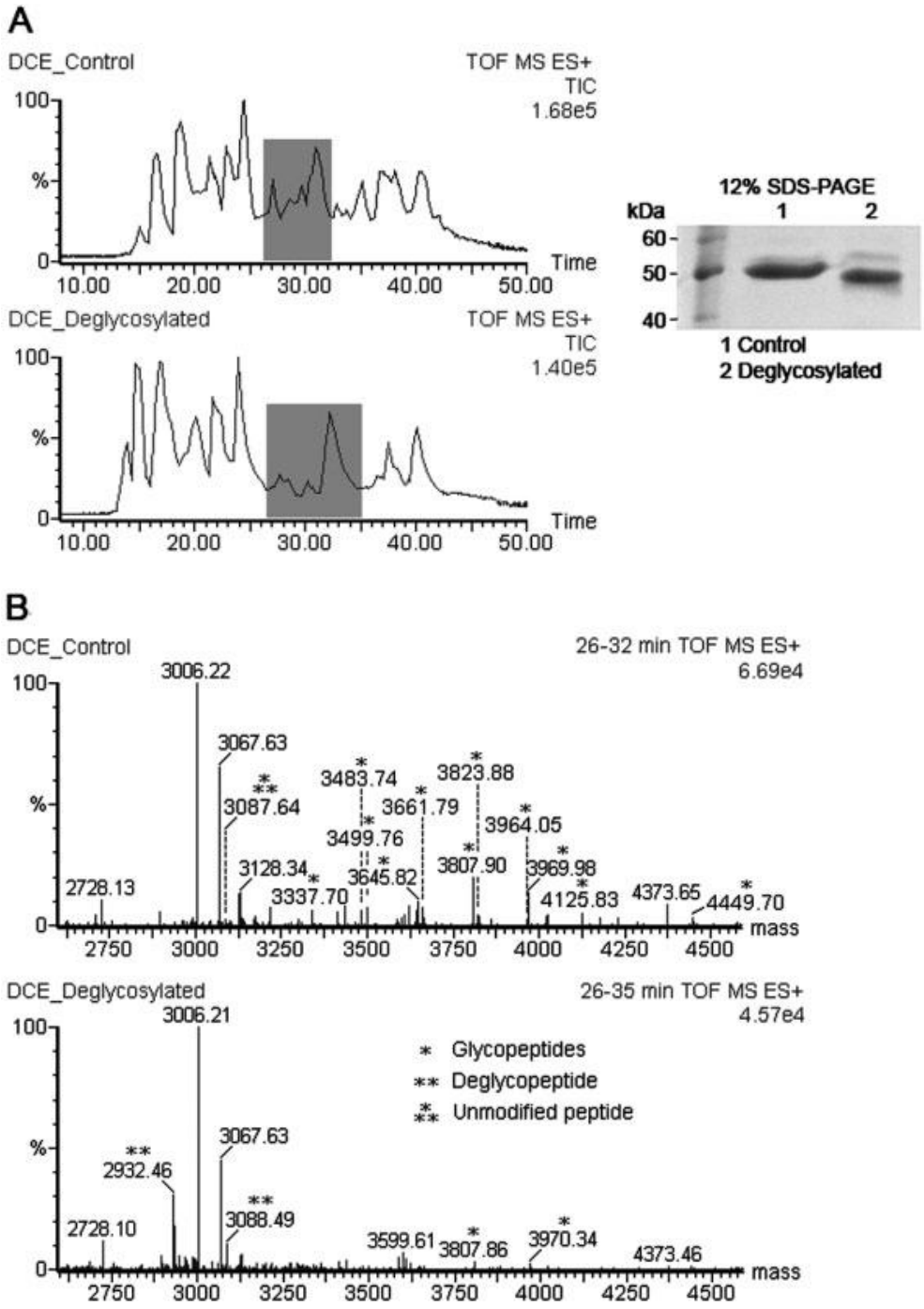


**Figure 3.7** Confirmation of DCE deglycosylation by nano-LC/ESI/MS and SDS-PAGE. (A) SDS-PAGE of the control and PNGase-deglycosylated DCE, and TIC of their tryptic peptides. The shadowed areas indicate the elution window of relevant peptides and their peak shift. (B) ESI/MS spectra of the relevant peptides of the control (Top) and deglycosylated (Bottom) DCE.

disappeared or diminished from the spectrum of PNGase F-treated DCE (Figure 3.7B, double asterisks labeled peaks). Two deglycosylated peptides, m/z 2932.46 and 3088.49, were observed in the treated DCE. In addition, a weak peak at m/z 3087 (Figure 3.7B, three asterisks) may be from trace amount of unmodified peptide at Asn285. Similar events were also observed in α-mannosidase or α-fucosidase-treated DCE (data not shown). These ESI-MS/MS data further confirmed DCE deglycosylation and provide additional evidence for the elucidated oligosaccharide structures.

*Oligosaccharide Profile*

All glycopeptides were eluted within 3 min under the applied RP separation conditions. Figure 3.8 (A and B) illustrates the TIC of *A. aegypti* DCE glycopeptides and their oligosaccharide structures, respectively. These oligosaccharides had dominant $Hex_3GlcNAc_2$, $Hex_3(Fuc)_{1\text{-}2}GlcNAc_2$, and truncated structures, including $GlcNAc_{1–2}$, $Hex_{1–2}GlcNAc_2$, and $Hex_{1–2}(Fuc)_{1–2}GlcNAc_2$. In addition, high hexose-type structures ($Hex_{4–7}(Fuc)GlcNAc_2$) were also detected. Overall, the oligosaccharides confirmed by MS/MS are consistent with the result of monosaccharide analysis, and no other glycosylation was observed (Table 3.1). Therefore, *N*-glycosylation seems to be the dominant glycosylation in DCE. When DCE from *A. subalbatus* was purified and analyzed in the same manners, it had a quite similar profile of *N*-linked oligosaccharides at its $Asn^{285}$-Glu-Thr motif (Figure 3.8C).

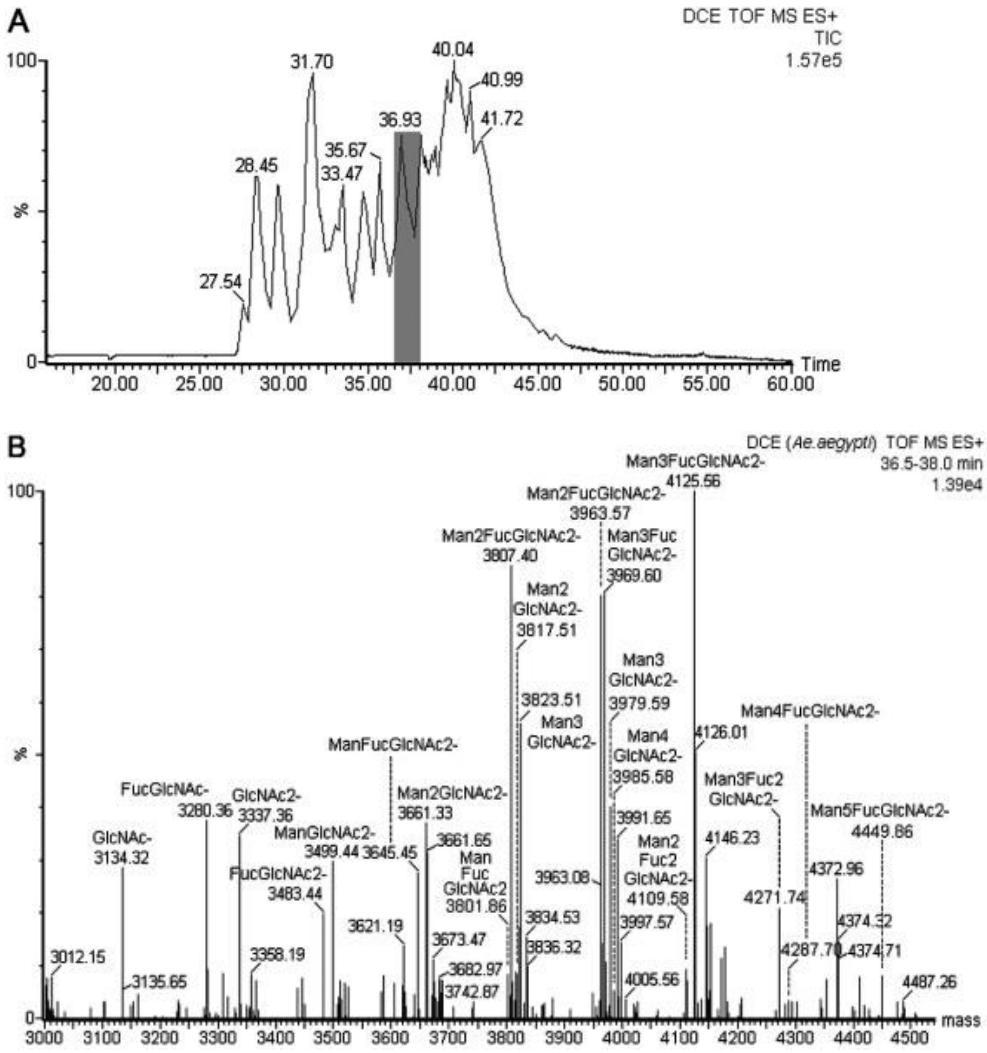


**Figure 3.8** Structure and profile of *N*-linked oligosaccharides in mosquito DCE. (A) TIC of tryptic peptides of DCE from *A. aegypti*. The shadowed area indicates the elution window of the glycopeptides which are shown in (B). (B) and (C) show the oligosaccharides and profile at $Asn^{285}$-Glu-Thr of *A. Aegypti* and *A. subalbatus* DCE, respectively. These oligosaccharide structures are elucidated based on the data from fragmentation spectra, monosaccharide analysis, and glycosidase deglycosylation. Man, mannose; Fuc, Fucose; GlcNAc, *N*-acetylglucosamine.

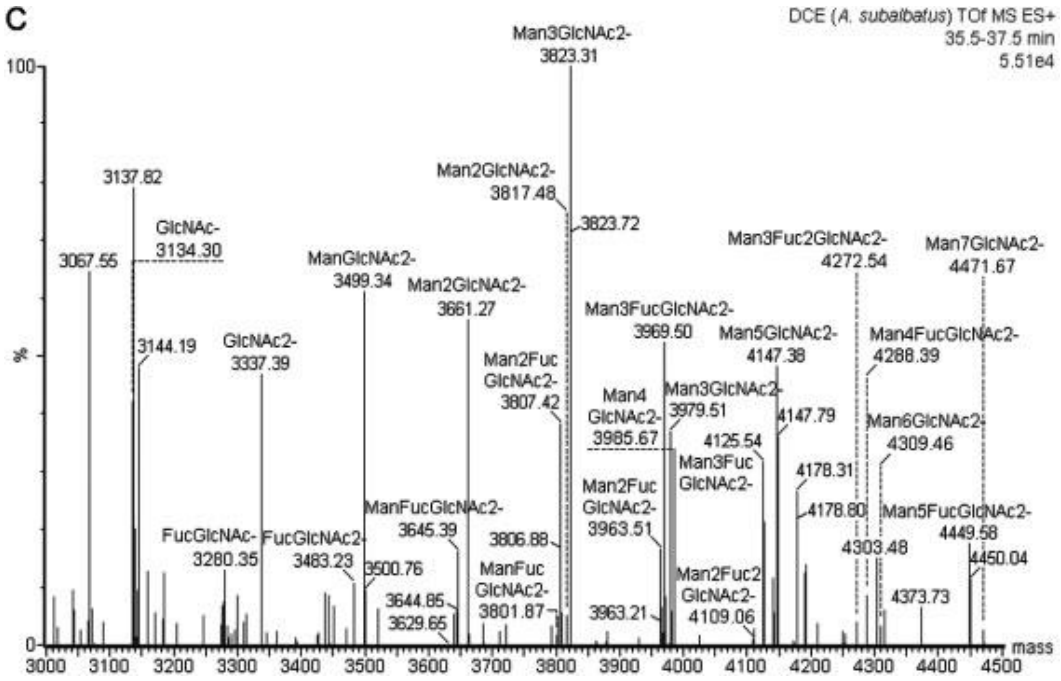


**Figure 3.8 (continued)** Structure and profile of *N*-linked oligosaccharides in mosquito DCE. (A) TIC of tryptic peptides of DCE from *A. aegypti*. The shadowed area indicates the elution window of the glycopeptides which are shown in (B). (B) and (C) show the oligosaccharides and profile at $Asn^{285}$-Glu-Thr of *A. Aegypti* and *A. subalbatus* DCE, respectively. These oligosaccharide structures are elucidated based on the data from fragmentation spectra, monosaccharide analysis, and glycosidase deglycosylation. Man, mannose; Fuc, Fucose; GlcNAc, *N*-acetylglucosamine.

### 3.4 Concluding Remarks

DCE was purified to its apparent homogeneity from mosquitoes. The protein is *N*-glycosylated at $Asn^{285}$. High- and paucimannose oligosaccharides, with quite a few truncated structures, were detected by nano-LC-ESI MS/MS and supported by monosaccharide composition analysis and glycosidase deglycosylation. The glycopeptides undergoes C-terminal rearrangement and complex formation, which further complicates its MS/MS spectrum. Although the oligosaccharides in DCE have been highly trimmed, they still have substantial effect on its activity and stability.

DCE is a novel insect protein that shares no similarity with any noninsect proteins from bacteria to humans. Although we have determined the biological function of the protein, its structural basis underlying the catalytic function is unclear. Results from this study demonstrate that mosquito DCE is a glycoprotein with dominant $Man_3GlcNAc_2$ and $Hex_3(Fuc)GlcNAc_2$ structures. In addition, high hexose-type structures ($Hex_{4-7}GlcNAc_2$) and truncated structures ($Hex_2GlcNAc_2$, $Man_2FucGlcNAc_2$) are also present. During glycoprotein synthesis in eukaryotic cells, a dolichol-linked precursor oligosaccharide ($Hex_{12}GlcNAc_2$) is first transferred to a newly synthesized protein. The oligosaccharide is then further processed in the ER and Golgi, involving removal and addition of monosaccharides by exoglycosidases and glycosyltransferases, leading to the production of a complex or hybrid type of oligosaccharides. It has been suggested that most insect cells have low levels of glycosyltransferase activities, but higher levels of exoglycosidases (such as α-mannosidase and β-*N*-acetylglucosaminidase) activity [16, 17], so that the processing pathway in insect cells is usually completed with the final structure of $Hex_3GlcNAc_2$, which is in agreement with our data.

The common approach for analyzing oligosaccharides in glycoproteins involves enzymatic release of oligosaccharides by PNGase A or F, direct analysis of oligosaccharides by MALDI-TOF-MS, LC-ESI MS/MS, or HPLC with fluorescent detection after oligosaccharide fluorescent labeling, sequential digestion of oligosaccharides by specific exoglycosidases, and final analysis of the digested products by normal phase HPLC or by MALDI-TOF-MS [17]. This overall process should provide information regarding the oligosaccharide profiles and the oligosaccharide structures. However, when the amount of glycoproteins is the limiting factor, it is difficult to determine the oligosaccharide structures using this approach. In addition, when a number of glycosylation sites are present in a glycoprotein, it is difficult to assign the specific oligosaccharide structures to a particular site. In our analysis of the DCE glycosylation site and oligosaccharide structures using LC-ESI MS/MS, oligosaccharides were not released from their associated peptide, so that the sensitivity or signal intensity of the glycopeptides was greatly improved due to the charge contribution from amino acid residues in the peptide. Moreover, the CID fragmentation pattern of the representative 3963 glycopeptide ion is highly interesting (Figure 3.4). Its precursor ion and MS/MS spectrum did not match to the DCE sequence, and its C-terminal rearrangement and formation of dimeric structures during CID considerably complicated structural analysis. Consequently, it is almost certain that the peptide would have easily been excluded for further analysis or treated as a contaminant. Through careful analysis, however, essentially all the major fragments could be assigned with confidence. This provides an interesting example in terms of potential complexity of the glycopeptide CID fragmentation pattern.

Based on the genomes of several model species, including *Drosophila melanogaster*, *Anopheles gambiae*, *A. aegypti*, *Apis mellifera*, and *Tribolium castaneum*, the yellow gene family is present in all of these insect species. Because members of the insect yellow gene family share no sequence similarity with other organisms, there is no shortcut to simulate the function by comparison of their protein functional correlates from noninsect species. To truly understand the biological function of insect DCE and other yellow proteins, one must study them at the protein level. Analysis of the deduced coding sequences of the mosquito and Drosophila yellow gene family by an *N*-glycosylation program (http://www.cbs.dtu.dk/services/NetNGlyc/) indicated that most of the yellow family proteins are potential glycoproteins and that some of them contain a conserved fragment with the same glycosylation site. For example, the VLRNETASQR, LQNETMAQL, and LRNET fragments in EAA08479, EAA09172, and EAA03946 coding sequences from the *A. gambiae* yellow gene family, and the VLQNET, LQNETYS, VLKNETLAR fragments in the EAT43230, EAT40936, and EAT48899 coding sequences from the *A. aegypti* yellow gene family share high similarity with the VLRNETASKR fragment of the *A. aegypti* DCE. All of these fragments contain the same *N*-glycosylation consensus (NET) sequence and they are located in similar positions in their deduced sequences. Therefore, the glycosylation site and oligosaccharide structures of mosquito DCE provide an essential basis for future studies of the glycosylation and oligosaccharide structures of other members of the insect yellow family proteins.

**Acknowledgements**

A majority of the analysis of DCE was carried out by Dr. Junsuo Li. This chapter has been published in the journal Proteomics with the following citation:

Li, J.S., et al., Proteomic analysis of N-glycosylation in mosquito dopachrome conversion enzyme. Proteomics, 2007. **7**(15): p. 2557-2569.

This work was supported in part by the College of Agriculture and Life Science and NIH grant AI 37789 and AI19769.

# LITERATURE CITED


1. Johnson, J. K., Li, J., Christensen, B. M., *Cloning and characterization of a dopachrome conversion enzyme from the yellow fever mosquito, Aedes aegypti*. Insect Biochem. Mol. Biol. 2001, *31*, 1125–1135.

2. Georgiev, P., Tikhomirova, T., Yelagin, V., Belenkaya, T. *et al*., Insertions of hybrid P elements in the yellow gene of Drosophila cause a large variety of mutant phenotypes. Genetics 1997, *146*, 583–594.

3. Wittkopp, P. J., Vaccaro, K., Carroll, S. B., *Evolution of yellow gene regulation and pigmentation in Drosophila*. Curr. Biol. 2002, *12*, 1547–1556.

4. Prud'homme, B., Gompelm, N., Rokas, A., Kassner, V. A. *et al., Repeated morphological evolution through cis-regulatory changes in a pleiotropic gene.* Nature 2006, *440*, 1001–1002.

5. Jeong, S., Rokas, A., Carroll, S. B., *Regulation of body pigmentation by the Abdominal-B Hox protein and its gain and loss in Drosophila evolution*. Cell 2006, *125*, 1387–1399.

6. Weitzhandler, M., Kadlecek, D., Avdalovic, N., Forte, J. G. *et al., Monosaccharide and oligosaccharide analysis of proteins transferred to polyvinylidene fluoride membranes after sodium dodecyl sulfate-polyacrylamide gel electrophoresis*. J. Biol. Chem. 1993, *268*, 5121–5130.

7. Anumula, K. R., *Quantitative determination of monosaccharides in glycoproteins by high performance liquid chromatography with highly sensitive fluorescence detection.* Anal. Biochem. 1994, *220*, 275–283.

8. Anumula, K. R., *Rapid quantitative determination of sialic acids in glycoproteins by high-performance liquid chromatography with a sensitive fluorescence detection.* Anal. Biochem. 1995, *230*, 24–30.

9. Anumula, K. R., *Advances in fluorescence derivatization methods for high-performance liquid chromatographic analysis of glycoprotein carbohydrates*. Anal. Biochem. 2006, *350*, 1–23.

10. Laemmli, U. K., *Cleavage of structural proteins during the assembly of the head of bacteriophage T4.* Nature 1970, *227*, 680–685.

11. Ballard, K. D., Gaskell, S. J., *Intramolecular [18O] isotopic exchange in the gas phase observed during the tandem mass spectrometric analysis of peptides*. J. Am. Chem. Soc. 1992, *114*, 64–71.

12. Gonzalez, J., Besada, V., Garay, H., Reyes, O. *et al.*, *Effect of the position of a basic amino acid on C-terminal rearrangement of protonated peptides upon collision-induced dissociation.* J. Mass. Spectrom. 1996, *31*, 150–158.

13. Fabini, G., Freilinger, A., Altmann, F., Wilson, I. B. H., *Identification of core a1,3-fucosylated glycans and cloning of the requisite fucosyltransferase cDNA from Drosophila melanogaster: Potential basis of the neural anti-horseradish peroxidase epitope.* J. Biol. Chem. 2001, *176*, 28058–28067.

14. Sudha, R., Kohtani, M., Jarrold, M. F., *Noncovalent interactions between unsolvated peptides: Helical complexes based on acid-base interactions.* J. Phys. Chem. B 2005, *109*, 6442–6447.

15. Aroca, P., Martinez-Liarte, J. H., Solano, F., Garcia-Borron, J. C., Lozano, J. A., *The action of glycosylases on dopachrome (2-carboxy-2,3-dihydroindole-5,6-quinone) tautomerase.* Biochem. J. 1992, *284*, 109–113.

16. Tomiya, N., Narang, S., Lee, Y. C., Betenbaugh, M. J., *Comparing N-glycan processing in mammalian cell lines to native and engineered lepidopteran insect cell lines.* Glucoconj. J. 2004, *21*, 343–360.

17. Varki, V., Cummings, R., Esko, J., Freeze, H., Hart, G., Marth, J., *Essentials of Glycobiology*, Cold Spring Harbor

# IV

# METHYLDOPA RESISTANT PROTEIN

## 4.1 Abstract

The α-methyldopa resistant protein (AMD) was originally identified in *Drosophila* mutants hypersensitive to α-methyldopa, an inhibitor of dopa decarboxylase (DDC). Production of dopamine by DDC is critical for developing insects because dopamine conjugates are used as crosslinking precursors for cuticle sclerotization. Although there has been much discussion into the phenotypic effects of AMD, the actual function of this protein is not clear. In this study, we expressed a recombinant AMD and assessed its activity to α-methyldopa and dopa. Incubation of AMD in the presence of α-methyldopa results in accumulation of 3,4-dihydroxyphenylacetone in the reaction mixture and incubation of the protein in the presence of dopa produces 3,4-dihydroxyphenylacetaldehyde (DOPAL) as a major product and dopamine as a minor product. These results demonstrate that AMD is an enzyme that can use α-methyldopa and L-DOPA as its substrates. Based on the identified enzymatic products, we propose that AMD catalyzes an oxidative decarboxylation of α-methyldopa and dopa, leading to the production of the deaminated intermediates 3,4-dihydroxyphenylacetone and DOPAL, respectively. The ability to catalyze α-methyldopa to 3,4-dihydroxyphenylacetone by AMD may explain why Drosophila becomes more resistant to α-methyldopa in the presence of AMD.

## 4.2 Introduction

An α-methyldopa hypersensitive loci adjacent to the dopa decarboxylase (DDC) gene was originally identified in *Drosophila* strains resistant to α-methyldopa and the gene

product was termed α-methyldopa resistant protein (AMD) [1, 2]. The compound, α-methyldopa, is a competitive inhibitor of DDC that catalyzes the decarboxylation of L-DOPA to dopamine [3]. AMD mutants are highly sensitive to α-methyldopa and die more rapidly than wild type in the presence of this compound. The AMD protein has been named after its phenotype; however, what exactly the AMD does to make *Drosophila* resistant to α-methyldopa is unknown.

AMD shares 48% sequence identity to DDC; which may seem sufficient to classify AMD as a DDC isozyme. However, the potential function in dopa decarboxylation by AMD has never been described. DDC is a ubiquitous protein that is present in living organisms from bacteria to humans [3]. Compared to other species, however, DDC plays some unique functions in insects. For example, DDC is involved in cuticle formation/sclerotization and immune responses in insects, which has not been discussed in other species except in some arthropods [4]. Dopamine (DA), the product of insect DDC, is used to produce *N*-acetyldopamine and *N*-β-alanyl-dopamine that are important crosslinking precursors used by insects to crosslink cuticle proteins during cuticle sclerotization, an essential biochemical event leading to the production of highly protective exoskeleton in insects [4]. DA is an intermediate in the insect melanization pathway that is involved in insect immune responses and wound healing [5]. This may explain why DDC is highly regulated in insects than in most other species.

Although mammalian DDC is able to catalyze the decarboxylation of L-DOPA, tryptophan and 5-HTP, insect DDC is more specific and is only able to catalyze the

decarboxylation of L-DOPA, and 5-HTP, but not tryptophan. In addition to DDC and histidine decarboxylase, which both mammals and insects contain, two separate tyrosine decarboxylase enzymes and AMD are both additionally present in insects, and are not found in mammalian systems. The higher specificity of insect DDC in addition to the presence of additional similar decarboxylase enzymes reflects the evolutionary pressure to regulate catecholamine metabolism in insects.

The high sequence identity between DDC and AMD raises an essential question regarding the relationship between DDC and AMD. A protein BLAST search of *Drosophila* AMD against the available sequences of several insect species identified the presence of AMD in their genomes. To understand the function of AMD and its relationship with DDC, we expressed *Drosopohila* AMD and assessed its potential function towards L-DOPA and α-methyldopa, which leads to the identification of AMD as an enzyme that is capable of mediating oxidative deamination of L-DOPA and α-methyldopa. In this report, we present data to describe and discuss the biochemical function of AMD and its relation with DDC. Expression and purification of recombinant *Drosophila* AMD produced a protein that displays high activity toward L-DOPA and α-methyldopa. GC-MS analysis of TMS derivatized AMD enzymatic metabolites revealed 3,4-dihydroxyphenylacetaldehyde (DOPAL) as the major enzymatic product of L-DOPA and 3,4-dihydroxyphenylacetone as the AMD product of α-methyldopa. Unlike DDC, which simply catalyzes a decarboxylation of L-DOPA to dopamine, AMD catalyzes an oxidative decarboxylation of L-DOPA to DOPAL.

```
DDC             -----------------------------------MEAPEFKDFAKTMVDFIAEYLENIR 25
AMD Isoform A   -----------------------------------MDAKEFREFGKAAIDYIADYLENIR 25
AMD Isoform B   -----------------------------------MDFDEFREFGHASIEFLINYLSGIR 25
                                                    *:  **::*.:: :::: :**..**

DDC             ERRVLPEVKPGYLKPLIPDAAPEKPEKWQDVMQDIERVIMPGVTHWHSPKFHAYFPTANS 85
AMD Isoform A   DDDVLPNVEPGYLLDLLPTEMPEEPEAWKDVLGDISRVIKPGLTHWQSPHMHAYYPTSTS 85
AMD Isoform B   ERDVLPSTAPYAVINQLPKEIPEQPDHWREVLKDLENIILPGLTHWQSPYFNAFYPSSSS 85
                :  ***.. *  :   :*   **:*: *::*: *:..:* **:***:** ::*::*::.*

DDC             YPAIVADMLSGAIACIGFTWIASPACTELEVVMMDWLGKMLELPAEFLACSGGKGGGVIQ 145
AMD Isoform A   YPSIVGEMLASGFGVIGFSWICSPACTELEVVVMDWLAKFLKLPAHFQHASDGPGGGVIQ 145
AMD Isoform B   AGSIIGELLIAGIGVLGFSWICSPACTELEVVVMDWLAKFLKLPAHFQHASDGPGGGVIQ 145
                  :*:.::* ..:. :**:**.**********:****.*:*:***.*  .*.* ******

DDC             GTASESTLVALLGAKAKKLKEVKELHPEWDEHTILGKLVGYCSDQAHSSVERAGLLGGVK 205
AMD Isoform A   GSASEAVLVAVLAAREQAVANYRESHPELSESEVRGRLVAYSSDQSNSCIEKAGVLAAMP 205
AMD Isoform B   GSASEAVLVAVLAAREQAVANYRESHPELSESEVRGRLVAYSSDQSNSCIEKAGVLAAMP 205
                *:***:.***:*.*: : : : :* *** .*  : *:**.*.***::*.:*:**:*..:

DDC             LRSVQS-ENHRMRGAALEKAIEQDVAEGLIPFYAVVTLGTTNSCAFDYLDECGPVGNKHN 264
AMD Isoform A   IRLLPAGEDFVLRGDTLRGAIEEDVAAGRIPVICVATLGTTGTCAYDDIESLSAVCEEFK 265
AMD Isoform B   IRLLPAGEDFVLRGDTLRGAIEEDVAAGRIPVICVATLGTTGTCAYDDIESLSAVCEEFK 265
                :* : : *:. :** :*. ***:*** * **. .*.*****.:**:* ::. ..* ::.:

DDC             LWIHVDAAYAGSAFICPEYRHLMKGIESADSFNFNPHKWMLVNFDCSAMWLKDPSWVVNA 324
AMD Isoform A   VWLHVDAAYAGGAFALEECSDLRKGLDRVDSLNFNLHKFMLVNFDCSAMWLRDANKVVDS 325
AMD Isoform B   VWLHVDAAYAGGAFALEECSDLRKGLDRVDSLNFNLHKFMLVNFDCSAMWLRDANKVVDS 325
                :*:********.**   *  .* **:: .**:*** **:************:*.. **::

DDC             FNVDPLYLKHDMQG--SAPDYRHWQIPLGRRFRALKLWFVLRLYGVENLQAHIRRHCNFA 382
AMD Isoform A   FNVDRIYLKHKHEGQSQIPDFRHWQIPLGRRFRALKVWITFRTLGAEGLRNHVRKHIELA 385
AMD Isoform B   FNVDRIYLKHKHEGQSQIPDFRHWQIPLGRRFRALKVWITFRTLGAEGLRNHVRKHIELA 385
                **** :****. :*  . **:****************:*:.:*  *.*.*: *:*:* ::*

DDC             KQFGDLCVADSRFELAAEINMGLVCFRLKGSNERNEALLKRINGRGHIHLVPAKIKDVYF 442
AMD Isoform A   KQFEQLVLKDSRFELVAPRALGLVCFRPKGDNEITTQLLQRLMDRKKIYMVKAEHAGRQF 445
AMD Isoform B   KQFEQLVLKDSRFELVAPRALGLVCFRPKGDNEITTQLLQRLMDRKKIYMVKAEHAGRQF 445
                *** :* : ******.*   :****** **.** .  **:*: .* :*::* *:  .  *

DDC             LRMAICSRFTQSEDMEYSWKEVSAAADEMEQEQ---------------------------- 475
AMD Isoform A   LRFVVCGMDTKASDIDFAWQEIESQLTDLQAEQSLVARKSGNVGDLAQHFQIHLSTENAT 505
AMD Isoform B   LRFVVCGMDTKASDIDFAWQEIESQLTDLQAEQSLVARKSGNVGDLAQHFQIHLSTENAT 505
                **:.:*.  *::.*::::*:*:.:   ::: **

DDC             -----
AMD Isoform A   HEKSQ 510
AMD Isoform B   HEKSQ 510


SeqA Name   Len(aa)  SeqB Name   Len(aa)  Score
================================================
1    DDC    475      2    AMD A  510      52
1    DDC    475      3    AMD B  510      48
2    AMD A  510      3    AMD B  510      90
================================================
```

**Figure 4.1** Multiple Sequence alignment of DDC and AMD. Gene accession numbers: DDC, 724164; AMD isoform A, NP 476592; AMD isoform B, NP 724162.

## 4.3 Materials and Methods

*Materials*

L-α-methyl-3,4-dihydroxyphenylalanine (α-methyldopa), L-3,4-dihydroxyphenylalanine (L-DOPA), L-3,4-dihydroxyphenethylamine (dopamine, DA) pyridoxal-5-phosphate, pyridine, sodium phosphate, formic acid, trifluroacetic acid (TFA), acetonitrile, sodium hypochlorite, boric acid, benzene, were from Sigma (St. Louis, MO). *N*,*O*-*bis*[Trimethylsilyl]trifluoroacetamide (BSTFA) and trimethylchlorosilane (TMCS) were from Pierce (Waltham, MA). The IMPACT-CN protein expression and purification system was from New England Biolabs (Ipswich, MA). A pursuit $C_{18}$ 5u column was from Varian (Palo Alto, CA). HPLC with UV detection was from Hitachi (Pleasanton, CA).

*Expression and Purification*

Recombinant AMD (NP_476592.1) was obtained using an intein-mediated purification with an affinity chitin-binding tag system (IMPACT-CN, New England Biolabs). The AMD protein was expressed and purified according to methods described previously [6]. An AMD isoform B coding sequence was amplified from a *Drosophila melanogaster* cDNA pool. The PCR amplified AMD coding sequence was cloned into the pTYB12 plasmid (New England Biolabs) for expression of a fusion protein containing a chitin-binding domain. Transformed *Escherichia coli* cells (6 L) were cultured at 37 °C and induced with 0.2 mM isopropyl-1-thio-β-D-galactopyranoside. Following induction, the cells were cultured at 15°C for 24 h. Cells were collected and sonicated in 10 mM sodium phosphate (pH 7.5) with 1 mM phenylmethanesulphonylfluoride (PMSF). The soluble

protein extract was applied to a column packed with chitin beads and subsequently hydrolyzed under reducing conditions. The recombinant AMD was concentrated in 5 mM phosphate buffer (pH 7.5) using a Centricon YM-30 concentrator (Millipore). The identity of the protein was verified as AMD isoform B by MALDI-TOF/TOF analysis of its tryptic peptides.

*Identification of Products Formed*

AMD (10 ug in 100 uL reaction volume) was incubated with 2 mM L-DOPA or α-methyldopa for 10 minutes in 20 mM sodium phosphate (pH 6.8). The reaction mixture was treated with formic acid and then centrifuged to precipitate the enzyme. The components of the enzymatic reaction were separated and analyzed using a pursuit 5u $C_{18}$ column (Varian) with UV (280 nm) or electrochemical detection (Hitachi). The mobile phase was 6% acetonitrile 0.1% TFA for separation of the L-DOPA reaction and 30% acetonitrile 0.1% TFA for α-methyldopa using isocratic elution. Sodium phosphate was included during electrochemical detection. The major peaks were collected and dried using a speedvac.

Fractions were derivatized with TMS and analyzed with GC-MS in a similar manner to the methods described by Loutelier-Bourhis et al. [7]. The dried enzymatic fractions separated by HPLC were treated with pyridine (50 uL) and BSTFA/TMS (99:1, 50 uL). Each sample was transferred to a glass tube for GC-MS analysis. Products were identified after an exact match with a TMS derivatized standard. All products were identified as the dominant component of the sample by observation of the total ion count. All standards were available to run under the same conditions with exception of DOPAL;

a quality TMS derivatized DOPAL reference spectrum was obtained from Mattammal et al. [8].

*GC/MS Analysis of Catecholamine TMS Derivatives*

GC/MS analyses were performed using a Hewlett-Packard 5890 series gas chromatograph interfaced to a VG 70S mass spectrometer equipped with an Opus 3.1 data system.

Chromatographic separations were obtained using a RTX5MS 30M, 0.32mM i.d., 0.25 uM film thickness capillary column (Restek). Helium carrier gas was employed. Oven temperature was programmed from 80$^{o}$C (for 1 minute) to 280$^{o}$C at 8$^{o}$C/min. Injector temperature was 225$^{o}$C and the interface line was 250$^{o}$C. Injections of 2 to 5 uL were performed in the splitless mode.

Electron impact ionization mass spectra were obtained using an electron energy of 70eV, a trap current of 200uA, an acceleration voltage of 8kV and a resolution of 1000 (10% valley definition). The mass spectrometer was scanned at 1 second per decade over the range of m/z 50-550. The temperature of the ion source was 200$^{o}$C

*3,4-dihydroxyphenylacetone Standard*

3,4-dihydroxyphenylacetone was synthesized according to the methods of Slates et al. [9]. α-Methyldopa (211 mg) was dissolved in 0.5 M borax buffer (pH 8.5, 10 mL) and a layer of benzene (5 mL) was added. Nitrogen was bubbled through the borax and 0.34 N sodium hypochlorite was added drop wise. The red solution was collected and

dilute HCl was added. The 3,4-dihydroxyphenylacetone was extracted with ethylacetate and dried by rotary evaporation.

## 4.4 Results

*MALDI-TOF/TOF Verification*

MALDI-TOF/TOF analysis was carried out in the same manner as described for DCT (Chapter 2). The recombinant protein was verified as AMD isoform B through MALDI-TOF/TOF sequencing of tryptic peptides with 28% sequence coverage. AMD isoform A and B vary with regards to their N-terminal sequence. 3 N-terminal AMD isoform B specific peptides were identified (Figure 4.2).

*Identification of AMD Enzymatic Products of L-DOPA*

Three major peaks eluted during separation of the L-DOPA AMD enzymatic reaction mixture with reverse phase HPLC (Figure 4.3A). The first peak to elute was identified as the substrate L-DOPA (Figure 4.4). The second peak to elute was much smaller than the other two and was identified as dopamine (Figure 4.5). The third peak to elute was red when dried in the speedvac and was identified as 3,4-dihydroxyphenylacetaldehyde (DOPAL) (Figure 4.6) [8]. In contrast to the formation of DOPAL from DOPA by AMD, *Drosophila* DDC only forms DA from DOPA (Figure 4.3B).

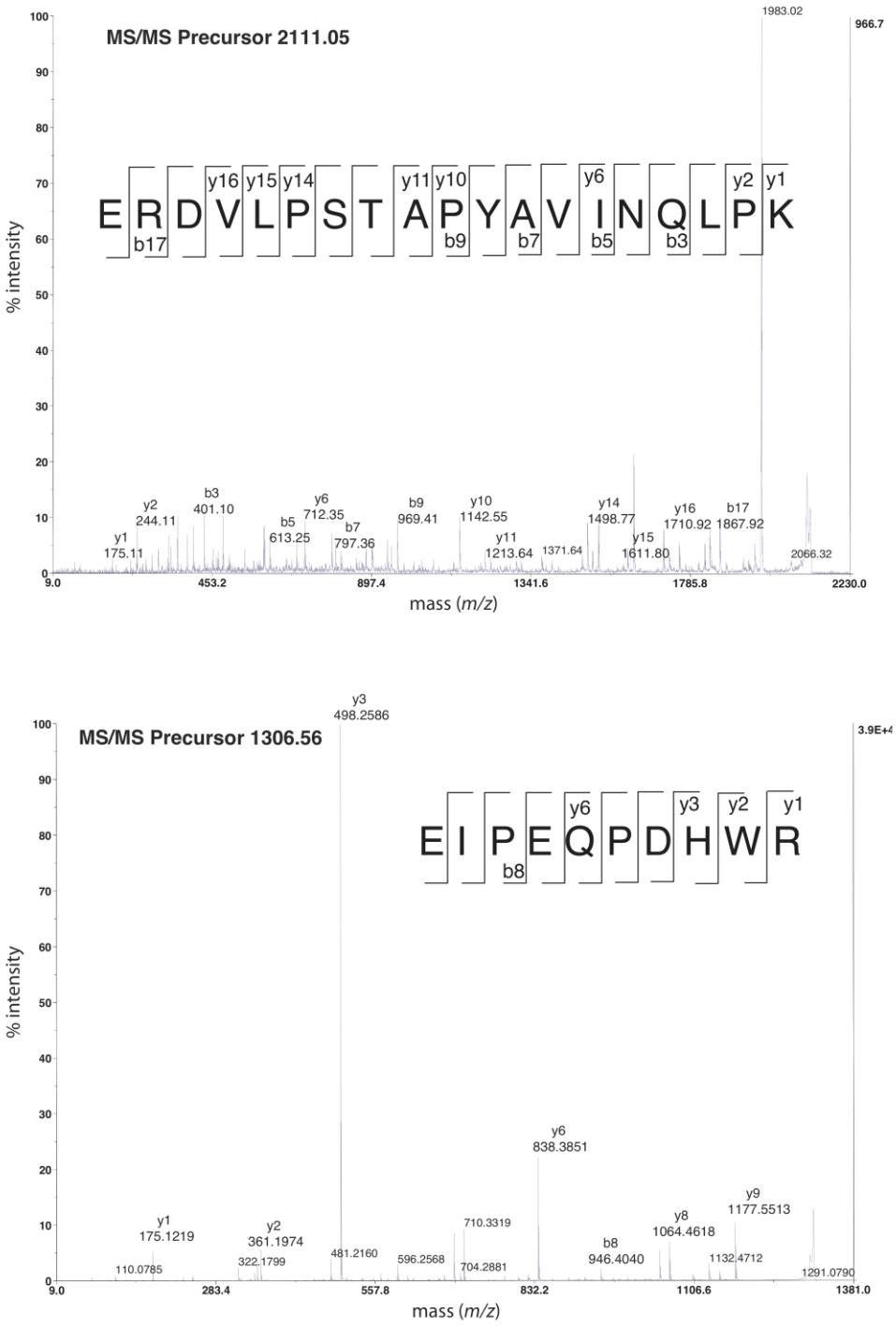


**Figure 4.2** AMD MALDI-TOF/TOF spectra of AMD isoform B specific tryptic peptides. Peptide ion *m/z* 2111.05 (top spectrum) corresponds to the AMD isoform B peptide $^{26}$ERDVLPSTAPYAVINQLPK$^{44}$, and peptide ion m/z 1306.56 (bottom spectrum) corresponds to the peptide $^{45}$EIPEQPDHWR$^{55}$.

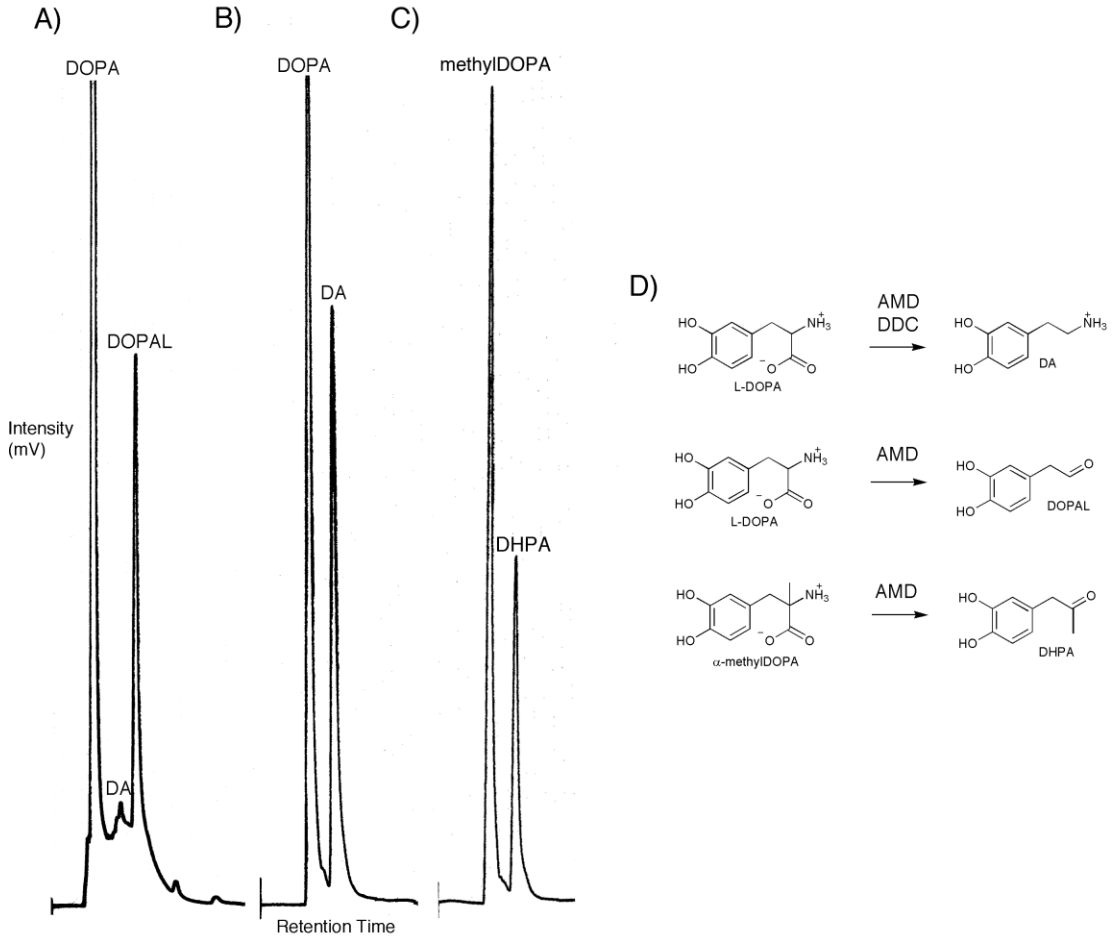


**Figure 4.3** Electrochemical detection of AMD (A and C) and DDC (B) enzymatic metabolites. Reaction conditions: (A) 100 ug/mL AMD, 2 mM L-DOPA, (B) 100 ug/mL DDC, 2 mM L-DOPA, (C) 100 ug/mL AMD, 2 mM methyldopa. All reactions were carried out in 20 mM sodium phosphate pH 6.8 for 10 minutes. The L-DOPA reactions were separated through C18 using 6% acetonitrile in the mobile phase; 30% acetonitrile was used for methyldopa. Figure 4.3D indicates the reactions catalyzed by AMD based on this analysis.

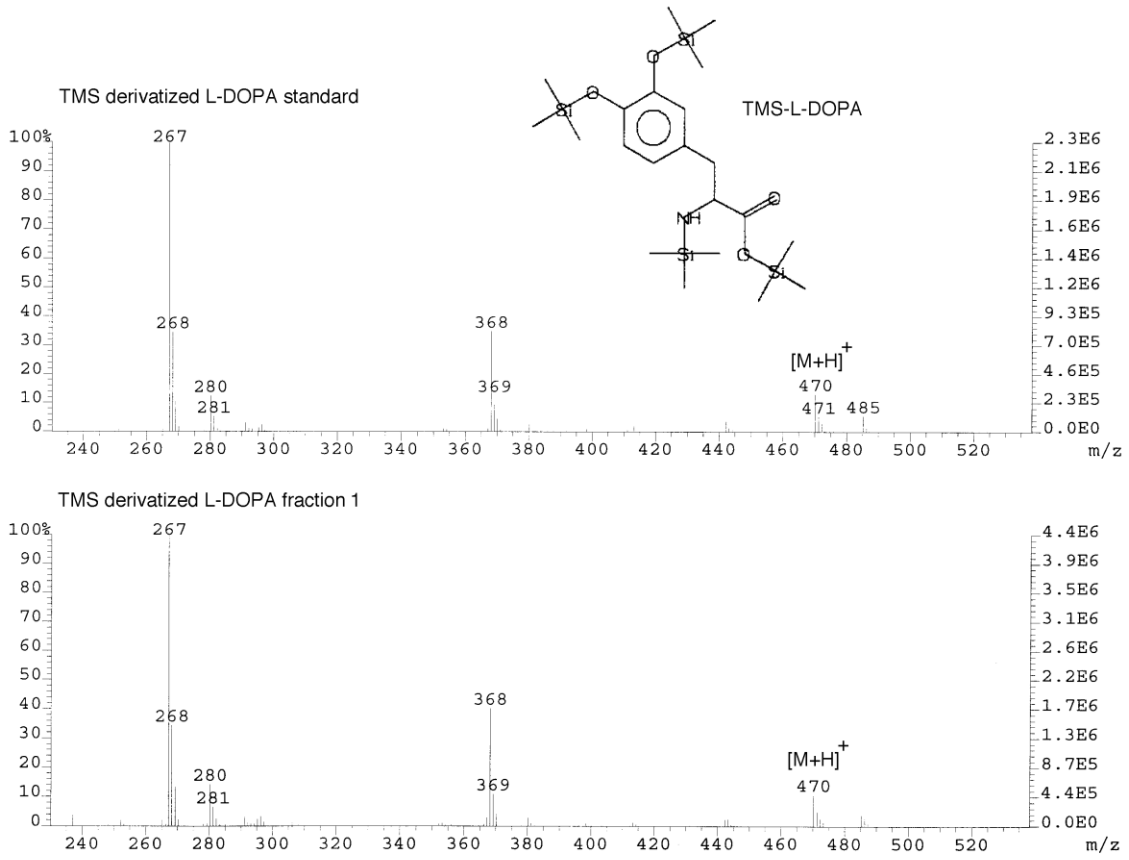


**Figure 4.4** Electron impact fragmentation spectrum of the TMS derivatized L-DOPA (above) and the EI spectrum of the TMS derivatized initial fraction from the AMD L-DOPA enzymatic reaction (below).

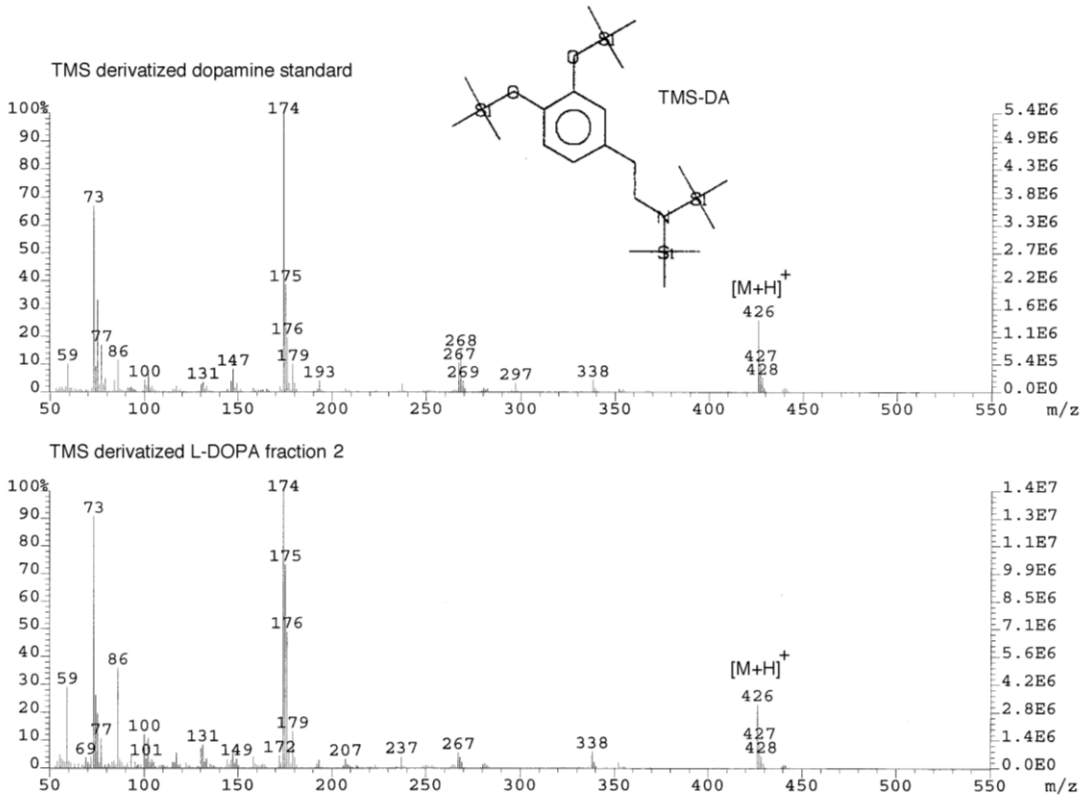


**Figure 4.5** Electron impact fragmentation spectrum of the TMS derivatized dopamine (above) and the EI spectrum of the TMS derivatized second fraction from the AMD L-DOPA enzymatic reaction (below).

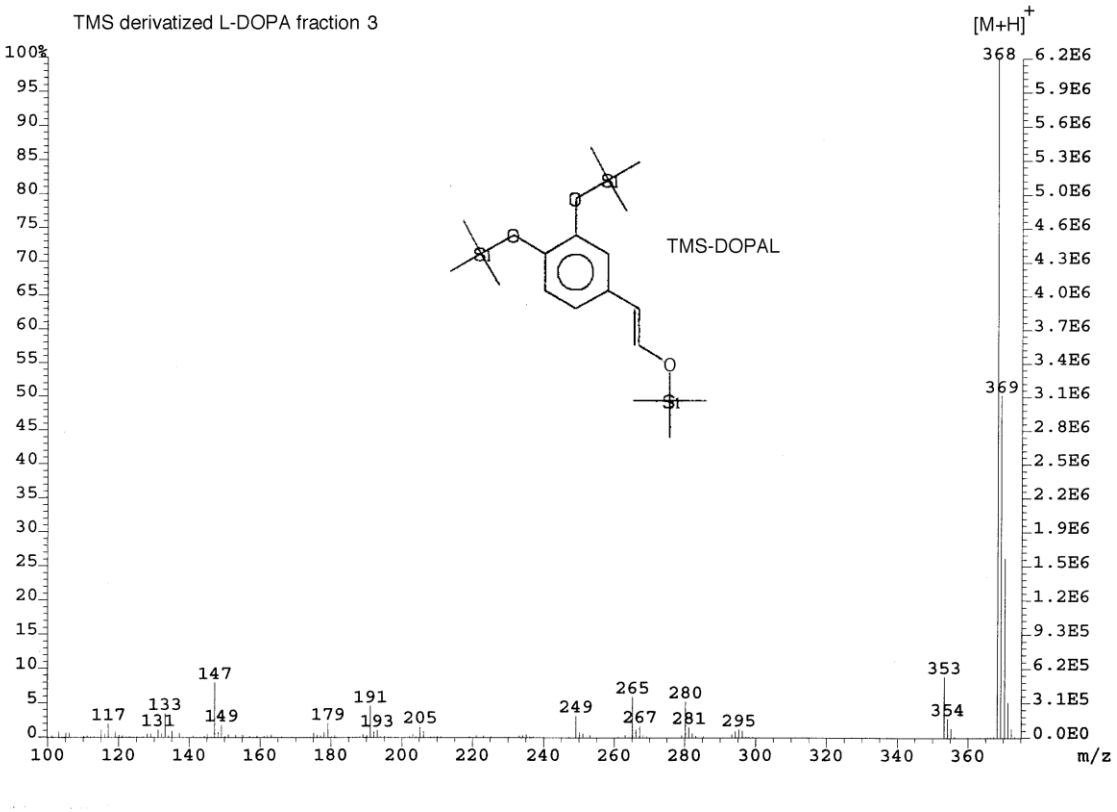


**Figure 4.6** Electron impact fragmentation spectrum of the TMS derivatized third fraction from the L-DOPA AMD enzymatic reaction. A TMS-DOPAL derivative standard ESI reference spectrum was obtained from Mattammal et al. [8]. These spectra indicate an enolization of the aldehyde during the process of TMS derivatization.

*Identification of AMD Enzymatic Products of α-methylDOPA*

A single product peak and single reaction peak were detected from the α-methyldopa, after separation of the reaction mixture with HPLC (Figure 4.3C). GC-MS of the TMS derivative of the initial fraction confirmed the identity of α-methyldopa (Figure 4.7). The TMS derivatized second fraction was identified as the enzymatic product 3,4-dihydroxyphenylacetone (Figure 4.8 and 4.9).

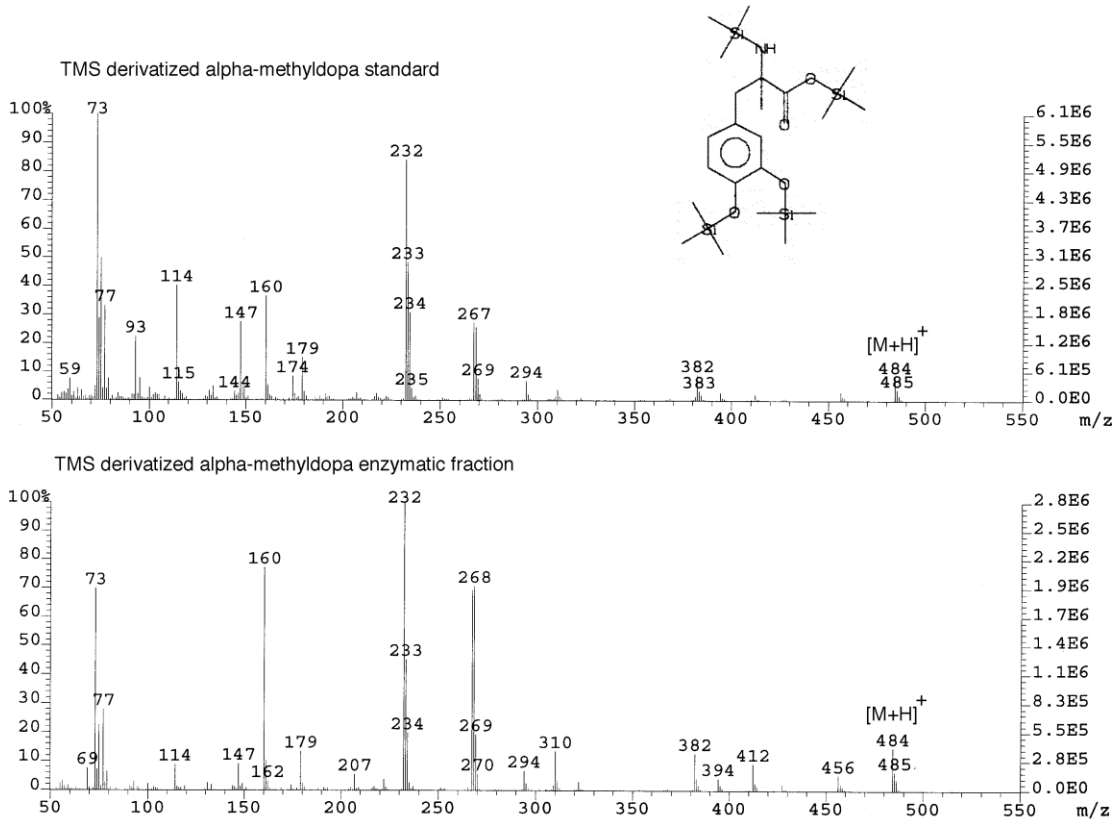


**Figure 4.7** Electron impact fragmentation spectrum of the TMS derivatized methyldopa (above) and the EI spectrum of the TMS derivatized initial fraction from the methyldopa reaction (below).

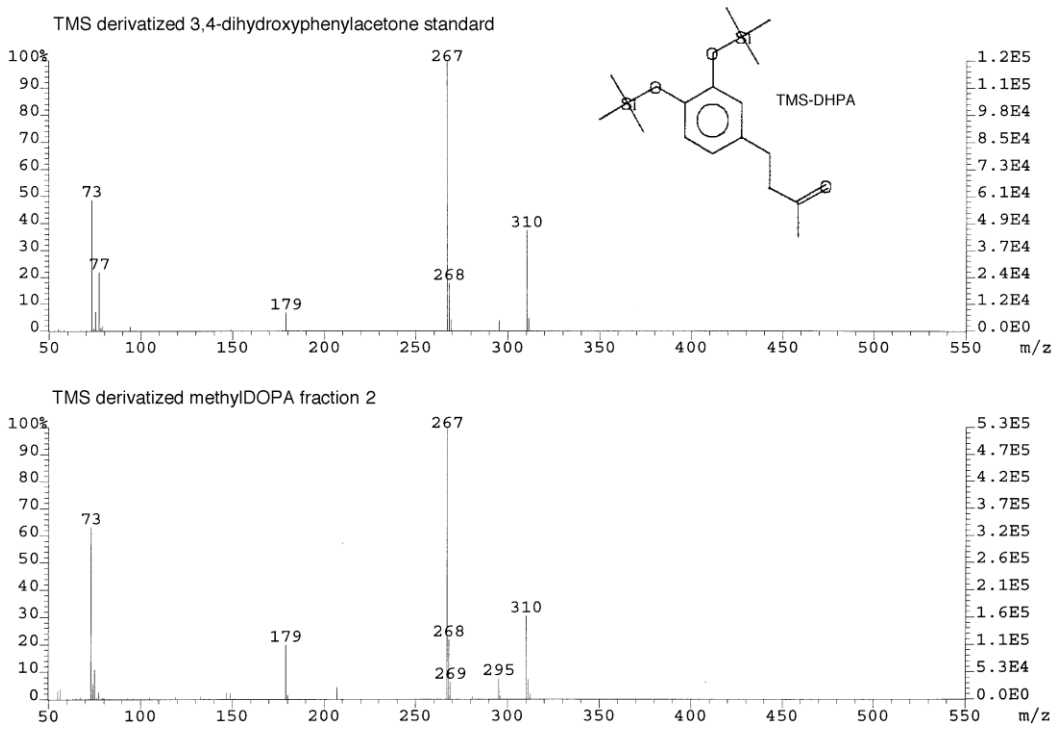


**Figure 4.8** Electron impact fragmentation spectrum of the TMS derivatized 3,4-dihydroxyphenylacetone (DHPA) standard (above) and the EI spectrum of the TMS derivatized second fraction from the α-methyldopa reaction (below).

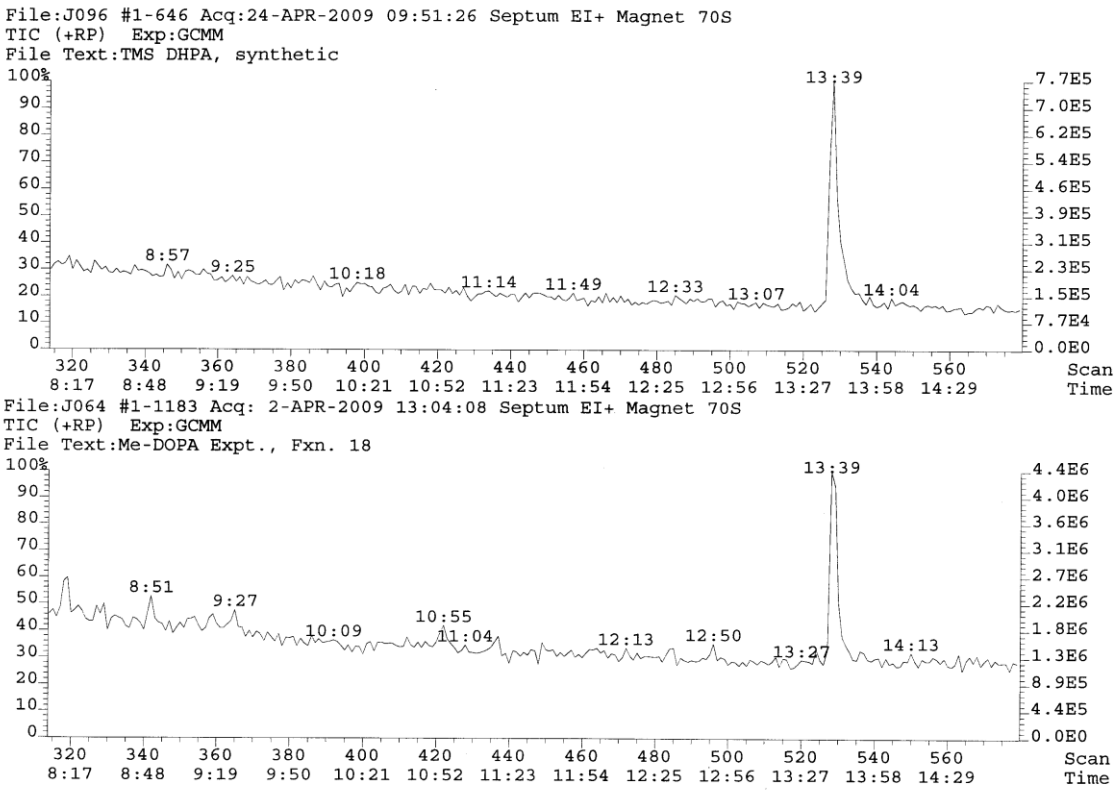


**Figure 4.9** GC-MS TIC for the dihydroxyphenylacetone standard (above) and product fraction from incubation of AMD with methyldopa (below).

## 4.5 Discussion

Although DDC has been shown to catalyze an oxidative deamination of α-methyldopa to some extent, the primary activity of DDC is to produce dopamine from L-DOPA [10]. Unlike DDC, AMD catalyzes the formation of oxidatively deaminated DOPAL from L-DOPA to a large extent (Figure 4.3).

AMD was originally isolated in *Drosophila* mutants that display high resistance to α-methyldopa. However, its primary function is likely not detoxification. α-Methyldopa is not a common metabolite in nature and furthermore AMD is highly active toward the common metabolite L-DOPA. Catecholamines are easily oxidized to quinones and when this happens intramolecular cyclization by way of the amino group occurs rapidly in order to gain stability (Figure 4.10). Cyclization of quinones is a major reaction in melanogenesis. For example, when dopamine is oxidized to dopaquinone, the quinone is able to cyclize to dopaminechrome, a primary intermediate in formation of DHI melanin. By oxidizing the amino group of its substrate, AMD prevents intramolecular cyclization from occurring. Cuticle crosslinking agents NBAD and NADA both have their amino groups blocked and are believed to be major crosslinking agents for cuticle sclerotization. DOPAL and further dopamine metabolites could potentially act in a similar manner.

*Drosophila* strains with both elevated resistance to α-methyldopa and increased DDC activity were also previously identified [2]. This posed the question whether DDC could be responsible for the α-methyldopa resistance. However, through comparison of DDC and AMD mutants, it was concluded that the resistance to α-methyldopa was generated from AMD alone [2]. Our finding that AMD produces some residual dopamine

along with DOPAL from L-DOPA explains why higher AMD activity could have been mistaken as high DDC activity as well.

Based on the production of DOPAL from L-DOPA and production of 5,6-dihydroxyphenylacetone from α-methyldopa, a pyrodoxal reaction mechanism is outlined in Figure 4.11. Because there is no α-proton in α-methyldopa, the mechanism must begin with the decarboxylation of substrate and shifting of electrons to the pyrodoxal cofactor. Normally, in this type of decarboxylation mechanism, the electrons shift back toward the substrate along with the addition of a proton. However, hydrolysis of the shiff base at this point would leave the amino group on the substrate. Therefore, it is proposed that the shiff base is first hydrolyzed leaving the amino group on the pyridoxal, followed by the electrons shifting toward the amino group with the addition of a proton to the amino group (formation of pyridoxamine). In the case of L-DOPA, the presence of an α-proton may allow the mechanism to follow the standard route leaving the amino group on the substrate, hence formation of small amounts of dopamine.

In conclusion, a new protein function has been characterized for *Drosophila* AMD: an oxidative deamination of L-DOPA and methyldopa. This could potentially be used for production of DOPAL as a crosslinking agent for sclerotization or for the quick degradation of L-DOPA, without producing the melanization intermediate dopamine.

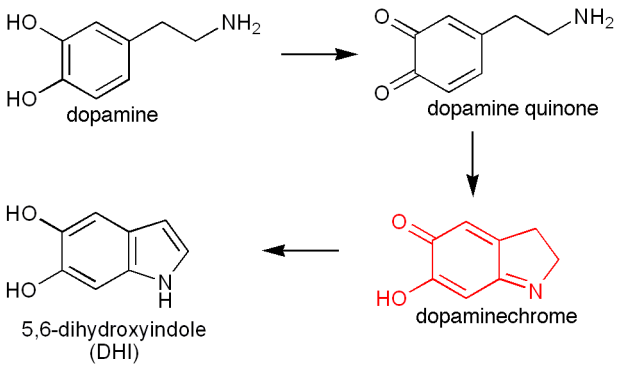


**Figure 4.10** Intramolecular cyclization of dopamine. This same process can occur with other catecholamines like L-DOPA, however not with sclerotization agents NADA and NBAD or oxidized DOPAL that contain no amino group.

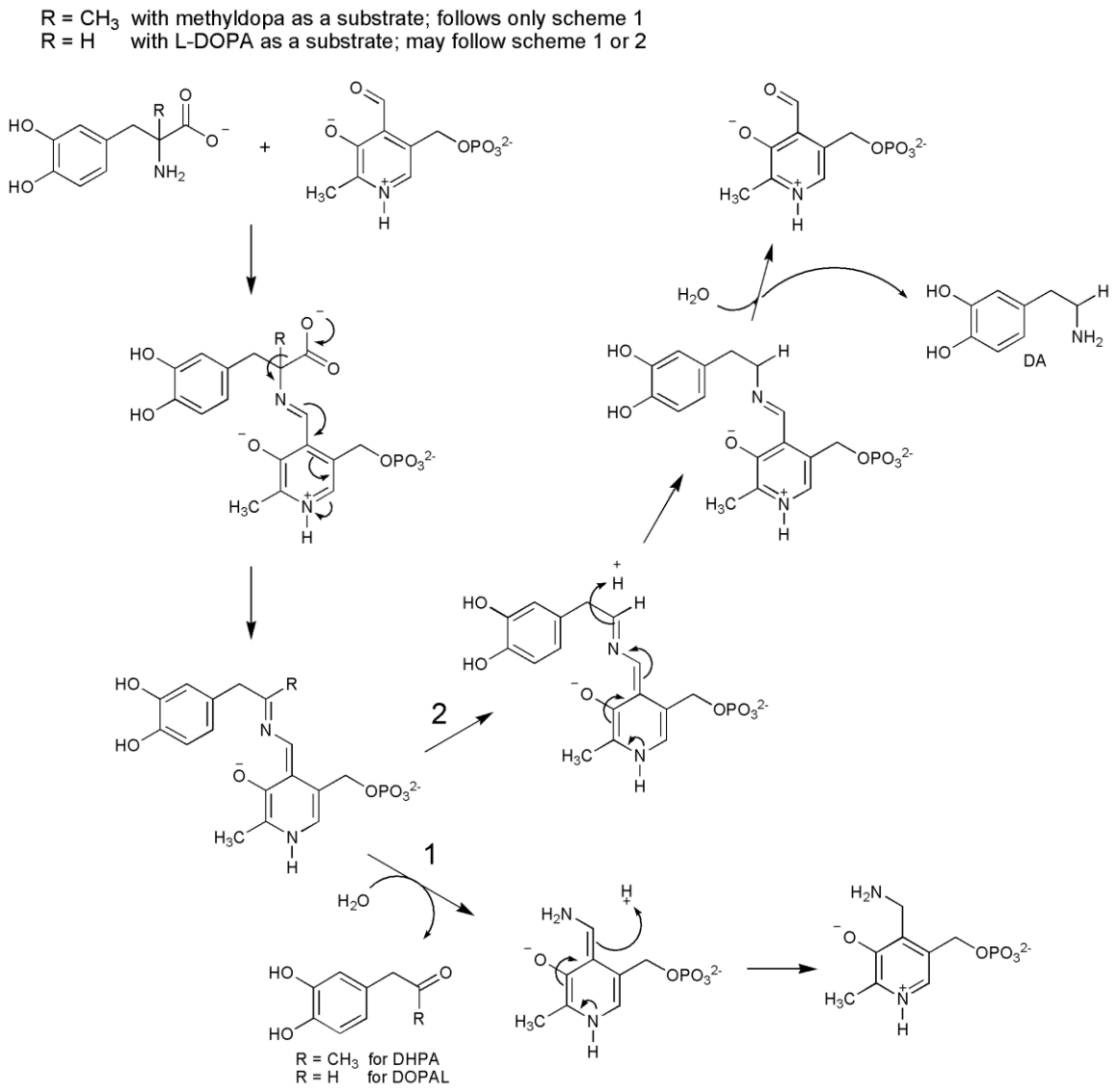


**Figure 4.11** Proposed reaction mechanism for the oxidative decarboxylation of L-DOPA and α-methyldopa catalyzed by AMD.

**Acknowledgements**

*This work was done in partnership with Kim Harich at the Virginia Tech Biochemistry Department GC-MS Faculity. Thanks to Dr. Keith Ray and Dr. Rich Helm at the Virginia Tech Mass Spectrometry Incubator (http://www.mass.biochem.vt.edu/) for their assistance with the analysis of AMD peptides. Thanks to Brian Hickory for assistance with the synthesis of 3,4-dihydroxyphenylacetone.*

# LITERATURE CITED


1. Wright, T.R.F., R.B. Hodgetts, and A.F. Sherald, *Genetics of Dopa Decarboxylase in Drosophila-Melanogaster .1. Isolation and Characterization of Deficiencies That Delete "Dopa-Decarboxylase-Dosage-Sensitive Region and Alpha-Methyl-Dopa-Hypersensitive Locus.* Genetics, 1976. **84**(2): p. 267-285.

2. Marsh, J.L. and T.R.F. Wright, *Evidence for Regulatory Variants of the Dopa Decarboxylase and Alpha-Methyldopa Hypersensitive Loci in Drosophila.* Genetics, 1986. **112**(2): p. 249-265.

3. Molinoff, P.B. and J. Axelrod, *Biochemistry of catecholamines.* Annu Rev Biochem, 1971. **40**: p. 465-500.

4. Andersen, S.O., M.G. Peter, and P. Roepstorff, *Cuticular sclerotization in insects.* Comparative Biochemistry and Physiology B-Biochemistry & Molecular Biology, 1996. **113**(4): p. 689-705.

5. Suderman, R.J., et al., *Model reactions for insect cuticle sclerotization: Cross-linking of recombinant cuticular proteins upon their laccase-catalyzed oxidative conjugation with catechols (vol 36, pg 353, 2006).* Insect Biochemistry and Molecular Biology, 2006. **36**(7): p. 610-611.

6. Han, Q., H. Robinson, and J. Li, *Crystal structure of human kynurenine aminotransferase II.* J Biol Chem, 2008. **283**(6): p. 3567-73.

7. Loutelier-Bourhis, C., et al., *Gas chromatography/mass spectrometric identification of dopaminergic metabolites in striata of rats treated with L-DOPA.* Rapid Commun Mass Spectrom, 2004. **18**(5): p. 571-6.

8. Mattammal, M.B., et al., *Confirmation of a dopamine metabolite in parkinsonian brain tissue by gas chromatography-mass spectrometry.* J Chromatogr, 1993. **614**(2): p. 205-12.

9. Slates, H.L., et al., *Degradation of α-Methyl-3,4-dihydroxyphenylalanine (α-MethylDOPA).* J Org Chem, 1964. **29**(6): p. 1424-1429.

10. Bertoldi, M., et al., *Reaction of Dopa decarboxylase with alpha-methyldopa leads to an oxidative deamination producing 3,4-dihydroxyphenylacetone: An active site directed affinity label.* Biochemistry, 1998. **37**(18): p. 6552-6561.

11. Marchitti, S.A., R.A. Deitrich, and V. Vasiliou, *Neurotoxicity and metabolism of the catecholamine-derived 3,4-dihydroxyphenylacetaldehyde and 3,4-dihydroxyphenylglycolaldehyde: The role of aldehyde dehydrogenase.* Pharmacological Reviews, 2007. **59**(2): p. 125-150.

# IV

# GENERAL DISCUSSION

The purification and analysis of recombinant DCT and AMD, as well as native DCE is outlined in this dissertation. Through these studies, many valuable insights in terms of the structural and functional characteristics of these important proteins have been gained. For example, *N*-glycosylation sites from DCT and DCE have been characterized. Furthermore, a new protein function has been demonstrated for AMD. These contributions were gained through the purification and mass spectrometric analysis of these enzymes or their metabolites.

The highly purified and active DCT, DCE and AMD were obtained using conventional biochemical methods. The technology and means used for the purification of these enzymes have existed for quite a while now, however these methods are still are very powerful tools for the elucidation of protein structure and function. Furthermore, the analysis of the products and substrates of the AMD enzymatic reaction were done using a VG 70S mass spectrometer.

In the post-genomic era, direct structural and functional characterization at the protein level has become an extremely important task [1]. Despite heavy interest into tyrosine metabolism fueled by the demand for insight into Parkinson's disease, dopamine related pharmacology and melanoma, many of the core enzymes in these pathways are still not understood. In the case of DCT, tyrosinase and TRP1, this is likely due to the level of difficulty required to isolate these enzymes. The major factors contributing to the difficulty in purifying these three enzymes are the transmembrane domain and high level of post-translational processing.

To avoid the complications that arise when working with membrane proteins, DCT was expressed without the C-terminal transmembrane domain and cytosolic tail

using an Sf9 insect cell expression system. Purification of the truncated, recombinant DCT proved to be much easier than the native protein from B16 cells. This recombinant DCT is soluble in the absence of detergent and is expressed at higher levels than from B16 mouse melanoma cells. The successful expression tyrosinase and TRP1 in insect cells (see appendix) is also a move in the right direction for the proteomic characterization of the entire tyrosinase related protein family. Tyrosinase has been extensively characterized and a crystal structure for a bacterial tyrosinase has recently been reported. There is still much work to be done with TRP1. However, the reactions catalyzed by tyrosinase and TRP1 are more difficult to assay for than DCT. For these reasons, DCT was an ideal starting point for the purification of tyrosinase related proteins.

Despite the many advantages of working with recombinant protein, the physiological relevance may be brought into question. In the case of proteins that are able to be expressed in bacterial systems, like AMD, the differences between the recombinant and native protein are likely to be much less significant than for highly processed proteins like DCT. In regards to *N*-glycosylation, the complexity of the final occupied *N*-glycosylation sites varies between the eukaryotic expression systems. For example, yeast generate high mannose, "complex type" *N*-glycans and vertebrates produce the most complex *N*-glycan structures [2]. The processing pathway in insect cells is the least complicated and is usually completed with the final structure of $Man_3GlcNAc_{2\ [2]}$, as was found in our analysis of DCE and DCT expressed in insect cells [3].

Although production of a mammalian glycoprotein in an insect cell expression system would therefore lead to production of less complex glycan structures as was found

in the case with DCT, it has been found that the same glycosylation sites are occupied between different eukaryotic expression systems [4-6]. Furthermore, the less complex and more uniform processing in the insect cell expression system will be highly advantageous for obtaining protein crystals.

*N*-glycosylation is critical for the correct folding and processing of glycoproteins through the ER and Golgi. Mutation of glycosylation sites in tyrosinase have been found to disrupt the processing of the protein. Furthermore, disruption of glycosylation sites through mutation is also linked to various forms of oculocutaneous albinism. Although DCT plays a very important role in melanogenesis, no direct analysis of its *N*-glycosylation sites has previously been carried out.

The purification of DCE is somewhat more manageable than for the tyrosinase related proteins. The activity of DCE can be measured in the same manner as DCT, by observing the disappearance of dopachrome. Furthermore, the activity of DCE is higher than DCT, which makes it even easier to track during purification. DCE contains no membrane domain and is not as highly processed; DCE contains only a single glycosylation site in comparison to the multiple sites in DCT and mammalian tyrosinase. This allowed for extensive analysis of the native protein. However, recombinant protein is also being explored as a good option to produce uniform protein for crystallography purposes.

In the case of AMD, it is not a matter of difficulty that has left this interesting protein uncharacterized. This may demonstrate the enormity of the task of proteomics, as there still is an abundant number of proteins that have yet to be characterized. However, this may simply reflect the amount of interest in insect proteins relative to mammals.

There are still quite a number of uncharacterized proteins involved in the metabolism of tyrosine.

Comparison between the enzymes of melanogenesis and dopamine metabolism between insects and mammals reveals many interesting evolutionary differences. In regards to melanogenesis, the direct enzymatic regulation by the mammalian system may appear to be more highly controlled. However the insect pathway is highly evolved; insects contain multiple phenoloxidases and DCE is a member of a yellow gene family with a number of similar enzymes. As a model species, *Drosophila* contains 13 phenoloxidases and up to 14 yellow family proteins [7]. Insects must invest a great deal of energy to hardening of their eggs and formation of their cuticle. It is therefore logical that they have evolved a highly complex network of enzymes to assist in these processes. Currently, most of the yellow proteins and phenoloxidases remain uncharacterized.

The evolutionary difference is also pronounced when examining DDC from both phyla. Mammals utilize just a single DDC termed aromatic amino acid decarboxylase (AADC) for the decarboxylation of L-DOPA to dopamine, and the decarboxylation of 5-hydroxytryptophan to serotonin. Drosophila contains multiple DDC isoforms, two tyrosine decarboxylases and AMD. Similar to the situation with melanization related enzymes, insects must also invest a great deal into L-DOPA metabolism, as they require dopamine for cuticle formation.

There is still much to be done in regards to understanding the enzymes involved in melanogenesis and sclerotization at the protein level. The purification and characterization of DCT, DCE and AMD have answered many questions, however crystal structures of these proteins are an essential piece of the complete picture.

Hopefully, this dissertation will serve as a useful reference for the comprehensive understanding of the enzymes of melanogenesis and sclerotization.

## LITERATURE CITED


1. Eisenberg, D., et al., *Protein function in the post-genomic era.* Nature, 2000. **405**(6788): p. 823-826.

2. Varki, A., *Essentials of glycobiology*. 1999, Cold Spring Harbor, NY: Cold Spring Harbor Laboratory Press. xvii, 653 p.

3. Li, J.S., et al., *Proteomic analysis of N-glycosylation in mosquito dopachrome conversion enzyme.* Proteomics, 2007. **7**(15): p. 2557-2569.

4. James, D.C., et al., *N-glycosylation of recombinant human interferon-gamma produced in different animal expression systems.* Biotechnology (N Y), 1995. **13**(6): p. 592-6.

5. Altmann, F., et al., *Insect cells as hosts for the expression of recombinant glycoproteins.* Glycoconjugate Journal, 1999. **16**(2): p. 109-123.

6. Yeh, J.C., et al., *Site-Specific N-Glycosylation and Oligosaccharide Structures of Recombinant Hiv-1 Gp120 Derived from a Baculovirus Expression System.* Faseb Journal, 1994. **8**(7): p. A1427-A1427.

7. Drapeau, M.D., *The family of yellow-related Drosophila melanogaster proteins.* Biochemical and Biophysical Research Communications, 2001. **281**(3): p. 611-613.

# APPENDIX

# SUPPLEMENTARY INFORMATION

## A.1 Supplementary DCT Information

*Supplementary DCT MS Data*

A few quality MS/MS spectra of DCT tryptic peptides were also collected using Q-TOF mass spectrometry (Figure A.1). These peptides were analyzed using the same methods described in Chapter 3 for Dopachrome Conversion enzyme. Additional MALDI-TOF/TOF spectra mentioned in Chapter 3 are also included (Figure A.2)

*Generation of DCT-TEV-$His_6$ Baculovirus Transfer Vector*

Although recombinant DCT was successfully purified from baculovirus transfected Sf9 insect cells, this process is difficult to reproduce. In an attempt to simplify the purification process, a polyhistidine tagged DCT has been produced. Because his-tags often interfere with chromatographic separations after metal affinity chromatography has already been used, a TEV cleavable his-tag is ideal.

No C-terminal TEV cleavable his-tag vector has been available commercially for baculovirus transfection. Because DCT contains an N-terminal signal sequence and a C-terminal transmembrane anchor, a C-terminal tag is best. An engineered Invitrogen vector pMelBacC with this modification was obtained from graduate student Michael Smout of University of Queensland, Australia (Figure A.3). DCT was amplified without its transmembrane domain using the forward primer ATATGTCGACATGGGCCTTGTGGGAT containing a SalI (SalI is compatible with XhoI) restriction site and the reverse primer TCAGAAGCTTGAGAGAGTTGTGGACC containing a HindIII restriction site. The amplified DCT coding sequence was inserted

into the modified vector, which was named pHotWax, however an extra nucleotide was detected in the vector before the stop codon after DNA sequencing. The DNA coding sequence containing DCT followed by a TEV site and histidine tag was reamplified with the reverse primer GGATCCTCAATGGTGATGGTGATG (BamHI restriction site) without the extra nucleotide and recloned into the transfer vector.

Sf9 insect cells were cotransfected with recombinant pHotWax and viral DNA in the same manner described in Chapter 2. The transfected cells contain high DCT activity, which indicates this recombinant DCT is also active and properly folded.

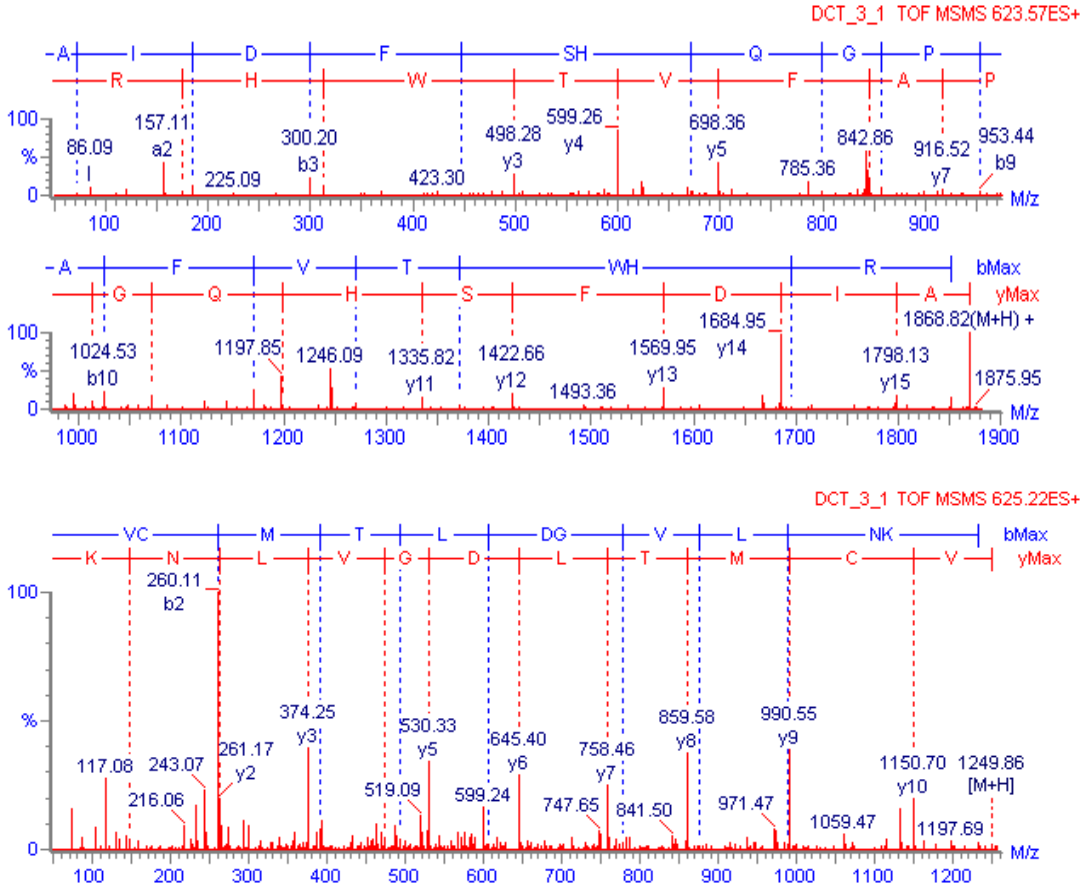


**Figure A.1** Q-TOF tandem spectra of DCT tryptic peptides

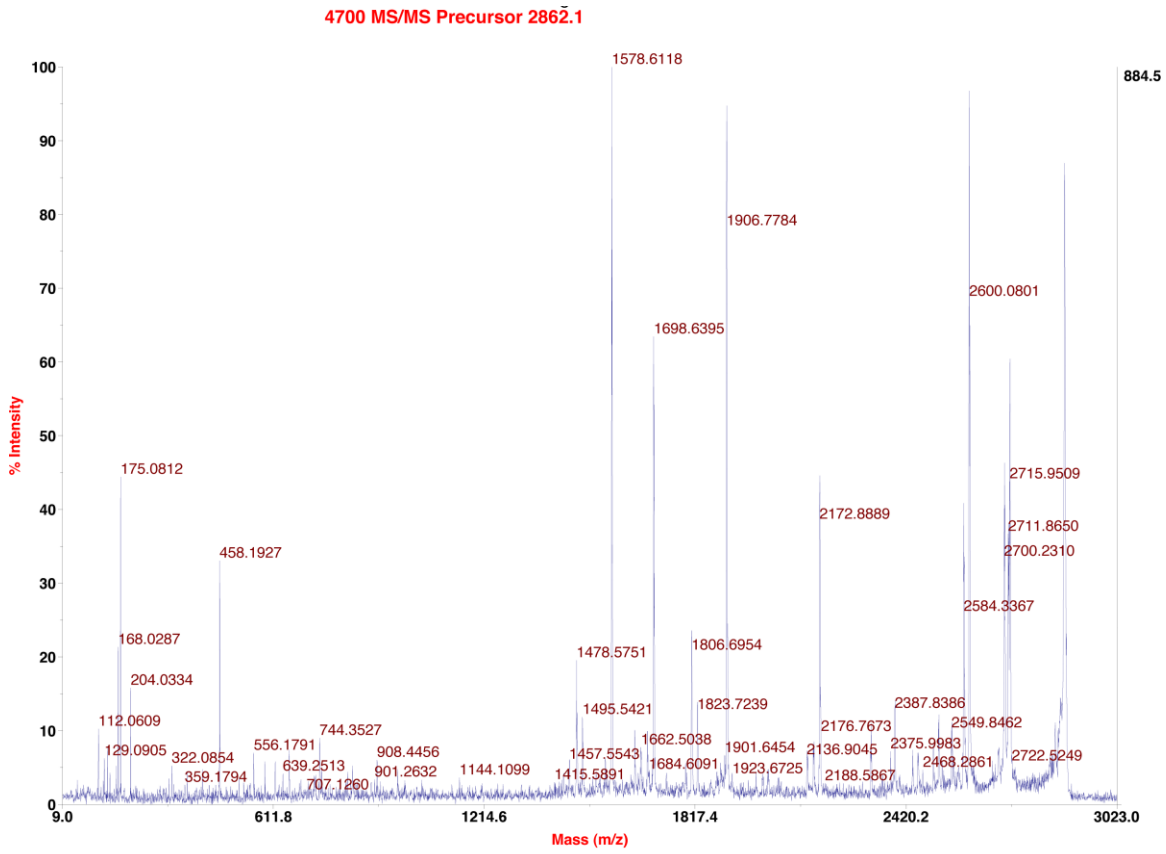


**Figure A.2** MALDI-TOF/TOF spectra of DCT glycosylated peptide ion *m/z* 2862.1

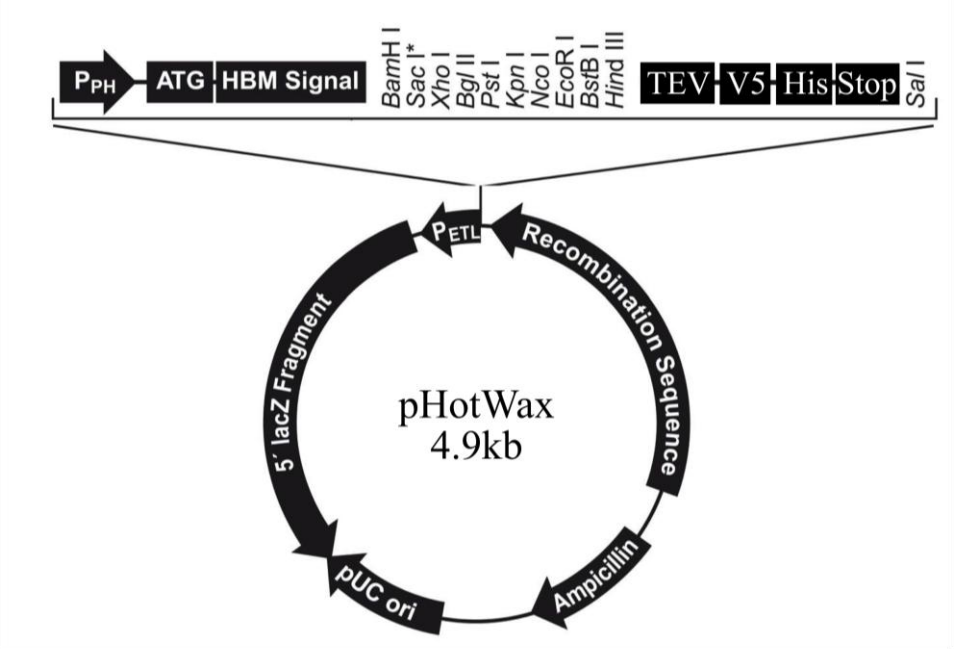


GTGTCCAGTGTGGCTTGATATCATGGAGATAATTAAAATRATAACCATCTCGCAAATAA
ATAAGTATTTTACTGTTTTCGTAACAGTTTTGTAATAAAAAAACCTATAAATATGAAAT
TCTTAGTCAACGTTGCCCTTGTTTTTATGGTCGTATACATTTCTTACATCTATGCGGAT
CGATGGGGATCCGAGCTCGAGATCTGCAGCTGGTACCATGGAATTCGAAGCTTGGAGGG
CCAGTTTTATCTGAACGAAGGTAAGCCTATCCCTAACCCTCTCCTCGGTCTCGATTCTA
CGCGTACCGGTCATCATCACCATCACCATTGAGTCGACTCTGCTGAAGAGGAGGAAATT
CTCCTTGAAGTTTCCCTGGTGTTCAAAGTAAAGGAGTTTGCACCAGACGCACCTCTGTT
CACTGGTCCGGCGTATTAAAACACGATACATTGTTATTAGTACATTTATTAAGCGCTAG
ATTCTGTGCGTTGTTGATTTACAGACAATTGTTGTACGTATTTTAATAATTCATTAAAT
TTATAATCTTTAG

**Figure A.3** Vector Map and multiple cloning site sequence of pHotWax. This vector was modified from pMelBacA (Invitrogen) and shares the exact sequence with exception to the multiple cloning site.

*PNGase F Purification*

PNGase F was produced by the methods of Loo et al. and the expression vector pOPH6 was obtained from Dr. Shaun Lott and the University of Auckland, New Zealand. BL21(DE3) *E. coli* was transformed with the expression vector pOPH6 and grown overnight at 37$^{o}$C with shaking. The overnight culture was diluted to 4% and the cells were grown for 4 hours before induction with 1 mM IPTG. Cells were harvested 4 hours after induction by centrifugation, washed and then suspended in 20 mM sodium phosphate pH 7.4. The cell extract was prepared using sonication where 1 mM PMSF was included. The cell extract was loaded onto Ni-NTA. Protein was eluted with a gradient from 0 - 150 mM imidazole in 20 mM sodium phosphate (pH 7.4) with 500 mM NaCl. PNGase F eluted at around 90 mM imidazole (Figure A.4).

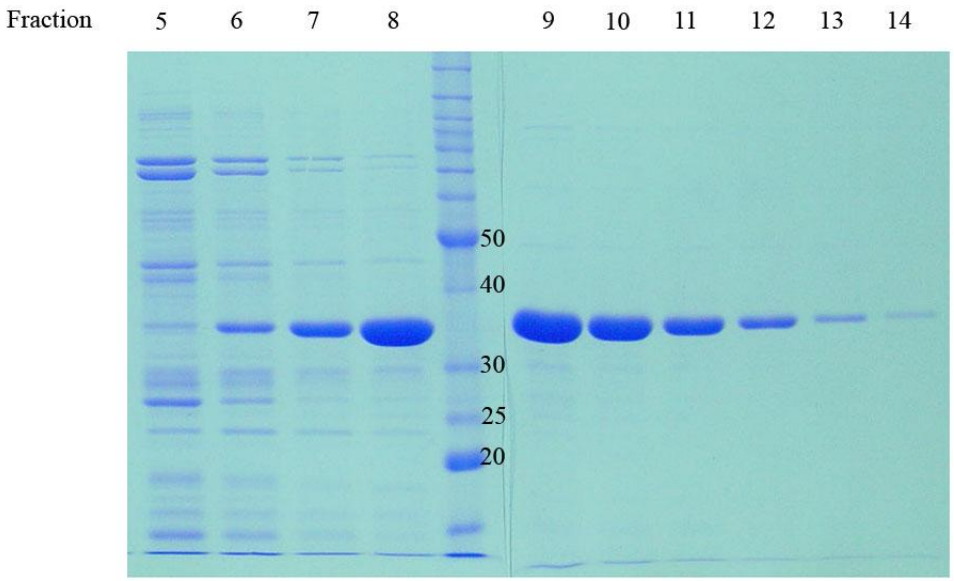


**Figure A.4** Higher purity fractions of PNGase F after elution from Ni-NTA with 0-150 mM imidazole

## A.2 Tyrosinase Related Proteins

DCT has only two close relatives within the same protein family: tyrosinase and tyrosinase-related protein 1 (TRP1) [1]. All three mammalian proteins share 38-47% sequence identity. Unlike DCT and TRP1, tyrosinase is also found in bacteria and a crystal structure of *Streptomyces castaneoglobisporus* tyrosinase has been solved [2]. This *Streptomyces* tyrosinase shares approximately 29% amino acid sequence identity with its three mammalian relatives.

Each protein contains an N-terminal signal peptide, 6-7 potential *N*-glycosylation sites, a C-terminal transmembrane domain and two highly conserved metal binding sites (Figure A.5). This high level of similarity in primary sequence strongly suggests a common evolutionary origin. A BLAST search against the NCBI non-redundant protein database using any one of these three sequences yields “tyrosinase” or “tyrosinase-like” sequences; however, their specific functions in the melanogenesis pathway are quite different. Tyrosinase functions as both a mono and dioxygenase using molecular oxygen as an electron acceptor to catalyze hydroxylation of tyrosine to 3,4-dihydroxyphenylalanine (L-DOPA) followed by the oxidation of L-DOPA to dopaquinone. In contrast, DCT serves as an intramolecular oxidoreductase and mediates a tautomerization of dopachrome to DHICA (Chapter 2). Although the exact function of TRP1 is not clear, it is most likely involved in the oxidation of DHICA units, a similar reaction to the tyrosinase oxidation of L-DOPA [3].

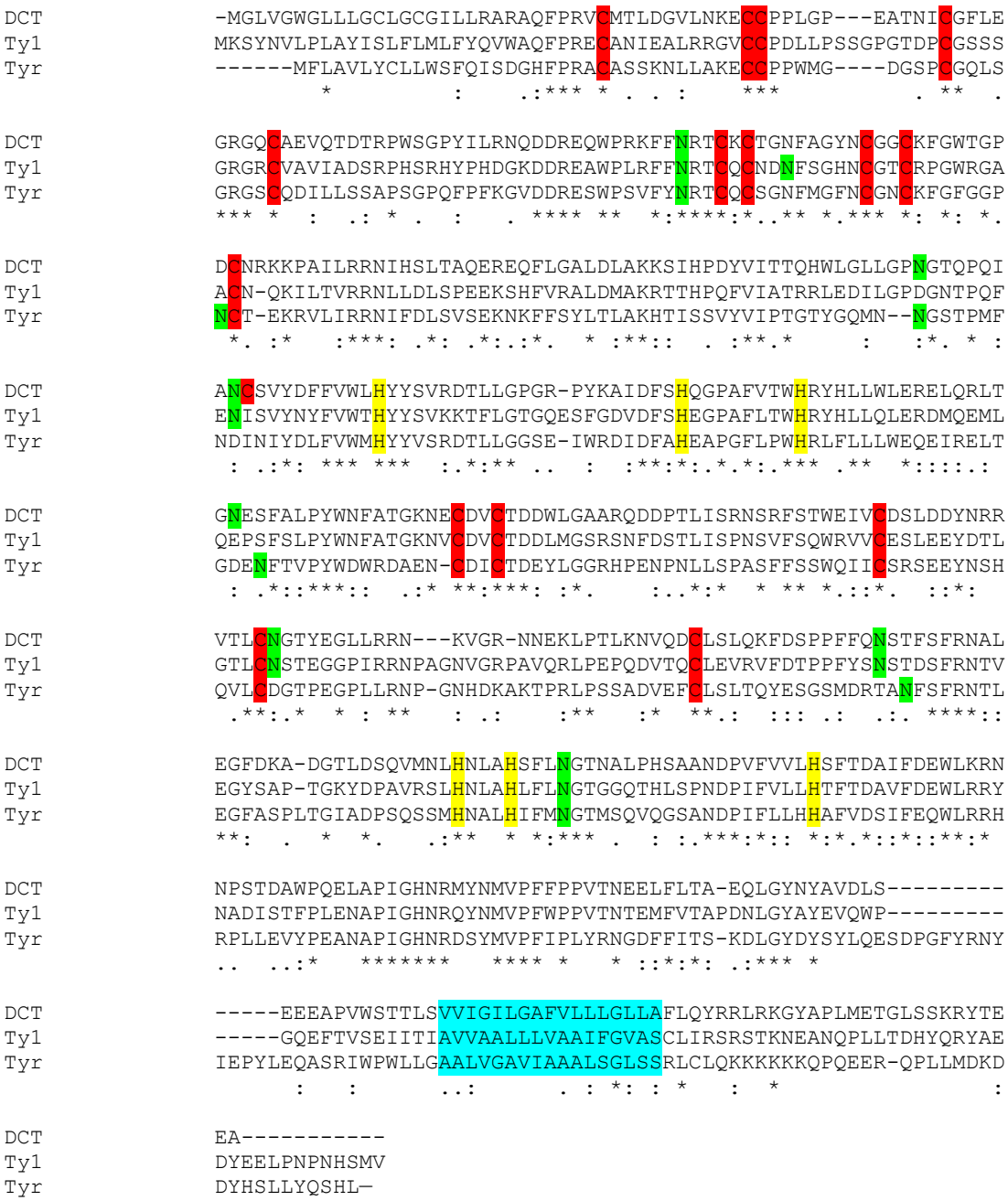


**Figure A.5** Annotated mouse DCT, Tyr and TRP1 (Ty1) sequence alignment. Potential N-glycosylation sites with an N-X-S/T motif are highlighted in green (X may represent any amino acid except proline). Cysteine residues are highlighted in red with the exception of those present in the signal sequence. The highly conserved metal binding histidine residues are highlighted in yellow. Putative transmembrane domains are highlighted in turquoise.

*Expression of Tyrosinase and Tyrosinase Related Protein 1*

Immunoaffinity purification of all three tyrosinase-related proteins has been reported, however this was done using antibodies specific for a portion of the C-terminal cytosolic domain [4]. We have successfully expressed truncated mammalian TRP1 and tyrosinase with the absence of their C-terminal hydrophobic and cytosolic domain using the same methods described in the DCT section. Tyrosinase was amplified using a forward primer (GACTGGATCCATGTTCTTGGCTGTTTTG) containing a BamHI restriction site and a reverse primer (GACTGAATTCTCACCAGATACGACTGGCTT) containing an EcoRI restriction site. TRP1 was amplified using a forward primer (CAGCACTCGAGATGAAATCTTACAACGTC) containing an XhoI restriction site and a reverse primer (GCGCGAATTCTCAAGATACAGTAAACTCCT) containing an EcoRI restriction site. The PCR protocol for the amplification of tyrosinase and tyrosinase-related protein 1 is identical to that described for DCT in Chapter 2.

Although the activity for tyrosinase and TRP1 are somewhat more difficult to monitor than DCT, the methods for purification of these proteins should be relatively similar since the proteins share high sequence identity and structural features.

## A.3 *Drosophila* AMD Mutant Analysis

The following *Drosophila melanogaster* AMD mutants were obtained from Bloomington *Drosophila* stock center (http://flystocks.bio.indiana.edu/). Stock number 18640, genotype: w[1118];PBac{w[+mC]=WH}amd[f03321]/CyO; stock number 3194, genotype: dp[ov1] b[1] amd[7] pr[1]/CyO; Dp(2;Y)H2; and stock number 3177, genotype: amd[1]/CyO. A DDC mutant was also obtained (stock number 3168, genotype: Ddc[DE1]). All mutants were grown in the presence of 0.1 mM methyldopa along with wildtype *Drosophila*. None of the flies grew except the DDC mutants. Because DDC and AMD have similar function, it is surprising that the DDC mutants were actually more resistant to methyldopa when the AMD mutants are hypersensitive.

Acetone extractions of the *Drosophila* mutants were also analyzed to determine their catecholamine levels using GC-MS in the same manner as described in Chapter 4. Unfortunately, no molecules resembling catechoamines were detected in any of the samples.

# LITERATURE CITED


1. Prota, G., *Melanins and melanogenesis*. 1992, San Diego: Academic Press. xiii, 290 p.

2. Matoba, Y., et al., *Crystallographic evidence that the dinuclear copper center of tyrosinase is flexible during catalysis.* J Biol Chem, 2006. **281**(13): p. 8981-90.

3. Kobayashi, T., et al., *Tyrosinase stabilization by Tyrp1 (the brown locus protein).* J Biol Chem, 1998. **273**(48): p. 31801-5.

4. Tsukamoto, K., et al., *A second tyrosinase-related protein, TRP-2, is a melanogenic enzyme termed DOPAchrome tautomerase.* EMBO J, 1992. **11**(2): p. 519-26.